

STRESS-DEPENDENT PERMEABILITY ON TIGHT GAS RESERVOIRS

A Thesis

by

CESAR ALEXANDER RODRIGUEZ

Submitted to the Office of Graduate Studies of  
Texas A&M University  
in partial fulfillment of the requirements for the degree of

MASTER OF SCIENCE

December 2004

Major Subject: Petroleum Engineering

STRESS-DEPENDENT PERMEABILITY ON TIGHT GAS RESERVOIRS

A Thesis

by

CESAR ALEXANDER RODRIGUEZ

Submitted to Texas A&M University  
in partial fulfillment of the requirements  
for the degree of

MASTER OF SCIENCE

Approved as to style and content by:

---

Robert A. Wattenbarger  
(Chair of Committee)

---

J. Bryan Maggard  
(Member)

---

Brann Johnson  
(Member)

---

Stephen A. Holditch  
(Head of Department)

December 2004

Major Subject: Petroleum Engineering

## ABSTRACT

Stress-Dependent Permeability on Tight Gas Reservoirs. (December 2004)

Cesar Alexander Rodriguez, B.S., Universidad Central de Venezuela

Chair of Advisory Committee: Dr. Robert A. Wattenbarger

People in the oil and gas industry sometimes do not consider pressure-dependent permeability in reservoir performance calculations. It basically happens due to lack of lab data to determine level of dependency. This thesis attempts to evaluate the error introduced in calculations when a constant permeability is assumed in tight gas reservoir.

It is desired to determine how accurate are conventional pressure analysis calculations when the reservoir has a strong pressure-dependent permeability. The analysis considers the error due to effects of permeability and skin factor. Also included is the error associated when calculating Original Gas in Place in the reservoir.

The mathematical model considers analytical and numerical solutions of radial and linear flow of gas through porous media. The model includes both the conventional method, which assumes a constant permeability (pressure-independent), and a numerical method that incorporates a pressure-dependent permeability.

Analysis focuses on different levels of pressure draw down in a well located in the center of a homogeneous reservoir considering two types of flow field geometries: radial and linear. Two different producing control modes for the producer well are considered: constant rate and constant bottom hole pressure.

Methodology consists of simulated tight gas well production with  $k(p)$  included. Then, we analyze results as though  $k(p)$  effects were ignored and finally, observe errors in determining permeability ( $k$ ) and skin factor ( $s$ ). Additionally, we calculate pore volume and OGIP in the reservoir.

Analysis demonstrates that incorporation of pressure-dependence of permeability  $k(p)$  is critical in order to avoid inference of erroneous values of permeability, skin factor and OGIP from well test analysis of tight gas reservoirs. Estimation of these parameters depends on draw down in the reservoir.

The great impact of permeability, skin factor and OGIP calculations are useful in business decisions and profitability for the oil company. Miscalculation of permeability and skin factor can lead to wrong decisions regarding well stimulation, which reduces well profitability.

In most cases the OGIP calculated is underestimated. Calculated values are lower than the correct value. It can be taken as an advantage if we consider that additional gas wells and reserves would be incorporated in the exploitation plan.

## DEDICATION

To Maria Raimunda, Yelitza, Maribel, Maria Alejandra, Maria Fernanda, Cesar  
Alejandro, Jacinto, Pastor, Pedro, Manuel and Janith.

## ACKNOWLEDGEMENTS

I would like to thank the Petroleum Department at Texas A&M University for allowing me to develop the current project. Special thanks to Dr. Wattenbarger, Dr. Maggard and Dr. Johnson. I want to also express thanks to PDVSA for providing funding for my master degree in petroleum engineering.

## TABLE OF CONTENTS

	Page
ABSTRACT.....	iii
DEDICATION.....	v
ACKNOWLEDGEMENTS.....	vi
TABLE OF CONTENTS.....	vii
LIST OF FIGURES.....	ix
CHAPTER	
I INTRODUCTION.....	1
1.1 Objectives.....	1
1.2 Problem Definition.....	2
1.3 Methodology.....	2
1.4 Previous Work.....	3
II LITERATURE REVIEW.....	7
2.1 Tight Gas Sands.....	7
2.2 Diffusivity Equation, Liquid Case.....	8
2.3 Diffusivity Equation, Gas Case.....	9
2.4 Stress-Dependent Formations.....	11
2.5 Linear Flow.....	14
2.6 Radial Flow.....	14
2.7 Transient Flow.....	15
2.8 Gas Simulator.....	15
2.9 Determination of OGIP.....	16
III PSEUDO PROPERTIES.....	18
IV STRESS-DEPENDENT PERMEABILITY RADIAL CASES.....	23
4.1 Infinite Acting, Constant $q_g$ .....	23
4.2 Infinite Acting, Constant $p_{wf}$ .....	33
4.3 Finite Acting, Constant $q_g$ .....	42
4.4 Finite Acting, Constant $p_{wf}$ .....	48

CHAPTER	Page
V STRESS-DEPENDENT PERMEABILITY LINEAR CASES.....	53
5.1 Infinite Acting, Constant $q_g$ .....	53
5.2 Infinite Acting, Constant $p_{wf}$ .....	59
5.3 Finite Acting, Constant $q_g$ .....	64
5.4 Finite Acting, Constant $p_{wf}$ .....	69
VI ANALYSIS OF RESULTS.....	74
VII CONCLUSIONS.....	77
NOMENCLATURE.....	79
REFERENCES.....	81
APPENDIX A REAL GAS DIFFUSIVITY EQUATION.....	85
APPENDIX B REAL GAS DIFFUSIVITY EQUATION CONSIDERING PRESSURE DEPENDENT PERMEABILITY.....	87
APPENDIX C RADIAL AND LINEAR MODELS.....	89
APPENDIX D GASSIM DATA FILES.....	91
APPENDIX E ANALYTICAL SOLUTION FOR RADIAL DIFFUSIVITY EQUATION.....	95
APPENDIX F ANALYTICAL SOLUTION FOR LINEAR DIFFUSIVITY EQUATION.....	102
APPENDIX G MISCELLANEOUS.....	110
VITA.....	117



## LIST OF FIGURES

FIGURE	Page
2.1 Stress-dependent permeability.....	12
3.1 Permeability as a function of pore pressure and gamma.....	20
4.1 Semi-log plot, analytical and numerical match for infinite acting radial case, constant $q_g$ .....	24
4.2 Semi-log plot, effect of pressure-dependent permeability for an infinite acting radial reservoir producing at constant $q_g=10\text{Mscf/D}$ .....	25
4.3 Permeability ratio vs. gamma, radial case, constant $q_g=10\text{Mscf/D}$ .....	26
4.4 Skin factor vs. gamma, radial case, constant $q_g=10\text{Mscf/D}$ .....	27
4.5 Plot $m'(p)$ vs. $m(p)$ , radial case, constant $q_g=10\text{Mscf/D}$ .....	28
4.6 Semi-log plot, effect of pressure-dependent permeability for an infinite acting radial reservoir producing at constant $q_g=40\text{Mscf/D}$ .....	29
4.7 Permeability ratio vs. gamma, radial case, constant $q_g=40\text{Mscf/D}$ .....	30
4.8 Skin factor vs. gamma, radial case, constant $q_g=40\text{Mscf/D}$ .....	31
4.9 Plot $m'(p)$ vs. $m(p)$ , radial case, constant $q_g=40\text{Mscf/D}$ .....	32
4.10 Semi-log plot, analytical and numerical match for infinite acting radial case, constant $p_{wf}$ .....	34
4.11 Semi-log plot, effect of pressure-dependent permeability for an infinite acting radial reservoir producing at constant $p_{wf}=4000$ psi.....	35
4.12 Permeability ratio vs. gamma, radial case, constant $p_{wf}=4000$ psi .....	36
4.13 Skin factor vs. gamma, radial case, constant $p_{wf}=4000$ psi .....	37
4.14 Plot $m'(p)$ vs. $m(p)$ , radial case, constant $p_{wf}=4000$ psi .....	38
4.15 Semi-log plot, effect of pressure-dependent permeability for an infinite acting radial reservoir producing at constant $p_{wf}=2000$ psi.....	39
4.16 Permeability ratio vs. gamma, radial case, constant $p_{wf}=2000$ psi .....	40
4.17 Skin factor vs. gamma, radial case, constant $p_{wf}=2000$ psi .....	41
4.18 Plot $m'(p)$ vs. $m(p)$ , radial case, constant $p_{wf}=2000$ psi .....	41
4.19 Semi-log plot, analytical and numerical match for finite acting radial case constant $q_g$ .....	43

FIGURE	Page
4.20 Cartesian plot, effect of pressure-dependent permeability for a finite acting radial reservoir producing at constant $q_g=10\text{Mscf/D}$ .....	44
4.21 OGIP ratio vs. gamma, radial case, constant $q_g=10\text{Mscf/D}$ .....	45
4.22 Cartesian plot, effect of pressure-dependent permeability for a finite acting radial reservoir producing at constant $q_g=20\text{Mscf/D}$ .....	46
4.23 Time and normalized pseudo time for a finite acting radial reservoir producing at constant $q_g = 20 \text{ Mscf/D}$ , Case $\gamma= 0.0$ .....	47
4.24 OGIP ratio vs. gamma, radial case, constant $q_g=20\text{Mscf/D}$ .....	48
4.25 Cartesian plot, effect of pressure-dependent permeability for a finite acting radial reservoir producing at constant $p_{wf}=4000 \text{ psi}$ .....	49
4.26 OGIP ratio vs. gamma, radial case, constant $p_{wf}=4000 \text{ psi}$ .....	50
4.27 Cartesian plot, effect of pressure-dependent permeability for a finite acting radial reservoir producing at constant $p_{wf}=2000 \text{ psi}$ .....	51
4.28 OGIP ratio vs. gamma, radial case, constant $p_{wf}=2000 \text{ psi}$ .....	52
5.1 Log-log plot, analytical and numerical match for infinite acting linear case, constant $q_g$ .....	54
5.2 Square root of time plot, effect of pressure-dependent permeability for an infinite acting linear reservoir producing at constant $q_g=10\text{Mscf/D}$ .....	55
5.3 Permeability ratio vs. gamma, linear case, constant $q_g=10\text{Mscf/D}$ .....	56
5.4 Skin factor vs. gamma, linear case, constant $q_g=10\text{Mscf/D}$ .....	57
5.5 Plot $m'(p)$ vs. $m(p)$ , linear case, constant $q_g=10\text{Mscf/D}$ .....	58
5.6 Log-log plot, analytical and numerical match for infinite acting linear case, constant $p_{wf}$ .....	59
5.7 Square root of time plot, effect of pressure-dependent permeability for an infinite acting linear reservoir producing at constant $p_{wf}=8000 \text{ psi}$ .....	60
5.8 Permeability ratio vs. gamma, linear case, constant $p_{wf}=8000 \text{ psi}$ .....	61
5.9 Skin factor vs. gamma, linear case, constant $p_{wf}=8000 \text{ psi}$ .....	62
5.10 Plot $m'(p)$ vs. $m(p)$ , linear case, constant $p_{wf}=8000 \text{ psi}$ .....	63
5.11 Log-log plot, analytical and numerical match for finite acting linear case constant $q_g$ .....	64

FIGURE	Page
5.12 Cartesian plot, effect of pressure-dependent permeability for a finite acting linear reservoir producing at constant $q_g=10\text{Mscf/D}$ .....	65
5.13 Normalized pseudo time for $\gamma=0$ , linear case, constant $q_g=10\text{Mscf/D}$ .....	66
5.14 Normalized pseudo time for $\gamma=0.0003$ , linear case, constant $q_g=10\text{Mscf/D}$ ....	67
5.15 OGIP ratio vs. gamma, linear case, constant $q_g=10\text{Mscf/D}$ .....	68
5.16 Log-log plot, analytical and numerical match for finite acting linear case constant $p_{wf}$ .....	69
5.17 Cartesian plot, effect of pressure-dependent permeability for a finite acting linear reservoir producing at constant $p_{wf}=8000$ psi .....	70
5.18 Semilog plot, pressure-dependent permeability, linear case, constant $p_{wf} = 8000$ psi.....	71
5.19 Normalized pseudo time for $\gamma=0$ , linear case, constant $p_{wf}=8000$ psi .....	72
5.20 OGIP ratio vs. gamma, linear case, constant $p_{wf}=8000$ psi .....	73

## CHAPTER I

### INTRODUCTION

The present work attempts to do an investigation on stress-sensitive tight gas formations. People in the oil and gas industry some times do not consider pressure-dependent permeability in engineering calculations, it basically happens due to lack of lab data to determine level of dependency. This works evaluate the error introduced in calculations when constant permeability is considered in well test analysis of tight gas reservoirs.

We want to determine how accurate is our conventional pressure analysis calculations when the reservoir has a strong pressure-dependent permeability. The analysis considers the error in term of permeability and skin factor. Also include estimation on error calculating Original Gas in Place due to a false reservoir limit.

#### 1.1 Objectives

This work has the objective to investigate pressure and production performance on tight gas reservoirs considering stress-dependent permeability during transient and pseudo steady state flow. It makes focus in the physics of the rock that cause such behavior, the level of dependency, analytical and numerical modeling regarding radial and linear flow.

In reservoirs with a significant stress-dependent permeability, reservoir models should include stress-dependent permeability to improve accuracy for purposes of oil and gas reserve determination and reservoir modeling. The benefits include a better understanding of the behavior of tight gas sands, lead to a more accurate modeling of that kind of unconventional reservoirs and get a more realistic forecasting of production performance and well test analysis

---

This thesis follows the style and format of *SPE Journal*.

## 1.2 Problem Definition

Porous media are not rigid and non-deformable but exhibit elastic and inelastic deformations. Furthermore, the properties of rock and fluid are pressure-dependent. Tight gas reservoirs exhibit stress-sensitive permeability. For such reservoirs, pressure-transient analysis and forecast performance based on constant rock properties, especially permeability, can lead to significant errors in parameters estimation. Nevertheless, in most field cases, is not common to have stress-dependent permeability data. This project investigates the permeability change as a function of pressure in tight gas reservoirs in the case where laboratory data is not available.

## 1.3 Methodology

The methodology consists of using both analytical and numerical models of a stress-sensitive formation saturated with irreducible water saturation and gas. The model considers analytical and numerical solutions of transient and pseudo steady state (PSS) flow of gas through porous media for linear and radial geometries. The methodology includes both the conventional method, which assumed no pressure-dependent permeability, and a numerical method that incorporate a mathematical function to describe the dependency of permeability on pressure.

The analysis is based on the concept of a real gas pseudo pressure function,  $m(p)$ , defined by Al-Hussainy<sup>1</sup>. It incorporates variation of gas properties with pressure.

Analysis focuses on different levels of pressure draw down for a well located in the center of a homogeneous reservoir. Two different producing control modes for the producer well are considered; constant rate and constant bottom hole pressure.

## 1.4 Previous Work

Many authors have studied the effect of pressure-dependent permeability on reservoir performance. Following is a review of some of them.

Raghavan et al.<sup>2</sup> have treated reservoir porosity, permeability and compressibility, together with fluid density and viscosity as functions of pressure, they worked with a second-order, nonlinear, partial differential equation. The equation was reduced by a change of variables to a form similar to the diffusivity equation, but with a pressure-dependent diffusivity. They provided correlations in terms of dimensionless potential and time for a closed radial flow system producing at a constant rate; the solution obtained also has been compared with the conventional van Everdingen and Hurst solutions.

Vairogs and Rhoades<sup>3</sup> present the results of a theoretical investigation of the use of conventional pressure transient analysis methods in stress-sensitive formations. It was found that values of  $kh$  and wellbore conditions determined from conventional analysis of drawdown gas well test could be significantly in error when permeability is stress-dependent. In addition, skin factors determined from buildup test may not be representative. Because of permeability reduction near the wellbore, a positive skin factor will be determined even when the well is not damaged.

Samaniego et al.<sup>4</sup> applied the concept of a continuous succession of steady states to obtain a solution to the nonlinear partial differential equation describing the transient flow of a pressure-dependent fluid through a stress-sensitive formation. Samaniego presents a performance-prediction procedure based on the drainage radius concept and a material-balance equation. Results were obtained for five different sets of rock and fluid property data considering radial and linear bounded systems.

Gochmour and Slater<sup>5</sup> describe the use of a single well gas simulation model to characterize the properties of gas wells in tight reservoirs. It demonstrates the effective application of a simulation model to complement a conventional well test analysis. The single well gas model was used to characterize the reservoir by history matching the well test data; after a suitable match was obtained, the model was then used to predict the deliverability of the well.

Walls<sup>6</sup> investigate the effects of pressure, partial saturation and salinity on permeability in several cores from the Spirit River tight gas sand of western Alberta and Cotton Valley formation of east Texas. Samples from both locations showed strong dependence of permeability on effective pressure and degree of water saturation. It was also found that pore structure seems to be the major factor in determining permeability behavior and clay content being of secondary importance.

Pedrosa<sup>7</sup> presents a mathematical model that take in account the reduction in permeability caused by an increase in effective stress. A perturbation technique is applied to determine approximate analytical solutions for transient flow in an infinite radial system with constant rate inner boundary. The model includes a new parameter, the permeability modulus, which measures the permeability dependency on pressure. The solution of the model leads to the construction of type curves that can be applied to drawdown and buildup analysis of well test data from stress-sensitive reservoirs.

In a similar way, Ostensen<sup>8</sup> presents a study of the effect of stress-dependent permeability on gas production and well testing in tight gas sands by using a modified pseudo-pressure that include stress dependence.

Samaniego and Cinco-Ley<sup>9</sup> present a practical procedure to determine the pressure-dependent characteristics of a reservoir from transient pressure analysis. Expressions are derived for flow in stress sensitive formations of pressure-dependent liquid flow and of

real gas flow, which allow through the analysis of draw down and buildup tests the determination of the stress sensitive characteristics of the reservoir. The authors concluded that draw down and buildup results are complementary. The draw down analysis yields good estimates of the pressure-dependent parameter  $\{k(p)/[1-\phi(p)]\}$  at low values of pressure and the buildup analysis yield good estimates at high values of pressure.

Kikani and Pedrosa<sup>10</sup> analyzed and discussed the nonlinear equation that result by taking into account the effect of pressure-dependent rock properties. By defining a permeability modulus, the nonlinearities associated with the governing equation become weaker and an analytical solution in terms of a regular perturbation series can be obtained for a radial, infinite acting reservoir. The work presented uses a regular perturbation technique to solve the nonlinear equation to third order of accuracy. Also investigated are the first order effects of wellbore storage, skin, and boundary effects.

Zhang and Ambastha<sup>11</sup> consider the numerical pressure-transient solutions for stress-sensitive reservoirs using the one-parameter model and the stepwise permeability model. The authors analyzed the effects of permeability modulus, wellbore storage, skin, outer boundary condition, and permeability models on both drawdown and buildup test. The stepwise permeability model may provide a means to infer permeability versus stress curves under in-situ reservoir conditions by a proper analysis of a long duration pressure transient test for a stress-sensitive reservoir.

Jelmert and Selseng<sup>12</sup> proposed a skin factor calculation that takes in account changes in permeability. The concept is consistent with steady state flow in a stress-sensitive reservoir.

Davies and Davies<sup>13</sup> considered stress-dependent permeability in unconsolidated, high porosity sand reservoirs and consolidated reservoirs (tight gas sands). The authors focus



on i) fundamental controls on stress-dependent permeability, ii) rock-based log modeling of stress-dependent permeability in cored and non-cored wells and iii) implications for production based on data from reservoir simulation. The practical, fast and cost efficient methodology improves and enhances the productivity and management of stress-dependent reservoirs.

## CHAPTER II

### LITERATURE REVIEW

#### 2.1 Tight Gas Sands<sup>6,14</sup>

Tight gas reservoirs are characterized by having poor rock properties. Those reservoirs typically have low porosity and permeability. Tight gas reservoirs have been considered as gas storage rock with low quality. A tight gas reservoir is generally recognized as any low permeability formation which special well completion technique are required to stimulate production. Typical values of porosity are lower than 10% and permeability is usually below 0.1 md.

There are some fundamental differences in rock-water-gas interactions between tight sandstones and ‘normal’ gas reservoirs. These differences result primarily from significant pore structure alterations as the rock undergoes compaction and diagenesis.

As gas production begins from the reservoir, pore pressure decreases and the effective stress increases; the relation between these variables is shown in the following equation:

$$S = \sigma + \alpha p \dots\dots\dots (2.1)$$

$S$  corresponds to total stress,  $\sigma$  is the effective stress (matrix stress, grain to grain pressure) and  $p$  is the fluid pressure. Eq. 2.1 states that every change in the pore-fluid pressure under otherwise constant conditions, result automatically in a change of the effective stress. Rock permeability in tight sands is significantly affected by changing the effective stress.

The behavior of tight gas sand permeability in response to changing effective stress can be explained qualitatively by the complex and tortuous pore structure that results from extensive compaction and diagenesis. Thin section and scanning electron microscope (SEM) images of the pore structure reveal very narrow slit-like apertures between pores. These thin cracks provide the major connectivity, which allows fluid to move when the rock is under low effective pressure conditions. However, increasing effective pressure easily closes such flats cracks.

## 2.2 Diffusivity Equation, Liquid Case<sup>15</sup>

The derivation of the diffusivity equation combines the law of conservation of mass, Darcy's law and equations of state for the isothermal flow of fluids in porous media. Several assumptions about the well and reservoir are introduced in the model. A summary of these assumptions are: homogeneous and isotropic porous medium of uniform thickness, pressure independent fluid and rock properties, small pressure gradients, radial flow, applicability of Darcy's' law (laminar flow), and negligible gravity forces. These assumptions lead to the following general partial differential equation:

$$\frac{\partial^2 p}{\partial r^2} + \frac{1}{r} \frac{\partial p}{\partial r} = \frac{\phi \mu c}{0.00633 k} \frac{\partial p}{\partial t} \dots\dots\dots (2.2)$$

The general solution of Eq. 2.2 considering liquid flow through a reservoir with a radial geometry is as follows:

$$p_D = \frac{1}{2} \ln(t_D) + 0.4045 + s \dots\dots\dots (2.3)$$

### 2.3 Diffusivity Equation, Gas Case

In the derivation of the diffusivity equation for real gas reservoirs, Al-Hussainy<sup>1</sup> defined in 1966 a pseudo function that account for gas properties variation with pressure as:

$$m(p) = 2 \int_{p_o}^p \frac{p}{z\mu} dp \dots\dots\dots(2.4)$$

Al-Hussainy introduces the real gas pseudo pressure function to transform the diffusivity equation for real gases. It takes in account the change with pressure of gas properties such as z-factor and viscosity. The variable  $m(p)$  has dimension of pressure squared per centipoises. Substitution of the real gas pseudo pressure has several important consequences<sup>1</sup>. First, second degree pressure gradient terms, which have commonly been neglected under the assumption that the pressure gradient is small everywhere in the flow system, are rigorously handled. Omission of second-degree terms leads to serious errors in estimated pressure distribution for tight formations. Second, flow equations in terms of the real gas pseudo pressure do not contain viscosity or gas law deviation factors, and thus avoid the need for selection of an average pressure to evaluate physical properties. Third, the real gas pseudo pressure can be determined by numerically in terms of pseudo reduced pressures and temperatures from existing physical property correlations.

The diffusivity equation for real gas can be expressed as:

$$\nabla \bullet k \frac{p}{z\mu} \nabla p = \frac{\partial}{\partial t} \left( \phi \frac{p}{z} \right) \dots\dots\dots(2.5)$$

Including pseudo pressure concept into Eq. 2.5 it can be transformed to:

$$\nabla^2 m = \frac{\phi \mu c_t}{k} \frac{\partial m}{\partial t} \dots\dots\dots(2.6)$$

Further detail on the derivation of Eq. 2.6 is found in Appendix A. The solution of Eq. 2.6 considering gas reservoir with radial geometry in terms of pseudo pressure is as follow:

$$m_D = \frac{1}{2} \ln(t_D) + 0.4045 + s \dots\dots\dots(2.7)$$

In 1967, Wattenbarger<sup>16</sup> showed that semi log straight lines (SLSL) of plot  $m_D$  vs  $t_D$  give correct reservoir properties for different constant gas rate cases. Wattenbarger established that the  $m(p)$  linearization is extremely good for the basic case of constant sand face flow rate, at rates that are likely to be found in practice. This verifies the results of Al-Hussainy et al.<sup>1</sup> for production cases. Furthermore, this means that the flow capacity  $kh$  of a gas well can be determined accurately from a draw down plot.

Agarwal<sup>17</sup>, working with build up well data, showed that Eq. 2.7 gave wrong values of permeability for cases with different gas rates. Then, Agarwal introduced a plotting function that account for properties changes with time and that lead to get better values of permeability. The plotting function was defined as:

$$t_a = \int_{t_o}^t \frac{1}{\mu c_t} dt \dots\dots\dots(2.8)$$

However, Eq. 2.8 defined by Agarwal does not linearize the diffusivity equation. It means, Eq. 2.8 is a partial integral, fluid viscosity and compressibility varies with time and pressure. Agarwal demonstrated that better values of permeability were obtained using that plotting function.

## 2.4 Stress-Dependent Formations

As early as 1928 it was recognized that porous media are not always rigid and non-deformable<sup>4</sup>. This problem is usually handled by means of properly chosen ‘average properties’. This method only reduces the errors involved and generally does not eliminate these errors. A second order, nonlinear, partial differential equation results when variation of permeability with pressure is considered in the continuity equation. A different kind of flow-reducing mechanism has been studied experimentally by a number of investigators<sup>3, 18</sup>. This mechanism is the reduction in permeability caused by an increase in effective frame stress. In the reservoir an increase in effective frame stress is caused by fluid withdrawal and the accompanying decrease in pore pressure. Since the overburden force on the reservoir rock remains the same, the decreasing pore pressure results in an increased effective frame stress. Because low permeability formations are more affected by stress changes<sup>3</sup>, this effect can be expected to be more significant in deep gas reservoirs.

### 2.4.1 Laboratory Experiments

The rate of permeability decline with increasing net effective stress is different for each rock type and is controlled by three interrelated, pore geometrical parameters, length, and shape and short axis dimension of the throats<sup>13, 19</sup>. Others important parameters are clay content, pore volume compressibility and authigenic cementation. The mechanisms of permeability reduction are much more pronounced in tight formations<sup>3</sup>. It can be expected that formations with pore distribution of smaller radio are very sensitive to compressive stress.

In September 1971, Vairogs et al.<sup>3</sup>, presented a work based on lab experiments showing the relation of rock permeability and net confining pressure for cores with different initial permeability. These results are shown in **Fig. 2.1**. In this plot, ‘y’ axes correspond

with the ratio of permeability to a given confining pressure to the permeability at a confining pressure of 500 psig. 'x' axes is net confining pressure. Vairogs et al. concluded that there is a greater degree of permeability reduction with low permeability cores than with high permeability cores. In cores with initial permeability less than 1 md, the permeability is significantly reduced at high net confining pressure. This behavior is extended to tight gas formations, which exhibit permeability lower than 0.1 md. Usually this dynamic permeability is not considered in engineering calculations. The current project evaluates the error introduced in calculations when constant permeability is considered in well test analysis of tight gas reservoir.

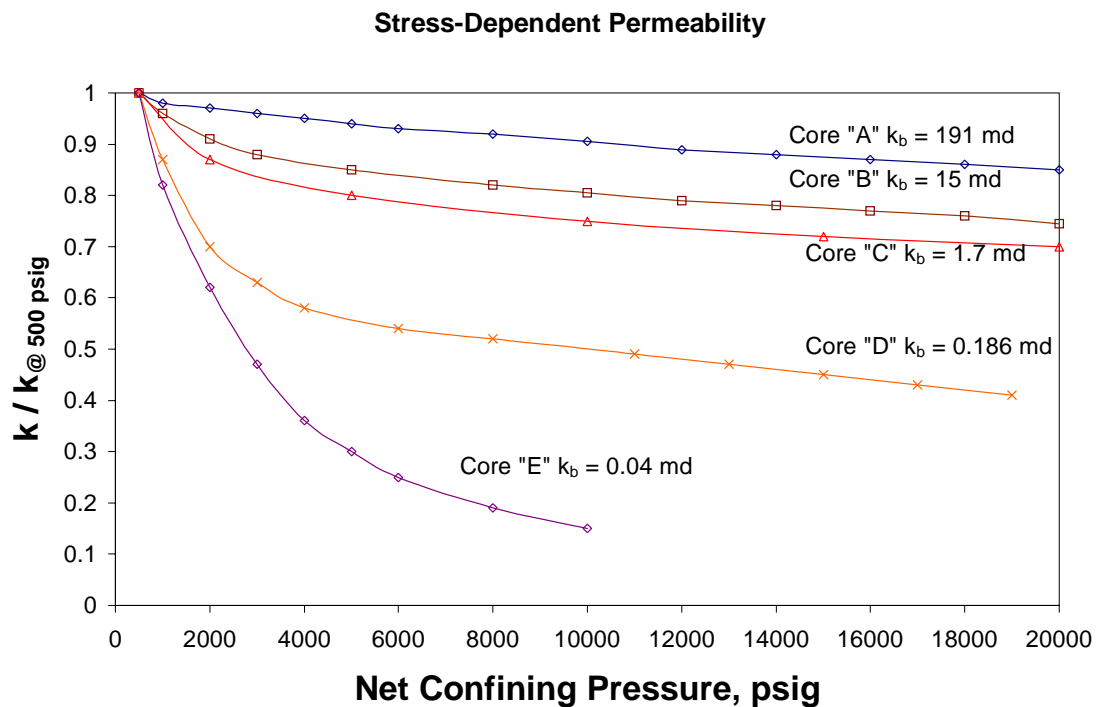


Fig. 2.1 – Stress-dependent permeability.

The plot shows an exponential dependence of permeability with pore pressure. A reduction in the pore pressure in tight gas formations leads to increase the effective rock stresses. This increasing is counterbalanced by the reduction in pore diameter, which

results in increased resistance to fluid flow and reduced fluid storage, lower rock permeability and porosity.

#### 2.4.2 Permeability Modulus

The dependence of permeability on pore pressure makes the flow equation strongly nonlinear<sup>4</sup>. To study fluid flow through stress-dependent porous media, a new parameter, permeability modulus or ‘ $\gamma$ ’, is defined by Nur *et al.*<sup>20</sup> and studied by Pedrosa and Kikani *et al.*<sup>10</sup> as follows:

$$\gamma = \frac{1}{k} \frac{\partial k}{\partial p} \dots\dots\dots (2.9)$$

This parameter plays a very important role in systems where changes in effective stress affect permeability. Basically, it measures the dependence of hydraulic permeability on pore pressure. For practical purposes, the permeability modulus is assumed constant. Thus, permeability varies exponentially with pore pressure.

$$k = k_i e^{-\gamma(p_i - p)} \dots\dots\dots (2.10)$$

In view of the similar appearance of permeability and density in the diffusion equation, it may be advantageous to assume an exponential relationship between permeability and pressure. This choice has some experimental support and mathematical convenience shown by Kikani and Pedrosa<sup>10</sup>. These authors were able to match an exponential rock model to real pressure data. Using the permeability modulus definition, the real gas pseudo pressure function can be modified to:

$$m'(p) = 2 \int_{p_o}^p \frac{p k(p)}{z \mu} dp \dots\dots\dots (2.11)$$



Now, the diffusivity equation considering flow of a real gas through a stress sensitive formation can be expressed as follow:

$$\nabla^2 m' = \frac{\phi \mu c_t}{k(p)} \frac{\partial m'}{\partial t} \dots\dots\dots(2.12)$$

Further detail on the derivation of Eq. 2.12 is found in Appendix B. Pedrosa<sup>7</sup> applied a perturbation technique to determine approximate analytical solutions for transient flow in an infinite radial system with constant rate inner boundary. The model includes the permeability modulus parameter, which measures the permeability dependency on pressure. The analytical solution presented by Pedrosa for constant gas rate infinite acting radial flow is:

$$m'_D = \frac{1}{2} \ln(t_D) + 0.4045 + s \dots\dots\dots(2.13)$$

## 2.5 Linear Flow<sup>21,22</sup>

Linear flow is a regime characterized by parallel flow lines in the reservoir. This results from flow to a fracture or a long horizontal well, or from flow in an elongated reservoir, such as a fluvial channel, or as a formation bounded by parallel faults. Linear flow is recognized as a +1/2 slope in the pressure derivative on the log-log diagnostic plot. Its presence enables determination of the fracture half-length or the channel or reservoir width, if permeability can be determined independently.

## 2.6 Radial Flow<sup>15,23</sup>

Radial flow represents the geometry that approximates fluid flow into a wellbore from a cylindrical reservoir of constant pay thickness. Flow lines converge to a concentric point located at the middle of the reservoir and is represented by the wellbore. The important

parameters that defined the radial flow geometry are: wellbore radius ( $r_w$ ), external radius ( $r_e$ ), thickness ( $h$ ).

## 2.7 Transient Flow<sup>15</sup>

This condition is only applicable for a relatively short period after some pressure disturbance has been created in the reservoir. In terms of the radial flow model this disturbance would be typically caused by altering the well's production rate at  $r = r_w$ . In the time for which the transient condition is applicable it is assumed that the pressure response in the reservoir is not affected by the presence of the outer boundary, thus the reservoir appears infinite in extent. In this period, the change of pressure with time in the reservoir is a function of location and time, thus

$$\frac{\partial p}{\partial t} = f(r, t) \dots \dots \dots (2.14)$$

## 2.8 Gas Simulator

During the development of this project, the computer-based program *GASSIM* was widely used. *GASSIM* is a single-phase simulator presented by Lee and Wattenbarger<sup>23</sup>. It is used in this work for simulating real gas flow for 2-D radial and linear models. It is a two-dimensional reservoir simulator that can work with  $x$ - $y$  or  $r$ - $z$  geometries. Originally this program was written in FORTRAN. This simulator has been modified and it is under development. Currently the code of the program is based in visual basic form (Visual Basic for Applications, VBA) and is run from Microsoft Excel program. The program has two main advantages that are the reasons of being selected during this project, the program's code can be modified and allow to introduce the changes necessities to account for stress sensitive formations. In addition, the program is time-

efficient and runs take few minutes. It is also friendly and well known by faculty in T A&M University.

## 2.9 Determination of OGIP<sup>24</sup>

This section deals with the determination of original gas in place (*OGIP*) for wells in pseudo steady state flow. The calculation of *OGIP* is based on analysis of gas well production performance. In this project is used the normalized pseudo time concept as a plotting function to calculate more accurate the *OGIP*. The use of this normalized pseudo time is particularly important in the analysis of highly depleted reservoirs with high compressibility where the superposition errors are largest.

The normalized pseudo time provides a plotting function for smoothing the production data by taking the effect of reservoir properties change with average pressure. The normalized pseudo time equation is given by the following expression:

$$t_n = (\phi \mu c_t)_i \int_0^t \frac{1}{\phi(\bar{p}) \mu(\bar{p}) c_t(\bar{p})} dt \dots\dots\dots (2.17)$$

This integration can be calculated by using Trapezoidal rule.

A plot of  $\frac{[m(p_i) - m(p_{wf})]}{q_g}$  vs.  $t_n$  for simulation results gives straight line. The slope from  $t_n$  plot, denoted  $\tilde{m}_{PSS}$ , is then used to calculate *OGIP* applying the following equations:

Constant  $q_g$  Case: 
$$OGIP = \frac{2 p_i S_{gi}}{z_i (\mu_g c_t)_i} \left( \frac{1}{\tilde{m}_{PSS}} \right) \dots\dots\dots (2.18)$$

Constant  $p_{wf}$  Case: 
$$OGIP = 0.5538 \frac{A_c k p_i S_{gi}}{T z_i (\mu_g c_t)_i L} \left( \frac{1}{\tilde{m}_{PSS}} \right) \dots\dots\dots (2.19)$$

The most important feature about normalized pseudo time is that it improves the accuracy of calculating  $OGIP$  because it takes into account the effect of properties change with average reservoir pressure.

CHAPTER III  
PSEUDO PROPERTIES

This project is based on the concept of real gas pseudo pressure  $m(p)$ . It was initially defined by Al-Hussainy<sup>1</sup> in 1966 as:

$$m(p) = 2 \int_{p_o}^p \frac{p}{z\mu} dp \dots\dots\dots(3.1)$$

Al-Hussainy introduces the real gas pseudo pressure function to transform the diffusivity equation for real gases. It takes in account the change with pressure of gas properties such as z-factor and viscosity. The variable  $m(p)$  has dimensions of pressure squared per centipoises.

The main objective of this project is to analyze stress sensitive formations, particularly tight gas reservoirs for radial and linear reservoir geometry. We want to determine the effect of pressure-dependent permeability  $k(p)$  on radial and linear flow analysis for infinite and finite acting, also investigate how it modify well test analysis results.

Methodology consists of simulation of tight gas well production with  $k(p)$  included. Then, analyze results as though  $k(p)$  effects were ignored and finally, observe errors in determining permeability ( $k$ ) and skin factor ( $s$ ).

The current method used to analyze gas well production is based in the solution of diffusivity equation with constant diffusivity term. The gas diffusivity equation in terms of  $m(p)$  is:

$$\nabla^2 m = \frac{\phi\mu c_t}{k} \frac{\partial m}{\partial t} \dots\dots\dots(3.2)$$

In Eq. 3.2, permeability is a constant parameter. In this case a plot of  $m(p)$  versus  $\log(t)$  is necessary to analyze the data. Then, from semi-log straight line is calculated the value of permeability and skin factor.

Now, we consider the case including pressure-dependent permeability  $k(p)$ . A new definition of pseudo pressure is introduced to incorporate pressure dependency of permeability; it is shown in Eq. 3.3:

$$m'(p) = 2 \int_{p_o}^p \frac{k(p) p}{z \mu} dp \dots\dots\dots(3.3)$$

Then, the diffusivity equation expressed in term of  $m'(p)$  corresponds with the following expression:

$$\nabla^2 m' = \frac{\phi \mu c_t}{k} \frac{\partial m'}{\partial t} \dots\dots\dots(3.4)$$

In this case, we analyze the gas well production data by plotting  $m'(p)$  versus  $\log(t)$ . The slope of semi-log straight line is related to the permeability and skin factor.

This project uses the concept of permeability modulus, introduced by Kikani and Pedrosa<sup>10</sup>. The permeability modulus,  $\gamma$ , called ‘gamma’ express an exponential relation between permeability and pressure. The mathematical function is:

$$\gamma = \frac{1}{k} \frac{dk}{dp} \dots\dots\dots(3.5)$$

Making a basic transformation of Eq. 3.5 lead to the following expression:

$$k = k_i e^{-\gamma(p_i - p)} \dots\dots\dots(3.6)$$

The use of permeability modulus is shown in **Fig. 3.1**.

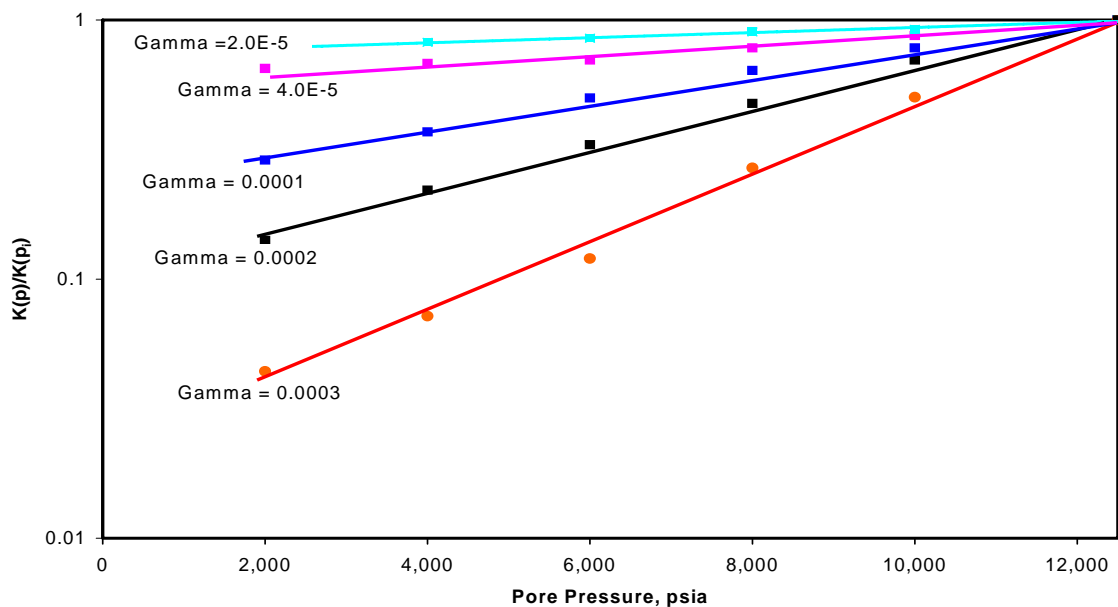


Fig. 3.1 – Permeability as a function of pore pressure and gamma.

Fig. 3.1 is a plot of permeability ratio versus pore pressure for different values of gamma corresponding with a stress-sensitive formation at an initial pore pressure of 12,600 psia. Permeability ratio is the permeability calculated as a function of pressure divided by the initial permeability. From the plot we can observe that as the reservoir is depleted the pore pressure decrease and permeability is significantly reduced. Another important observation is that as gamma increases the permeability reduction is higher.

The methodology used in the current project can be summarized for radial and linear modeling as follows.

#### Radial Infinite Acting Model

1. Simulate cases with  $k(p)$
2. Plot  $m(p)$ , not  $m'(p)$ , vs.  $\log t$
3. Find slope of semi-log straight line,  $m$
4. Calculate  $k$  and  $s$
5. Compare these with correct values

#### Radial Finite Acting Model

1. Simulate cases with  $k(p)$
2. Plot  $m(p)$ , not  $m'(p)$ , vs.  $t$
3. Find slope of straight line,  $\tilde{m}_{PSS}$
4. Calculate  $V_p$  and OGIP
5. Compare these with correct values

#### Linear Infinite Acting Model

1. Simulate cases with  $k(p)$
2. Plot  $m(p)$ , not  $m'(p)$ , vs.  $\sqrt{t}$
3. Find slope of straight line,  $m$
4. Calculate  $k$  and  $s$
5. Compare these with correct values



### Linear Finite Acting Model

1. Simulate cases with  $k(p)$
2. Plot  $m(p)$ , not  $m'(p)$ , vs.  $t$
3. Find slope of straight line,  $\tilde{m}_{PSS}$
4. Calculate  $V_p$  and OGIP
5. Compare these with correct values

Data used for each model, radial and linear, is described in Appendix C. In addition, in Appendix D have been included the data files used in GASSIM simulator for each case.

## CHAPTER IV

## STRESS-DEPENDENT PERMEABILITY RADIAL CASES

This chapter includes results and discussion of analytical and numerical simulation of stress-dependent permeability considering a reservoir with radial geometry. The analysis is presented for transient flow and pseudo-steady state flow, as well as constant gas rate and constant bottom hole pressure cases. Data files used in simulation runs are included in Appendix D. In addition, derivation of equations used to calculate permeability and skin factor as well as reservoir pore volume and OGIP are described in Appendix E.

- 4.1 Infinite Acting, Constant  $q_g$
- 4.1.1 Case 1:  $q_g = 10$  Mscf/D

This section starts presenting the numerical results from GASSIM simulator for the case with gas rate 10 Mscf/D. The important point is to analyze the portion of the curve that correspond with infinite acting or transient flow, to calculate permeability and skin factor from the slope of each curve that correspond with different values of gamma,  $\gamma$ . The analysis is made in terms of pseudo-pressure  $m(p)$ ; semi log plot of  $m(p)$  versus time indicate a straight line with a slope that is related directly to the value of permeability. **Fig. 4.1** show results of analytical and numerical simulation for  $\gamma = 0$ , that means; no stress dependent permeability is considered.

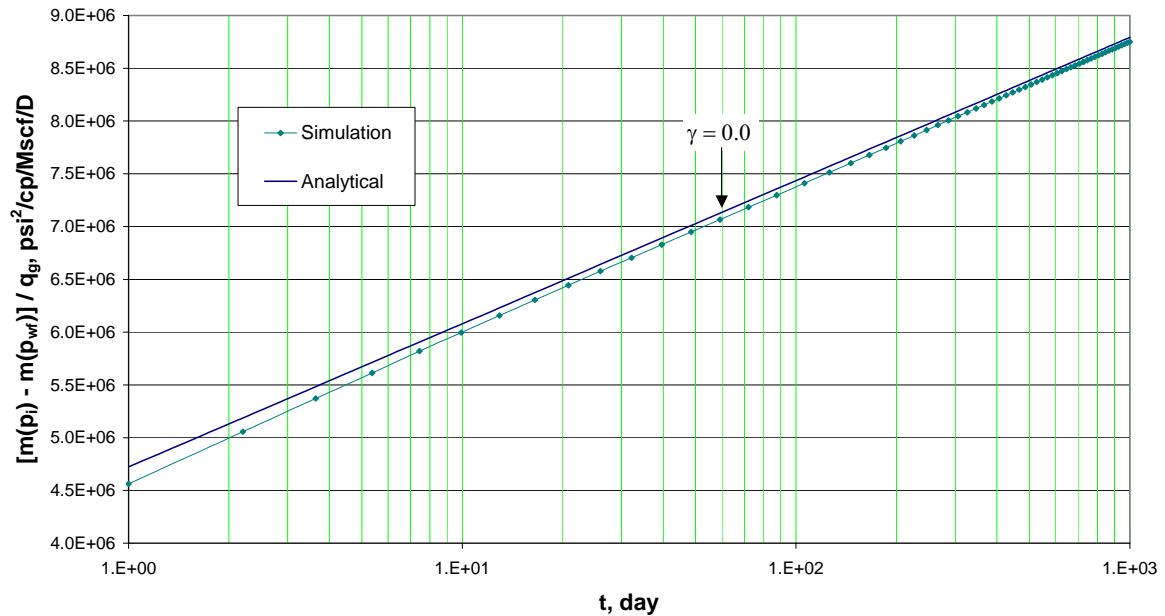


Fig. 4.1 – Semi-log plot, analytical and numerical match for infinite acting radial case, constant  $q_g$ .

Fig. 4.1 indicates a satisfactory match between analytical solution and numerical simulation regarding a radial model, constant gas rate and non-stress dependent permeability. In the plot is visible a small separation for early time, between 1 and 10 days due to numerical error. The numerical error can be minimized reducing the grid dimensions and time steps in the simulator. This results validate the simulation model for  $\gamma = 0$ .

To investigate the effect of stress-dependent permeability on the reservoir response, scenarios with different values of gamma ( $\gamma$ ) are considered. As the value of gamma increase, means that exists a stronger dependency of permeability on pressure. **Fig. 4.2** presents results in terms of pseudo pressure for a radial reservoir in transient flow.

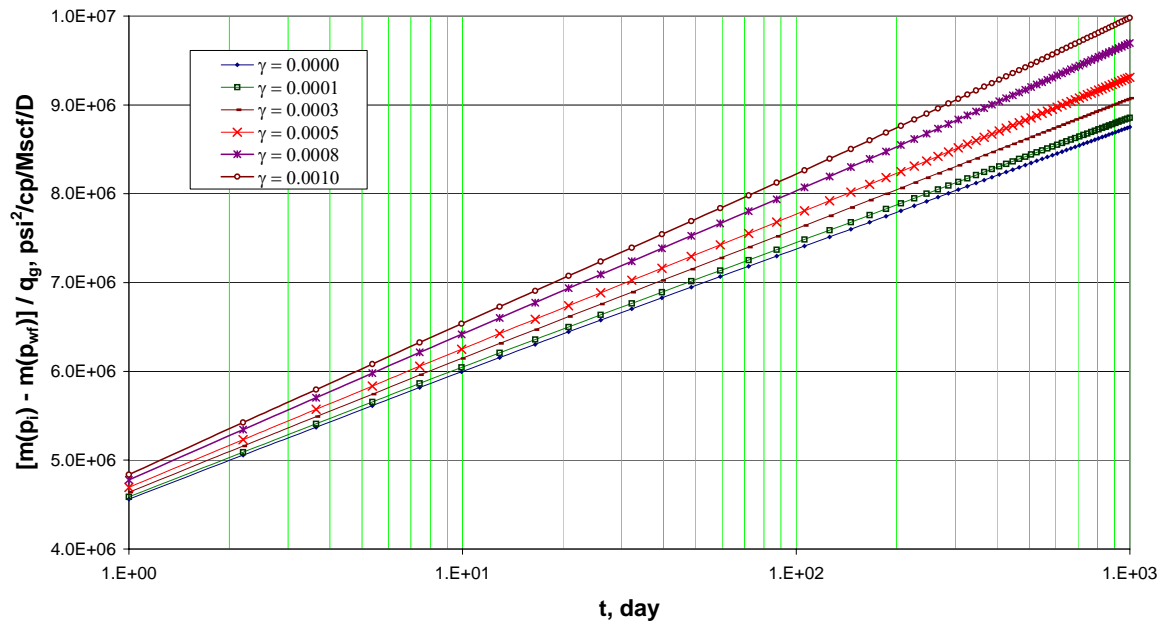


Fig. 4.2 – Semi-log plot, effect of pressure-dependent permeability for an infinite acting radial reservoir producing at constant  $q_g = 10$  Mscf/D.

Observing Fig. 4.2, we can see that for each value of gamma ( $\gamma$ ) considered, a semi log straight line (SLSL) is obtained. Each SLSL has a different slope, which is directly related to permeability and skin using the analytical solution. As expected, the permeability ( $k$ ) and skin factor ( $s$ ) calculated from the slope of the curve gamma zero ( $\gamma=0$ ) is the original reservoir permeability and zero skin. In other words; for  $\gamma=0$ ,  $k_{calc} = 0.0025$  md and  $s = 0$ . As the value of gamma increase, the slope obtained is higher; it is due to the permeability reduction in the reservoir as it is being depleted at constant gas rate. These results make sense and agree with Darcy's law; keeping the gas rate constant, whatever reduction in reservoir permeability during depletion time lead to a higher pressure drop, that explain the higher value of each slope as gamma increase. It is important to point out that for this particular case of  $q_g = 10$  Mscf/D, semi log plot indicate a straight line for each value of gamma, later on in this chapter, a case with a higher constant gas rate is also discussed.

Now, the discussion is moved to the permeability calculations. Permeability is calculated from the slope of each curve in Fig. 4.2 using the analytical solution equation. The initial reservoir permeability used in the GASSIM simulator was 0.0025 md. **Fig. 4.3** shows the results of calculations.

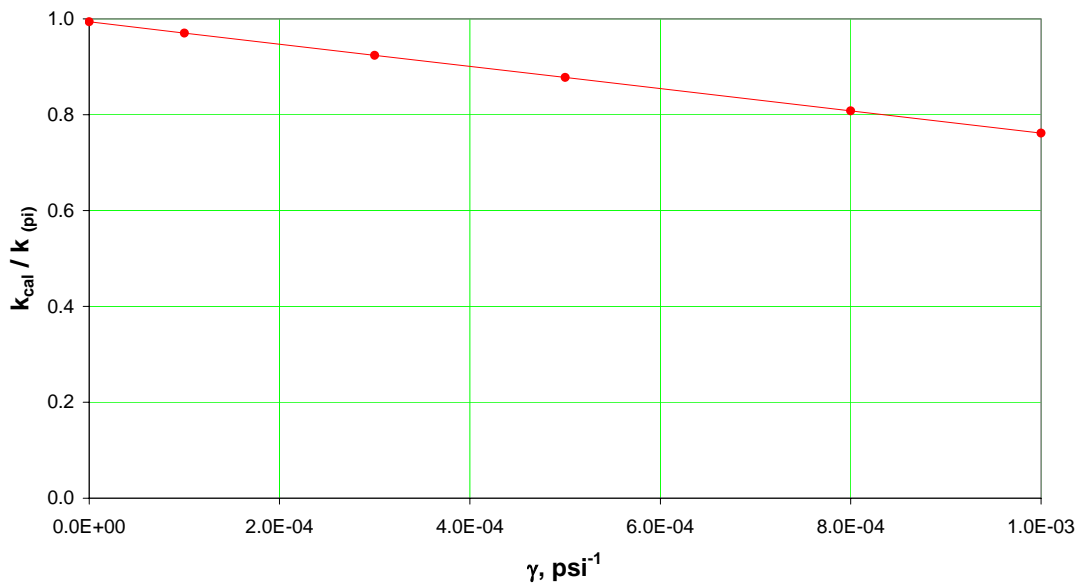


Fig. 4.3 – Permeability ratio vs. gamma, radial case, constant  $q_g = 10$  Mscf/D.

Fig. 4.3 is a plot of permeability reduction versus gamma. Permeability ratio is the permeability calculated in each run divided by the initial permeability ( $k=0.0025$  md). From that plot we can notice that the higher the value of gamma the higher is the permeability reduction in the reservoir, a 24% permeability reduction occur for  $\gamma=0.001$ . In addition, as a conclusion for this particular case, where  $q_g=10$  Mscf/D, a linear relation is obtained between permeability ratio and gamma.

The same analysis can be drawn for skin factor calculations. It is used the definition of skin factor to investigate the magnitude of permeability reduction in the reservoir in

terms of pore pressure. That means, the additional pressure drop necessary in the reservoir to maintain a gas rate constant meanwhile the permeability is reduced due to reservoir depletion. Skin factor is calculated from Fig. 4.2 at intersect of each curve with 'y' axe. **Fig. 4.4** shows the results.

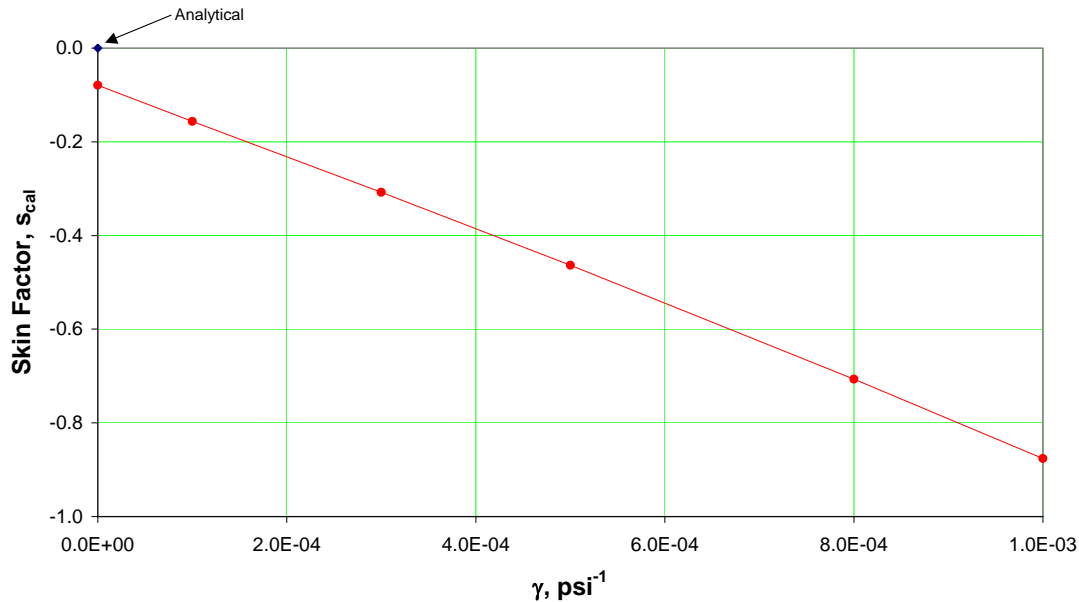


Fig. 4.4 – Skin factor vs. gamma, radial case, constant  $q_g = 10$  Mscf/D.

Fig. 4.4 corresponds with a plot of skin factor versus gamma. The analytical solution imply a non-skin case,  $s=0$ . For the range of gamma considered in this case, skin vary between -0.079 and -0.876. The fact that from numerical simulation we do not get a skin  $s=0$  for gamma  $\gamma=0$ , is explained as numerical error in the simulation runs. In addition, for this particular run, is obtained a straight-line relation between skin factor and gamma.

Analyzing the results for this particular scenario, is concluded that a linear response is obtained for  $[m(p_i)-m(p_{wf})]/q_g$  vs. time for all gamma. Now, it is important to investigate the range of pressure drop originated by the production at constant gas rate of 10 Mscf/D. Comparison is made in terms of  $m(p)$  and  $m'(p)$ . The term  $m(p)$  correspond to

the pseudo pressure defined originally by Al-Hussany<sup>1</sup>. The term  $m'(p)$  is the pseudo pressure including the stress-dependent permeability function. **Fig. 4.5** shows the results.

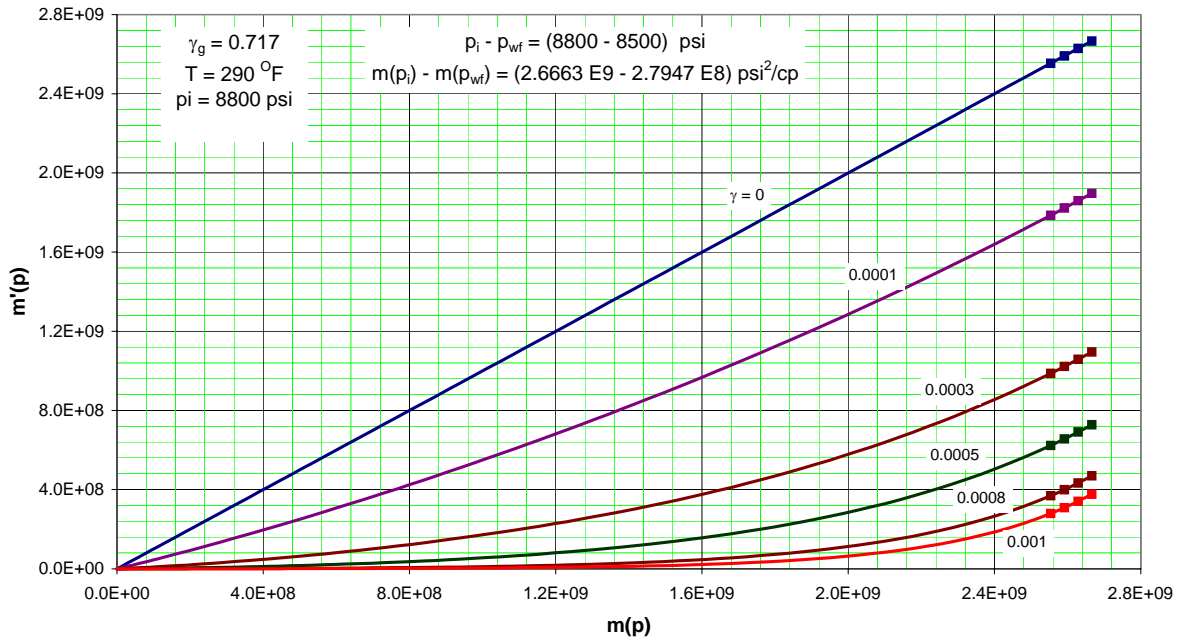


Fig. 4.5 – Plot  $m'(p)$  vs.  $m(p)$ , radial case, constant  $q_g = 10$  Mscf/D.

In Fig. 4.5 the plot correspond with  $m'(p)$  versus  $m(p)$ . Gas properties were calculated using a reservoir temperature of 290 °F, gas specific gravity of 0.717 and initial pressure of 8,800 psi. Each curve corresponds with a different value of gamma. The line in the top represents a non-stress sensitive scenario,  $\gamma = 0$ , for this case a straight line is obtained. As gamma start to increase from 0 to 0.001, the curves start to bend downward, and the relation is not longer linear. The maximum pressure drop ( $p_i - p_{wf}$ ) occurred for the case with  $\gamma = 0.001$  and it was 300 psi ( $p_i = 8,800$  psi;  $p_{wf} = 8,500$  psi). The squared dots localized at the end of each line indicate the range of pressure studied in this case ( $q_g = 10$  Mscf/D). It is noticeable that the squared dots are localized in a region over the continuous line where still exist a linear relation between  $m(p)$  and  $m'(p)$ , that explain the results analyzed in this case, where a linear response is obtained for  $[m(p_i) -$

$m(p_{wf})/q_g$  vs. time for all gamma. Further details about pseudo pressure and effect of non-linear term  $\phi \mu c_t$  on permeability and skin factor calculations for Case 1 are given in Appendix G.

#### 4.1.2 Case 2: $q_g = 40$ Mscf/D

In order to compare results with case 1, it is also considered a different scenario with a higher gas rate, fluid and reservoir properties are the same, and the only change is the constant gas rate that is set up to 40 Mscf/D. Running this case is desirable to validate results obtained in case 1 and try to get a correlation between permeability, skin and gamma. Similar to case 1, the range of gamma values is from 0 to 0.001. Results of case 2 are shown in **Fig. 4.6**.

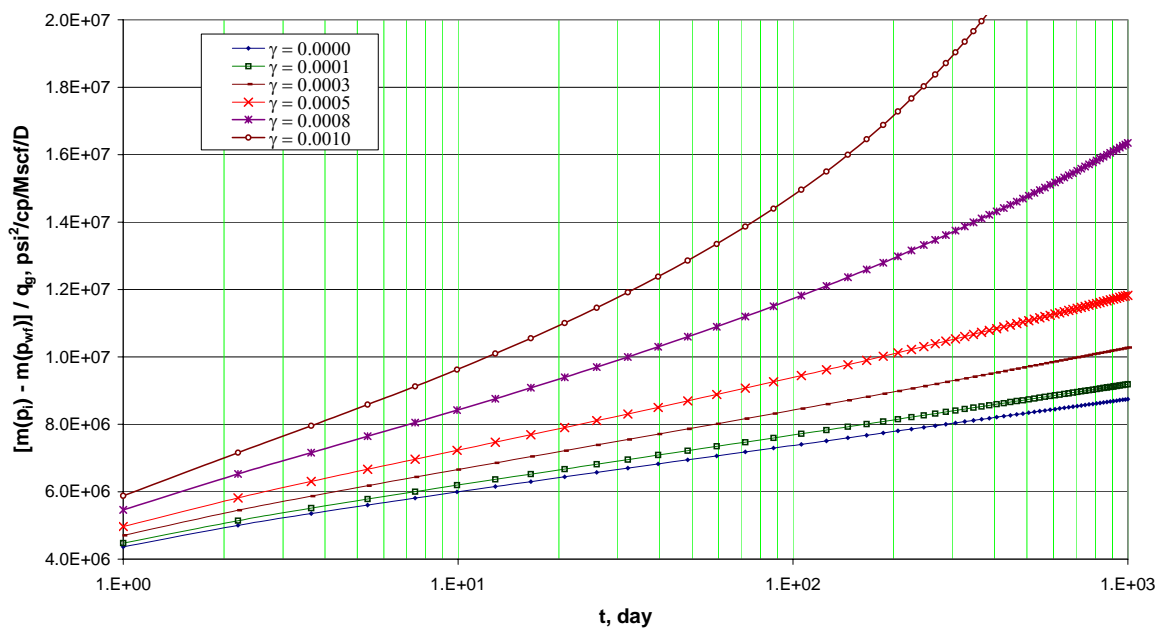


Fig. 4.6 – Semi-log plot, effect of pressure-dependent permeability for an infinite acting radial reservoir producing at constant  $q_g = 40$  Mscf/D.



Fig. 4.6 is a plot of  $[m(p_i)-m(p_{wf})]/q_g$  vs. time considering gas rate of 40 Mscf/D. The figure shows that for low values of gamma (between 0 and 0.005) there is a straight line from the semi log plot. For larger values of gamma the curves start to tilt upward indicating that no longer exist a linear relation. That behavior is caused by a significant reduction on permeability as the reservoir is depleted at constant rate. All the curves correspond with a transient flow period, however, the curves corresponding to  $\gamma=0.0008$  and  $\gamma=0.001$  behave like a response of a smaller reservoir; it means a reservoir with smaller dimensions than actual. This analysis lead to the fact that the values of permeability and skin factor calculated depend on the value of gamma and the case considered (gas rate).

Calculated permeability from the slope of each curve in Fig. 4.6 is compared with the initial reservoir permeability and results are shown in **Fig. 4.7**.

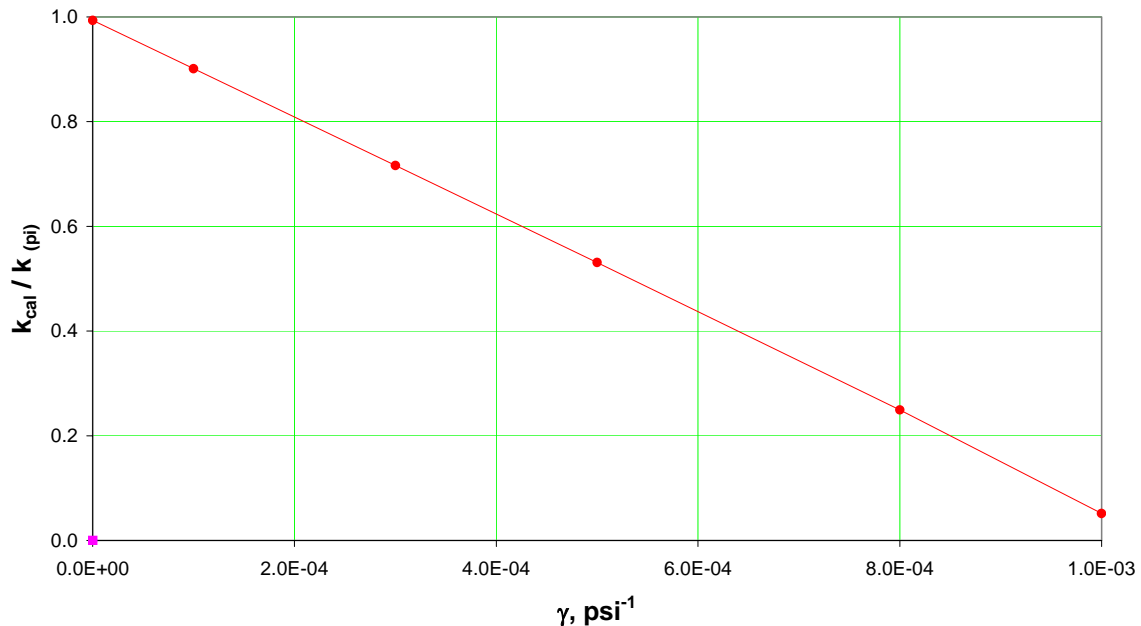


Fig. 4.7 – Permeability ratio vs. gamma, radial case, constant  $q_g = 40$  Mscf/D.

Fig. 4.7 is a plot of permeability ratio vs. gamma. The permeability ratio is obtained as the permeability calculated from each curve in Fig. 4.6 divided by the original

permeability. For  $\gamma=0$ , the permeability ratio is 1; implying a non-stress sensitive formation. As expected, for a higher value of gamma there is a significant reduction on the permeability of the reservoir as it is depleted at constant gas rate of 40 Mscf/D. In this case, a 95% permeability reduction occur for  $\gamma=0.001$ .

Skin factor are then calculated from intersect of each curve in Fig. 4.6. Results of skin calculations are presented in **Fig. 4.8**.

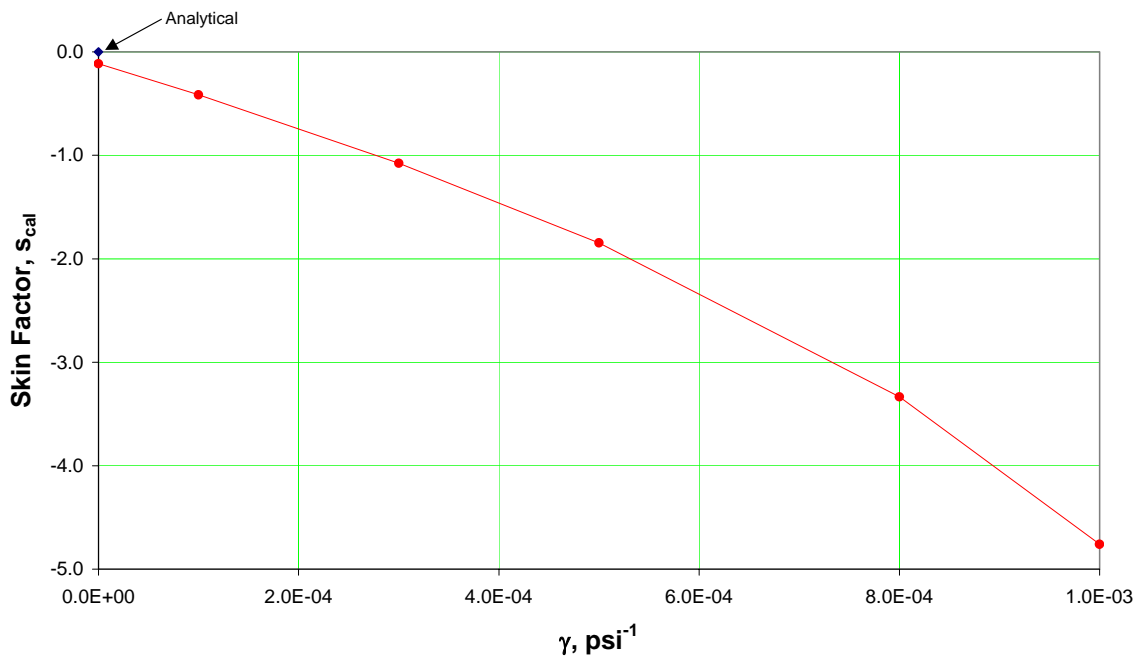


Fig. 4.8 – Skin factor vs. gamma, radial case, constant  $q_g = 40$  Mscf/D.

The calculated skin factor for this case shows a larger absolute value if compared with results of case 1, it is due to the higher constant gas rate used in the simulator. Skin varies from -0.113 to -4.758. The curve does not show a linear relation between skin and gamma.

Similar to case 1, is made an investigation about the range of pressure drop originated by the production at constant gas rate of 40 Mscf/D. Comparison is made in terms of  $m(p)$

and  $m'(p)$ . The term  $m(p)$  correspond to the pseudo pressure defined originally by Al-Hussany<sup>1</sup>. The term  $m'(p)$  is the pseudo pressure including the stress-dependent permeability function. **Fig. 4.9** shows the results.

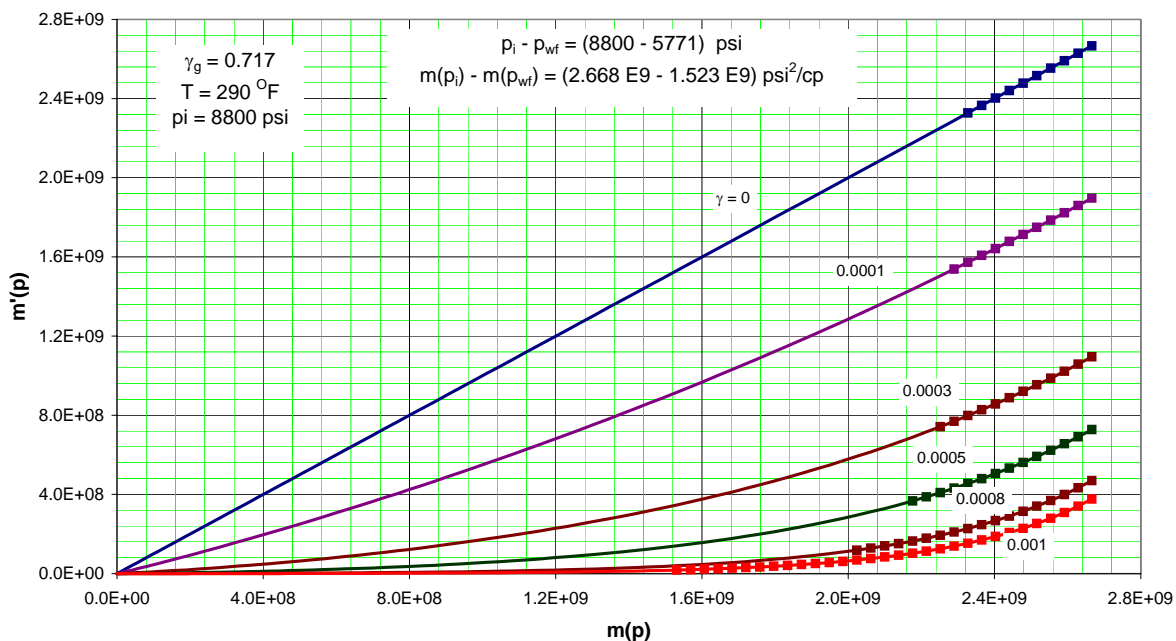


Fig. 4.9 - Plot  $m'(p)$  vs.  $m(p)$ , radial case, constant  $q_g = 40$  Mscf/D.

In Fig. 4.9 the plot correspond with  $m'(p)$  versus  $m(p)$ . Gas properties were calculated using a reservoir temperature of 290°F, gas specific gravity of 0.717 and initial pressure of 8,800 psi. Each curve corresponds with a different value of gamma. The line in the top represents a non-stress sensitive scenario,  $\gamma = 0$ , for this case a straight line is obtained. As gamma start to increase from 0 to 0.001, the curves start to tilt downward, and the relation is not longer linear. The maximum pressure drop ( $p_i - p_{wf}$ ) occurred for the case with gamma = 0.001 and it was 3029 psi ( $p_i = 8,800$  psi;  $p_{wf} = 5,771$  psi). The squared dots localized over each continuous line indicate the range of pressure studied in this case ( $q_g = 40$  Mscf/D). It is clear that only for gamma between 0 and 0.0005 the squared dots are localized in a region over the continuous line where still exist a linear

relation between  $m(p)$  and  $m'(p)$ , that explain the results analyzed in this case, where a linear response is obtained for  $[m(p_i)-m(p_{wf})]/q_g$  vs. time for all gamma. Something interesting happen for gamma higher than 0.0005, and it is that the pressure range studied cover a significant portion of the curve that is not straight line, that means, there is not longer a linear relation between  $m(p)$  and  $m'(p)$  that can explain the non linear response obtained for  $[m(p_i)-m(p_{wf})]/q_g$  vs. time for  $\gamma > 0.005$ .

## 4.2 Infinite Acting, Constant $p_{wf}$

### 4.2.1 Case 3: $p_{wf} = 4,000$ psi

Case 3 corresponds with a simulation run where the control mode is the bottom hole pressure and it is kept constant to 4,000 psi. It is the special interest to investigate the reservoir response for a stress dependent permeability in terms of pseudo pressure and time, and then calculate permeability and skin factor from transient flow period. First at all, a comparison is made between numerical and analytical solution for non-stress dependent permeability reservoir; that means gamma is zero ( $\gamma=0$ ). **Fig. 4.10** shows the match between both solutions.

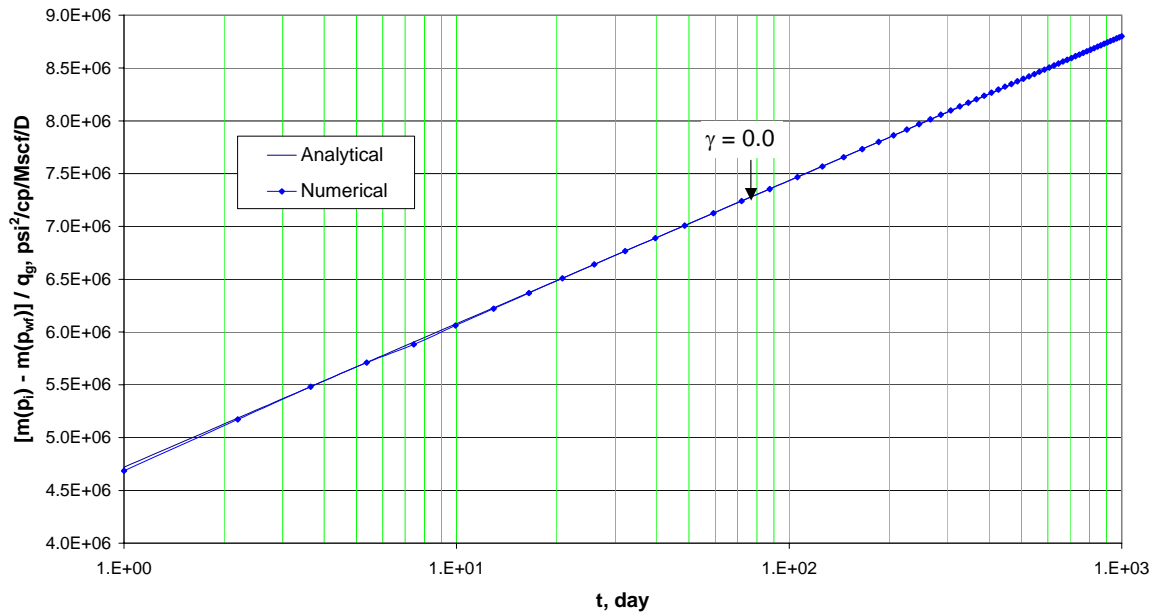


Fig. 4.10 - Semi-log plot, analytical and numerical match for infinite acting radial case, constant  $p_{wf}$ .

It is presented in Fig. 4.10 the numerical and analytical results in terms of pseudo pressure,  $m(p)$ , and time. Semi log plot of this variables indicate a straight line for transient flow period in a radial reservoir. From the plot is visible that there is a pretty good match between the numerical and analytical solution, however, the first 2 days of simulation there is a numerical error, due to time and space dimension specified in the simulator. The numerical error can be minimized reducing the grid dimensions and time steps in the simulator. This results validate the simulation model for  $\gamma = 0$ .

Then, we will move forward to see the results by incorporating the stress dependent permeability by increasing the values of gamma in each simulation run. Results are shown in **Fig. 4.11**.

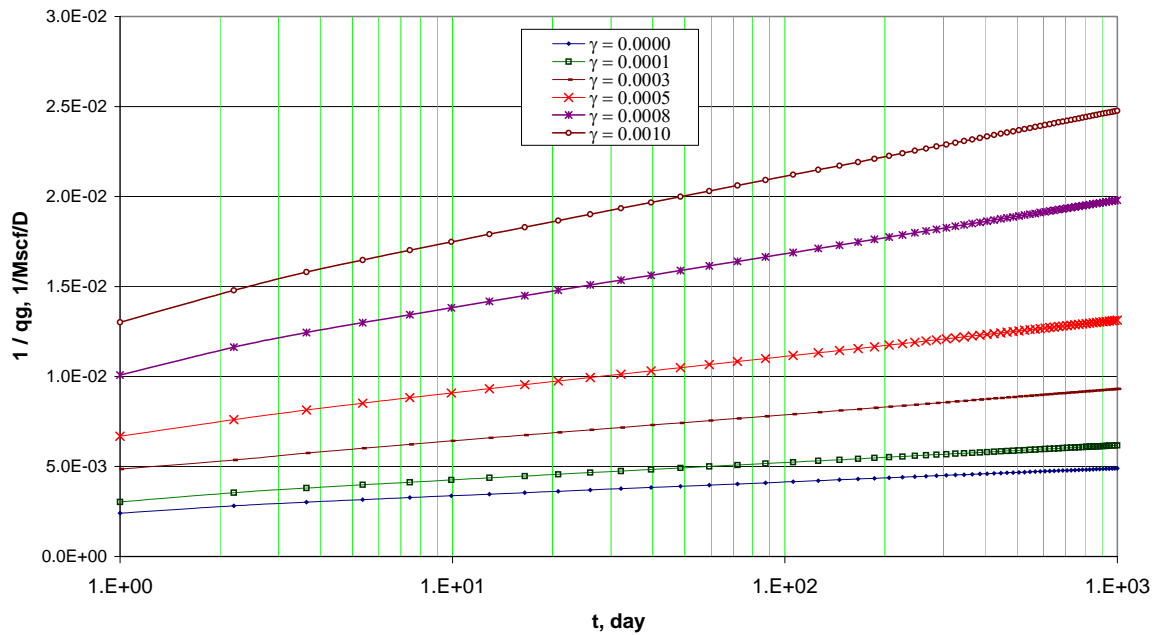


Fig. 4.11 – Semi-log plot, effect of pressure-dependent permeability for an infinite acting radial reservoir producing at constant  $p_{wf} = 4000$  psi.

Fig. 4.11 corresponds with the numerical simulation results for a radial reservoir with constant bottom hole pressure (4,000 psi). The plot is in the form  $1/q_g$  vs.  $\log t$ . For a non-stress dependent permeability formation this plot leads to a straight line and from the slope is calculated permeability and skin factor. As it is included stress dependent permeability by considering different values of gamma, the result indicate also a straight line for the transient flow period with a different slope. The higher the value of gamma the higher is the slope of the curve. That results imply a reduction on gas rate production with time as the permeability is reduced in the reservoir and the bottom hole pressure is kept constant, that obey Darcy's law. An important point to mention here is that for that particular case with a pressure draw down of 4,800 psi all the curves are straight lines.

Then, from each curve in Fig. 4.11 it is calculated the slope and consequently, the permeability of each simulation run to be compared with the initial permeability considered in the reservoir. Results are in **Fig. 4.12**.

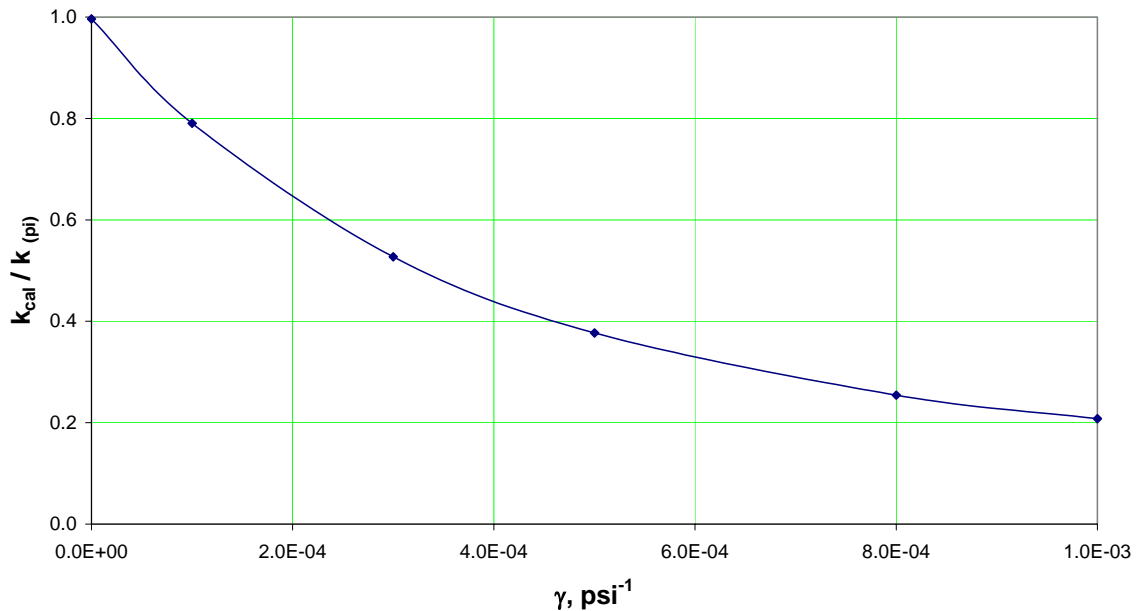


Fig. 4.12 - Permeability ratio vs. gamma, radial case, constant  $p_{wf} = 4000$  psi.

Fig. 4.12 shows permeability ratio versus gamma. It is perceived that for gamma zero there is not reduction on permeability ( $k_{\text{calc}} / k_{\text{pi}} = 1$ ). For higher values of gamma, the permeability calculated from each slope in Fig. 4.11 is lower, becoming almost 80% reduction on permeability for the case with  $\gamma = 0.001$ . The correlation between permeability reduction and gamma has an exponential form.

Skin factor is calculated in a similar way, using the slope of each curve from Fig. 4.11. Results are shown in **Fig. 4.13**. The calculation of skin factor for  $\gamma=0$  is very close to zero ( $s=-0.017$ ); difference is caused by numerical error introduced in the simulator by dimensions in the grid and time steps. As expected, for higher values of gamma, the calculated skin factor increase and is all the time positive. That indicates an introduction of damage in the reservoir due to the reduction on permeability as the reservoir is

depleted. The highest value of skin is 1.17 and correspond with the highest value of gamma,  $\gamma = 0.001$ .

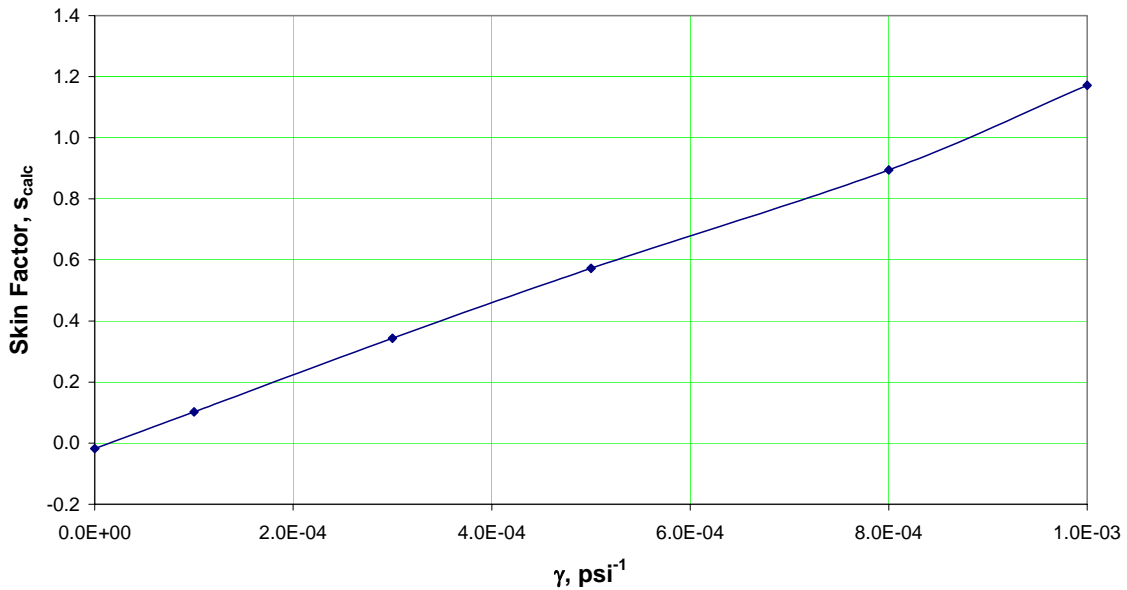


Fig. 4.13 - Skin factor vs. gamma, radial case, constant  $p_{wf} = 4000$  psi.

As it was discussed in the constant gas rate cases, for this constant bottom hole pressure case, an investigation on the range of pressure drop imposed in the reservoir is made. The important point here is to know the range of pressure where  $m(p)$  and  $m'(p)$  have a linear relation. Results are discussed in **Fig. 4.14**. The plot is  $m'(p)$  vs.  $m(p)$ . Both variables are the pseudo pressure defined by Al-Hussainy<sup>1</sup>, but the first include the effect of having a stress sensitive formation. Gas properties are calculated using as initial values, a specific gravity of 0.717 and a reservoir temperature of 290°F. Case 3 correspond with a constant bottom hole pressure of 4,000 psi, which imply that the pressure drop in the reservoir is constant to 4,800 psi. Each curve corresponds with a different value of gamma. The line in the top represents a non-stress sensitive scenario,  $\gamma = 0$ , for this case a straight line is obtained. As gamma start to increase from 0 to 0.001, the curves start to tilt downward, and the relation is not longer linear. The squared dots



localized over the continuous lines indicate the range of pressure studied in this case ( $p_{wf} = 4,000$  psi). From Fig. 4.14 is clear a very important difference between this case and the one with constant gas rate (cases 1 and 2). The squared dots are localized in a region over the continuous line where there is not a linear relation between  $m(p)$  and  $m'(p)$ . That results suggest that lines in Fig. 4.11 ( $1/q_g$  vs. time) should not be straight lines, however, based in simulation results they are straight lines.

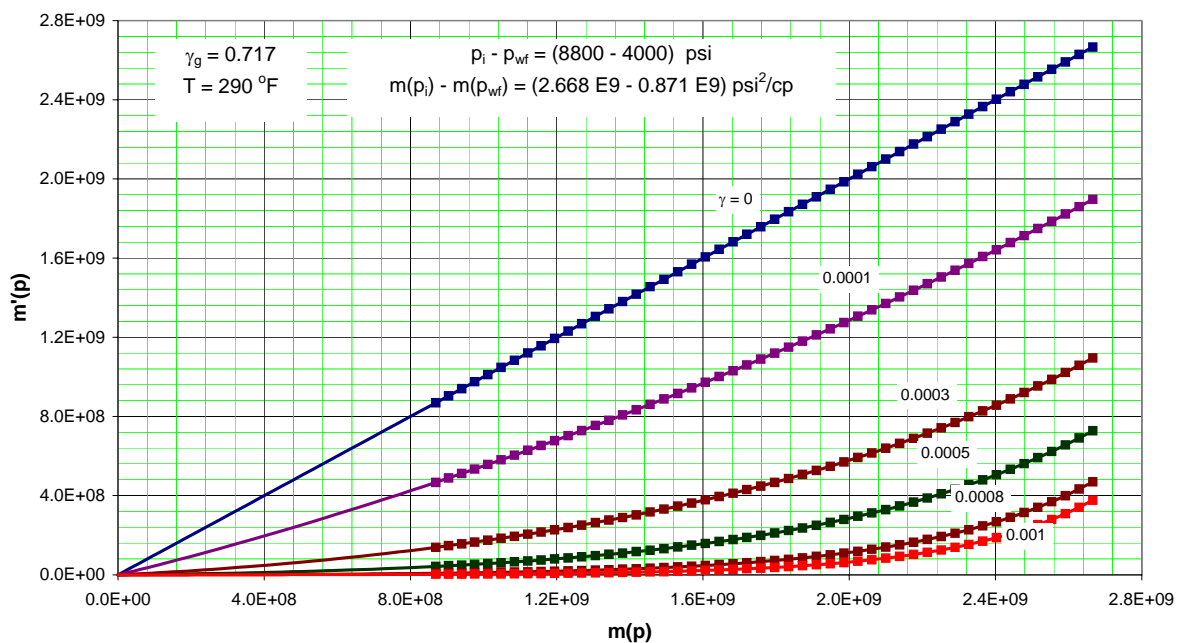


Fig. 4.14 - Plot  $m'(p)$  vs.  $m(p)$ , radial case, constant  $p_{wf} = 4000$  psi.

#### 4.2.2 Case 4: $p_{wf} = 2,000$ psi

In order to compare results from previous case, it is also considered a case with a different bottom hole pressure. Case 4 corresponds with a simulation run where the bottom hole pressure is 2,000 psi. The special interest is to investigate the reservoir response for a stress dependent permeability in terms of pseudo pressure and time, then

calculate permeability and skin factor from transient flow period. **Fig. 4.15** shows the simulation results.

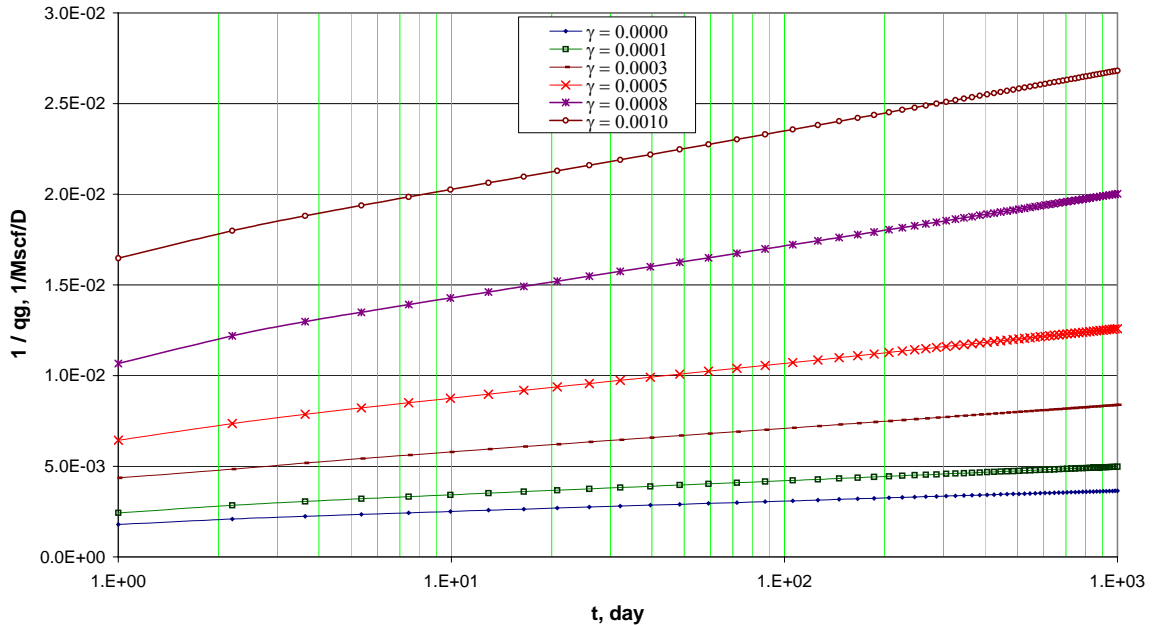


Fig. 4.15 – Semi-log plot, effect of pressure-dependent permeability for an infinite acting radial reservoir producing at constant  $p_{wf} = 2000$  psi.

Fig. 4.15 present the numerical solution for constant bottom hole pressure 2,000 psi. The plotting variable is  $1/q_g$  vs. time, and is observable that for transient flow period a straight line is obtained for each value of gamma considered. As the value of gamma increase a straight line with a higher slope is obtained, that obeys Darcy's law and implies that gas rate decline meanwhile permeability decrease as the reservoir is depleted. An important point to mention here is that for that particular case with a significant pressure draw down (6,800 psi) all the curves are straight lines. From that figure is calculated the slope of each curve and plugged into the corresponding equation to get the values of permeability. Permeability calculations are shown in **Fig. 4.16**.

The permeability calculated from each slope is lower as the values of gamma increase. That indicates a higher reduction in permeability in the reservoir as gamma is increased. An 86% permeability reduction is obtained for the case with the largest gamma ( $\gamma = 0.001$ ).

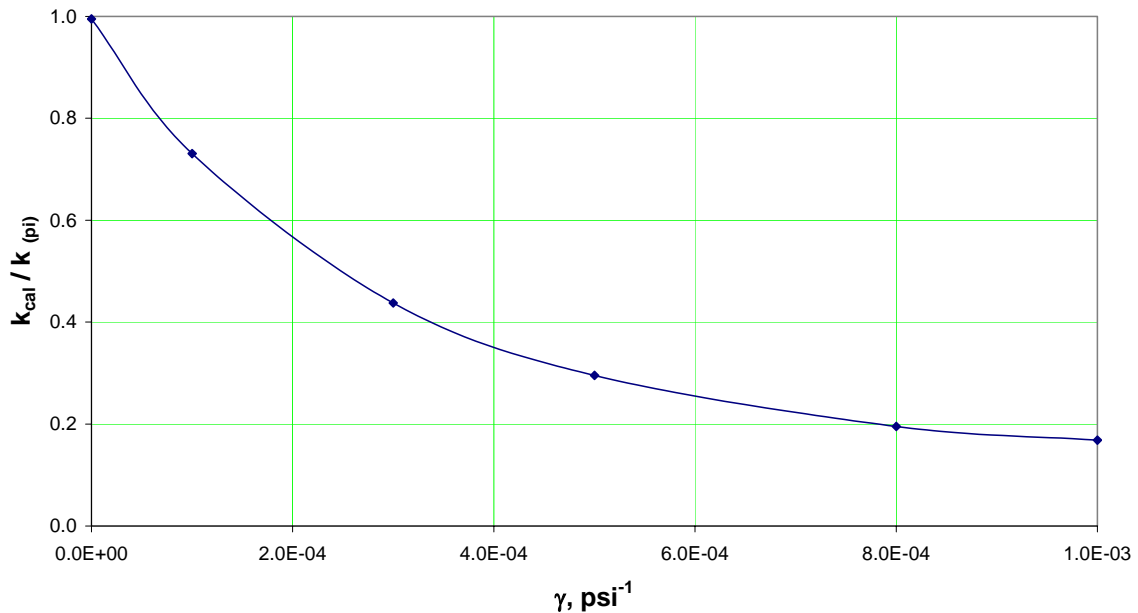


Fig. 4.16 - Permeability ratio vs. gamma, radial case, constant  $p_{wf} = 2000$  psi.

Skin factor is also calculated from results presented in Fig. 4.15. Getting the slopes of the curves, plugging them into the corresponding equations allow to get the values of skin for each gamma considered. Results are shown in **Fig. 4.17**. For this constant bottom hole pressure case calculated skin factors increase and are positive as gamma increase. Due to numerical error in the simulator, the value of skin factor obtained for  $\gamma=0$  is not zero ( $s=-0.063$ ), however it is close to zero and is considered satisfactory in this project. This can be improved reducing time and space dimensions in the simulator runs.

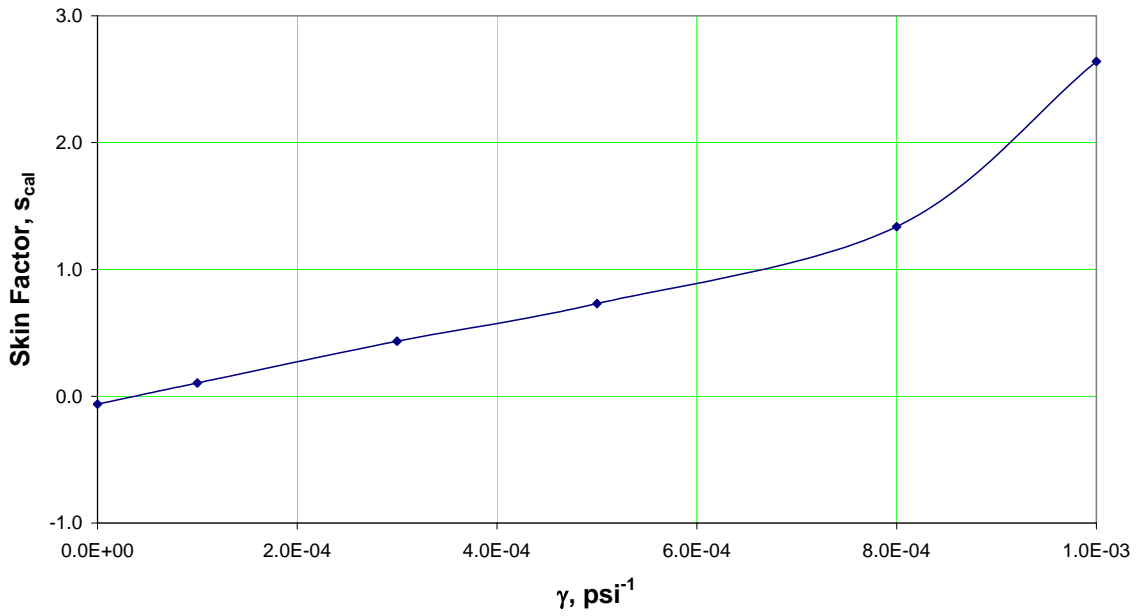


Fig. 4.17 - Skin factor vs. gamma, radial case, constant  $p_{wf} = 2000$  psi.

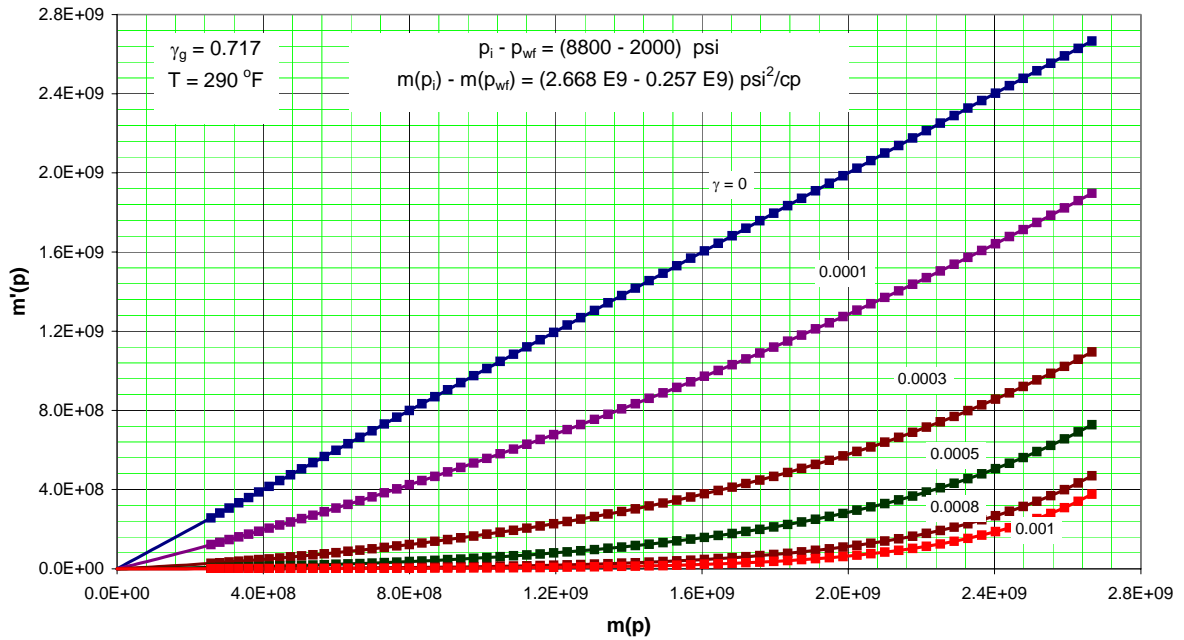


Fig. 4.18 - Plot  $m'(p)$  vs.  $m(p)$ , radial case, constant  $p_{wf} = 2000$  psi.

The range of pressure drop considered in this case is 6,800 psi ( $p_i=8,800$  psi;  $p_{wf}=2,000$ psi), and as it is seen in Fig. 4.18, it covers a significant range of pseudo pressures values. The squared dots over the continuous lines indicate that range of pressure. For high values of gammas the plot suggest that there is not linear relation between  $m(p)$  and  $m'(p)$ , however, numerical results presented in Fig. 4.15 indicate that for all values of gammas a straight line relation is obtained.

### 4.3 Finite Acting, Constant $q_g$

In this section is made a discussion of the pseudo steady state results, and particularly to calculate the Original Gas in Place (OGIP) in the reservoir. It is desirable to investigate how is affected the calculation of OGIP considering the stress dependent permeability through the introduction of the gamma function. The methodology is to deplete the reservoir at constant rate until it reaches the borders, then estimate the dimensions, pore volume and estimate the original volume of hydrocarbon in place.

#### 4.3.1 Case 5: $q_g = 10$ Mscf/D

The discussion starts with the first case that corresponds with a constant gas rate of 10 Mscf/D in a radial reservoir.

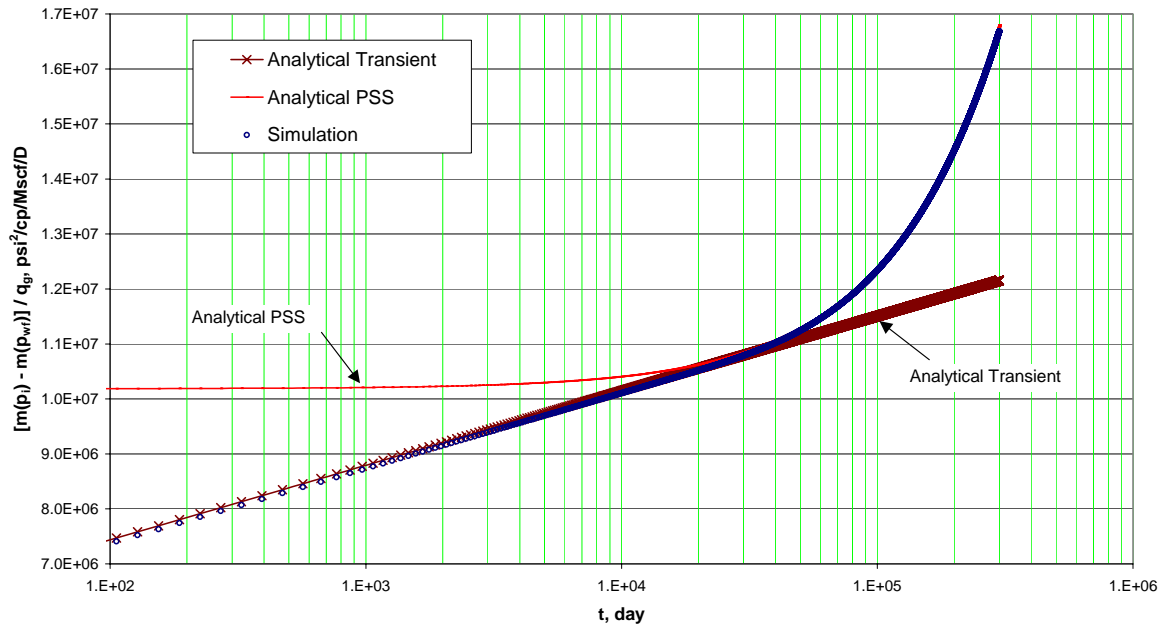


Fig. 4.19 – Semi-log plot, analytical and numerical match for finite acting radial case, constant  $q_g$ .

The method uses the analytical solution of pseudo steady state at the inner boundary, then estimate the reservoir pore volume from the slope of the cartesian plot  $[m(p_i) - m(p_{wf})]/q_g$  vs. time, as described in Appendix D.

**Fig. 4.19** shows the results of compare analytical and numerical solutions for a non-stress sensitive formation. It is clear that there is a satisfactory match for both early time and late time. Early time corresponds with transient flow where there the reservoir behaves like to be infinite; no limits are found in that portion, and the match is between numerical and transient analytical solutions curves. For about 5,000 days start the transition time to pseudo steady state period and the match corresponds with the PSS analytical solution curve, the match is pretty good. These results confirm and validate the numerical model.

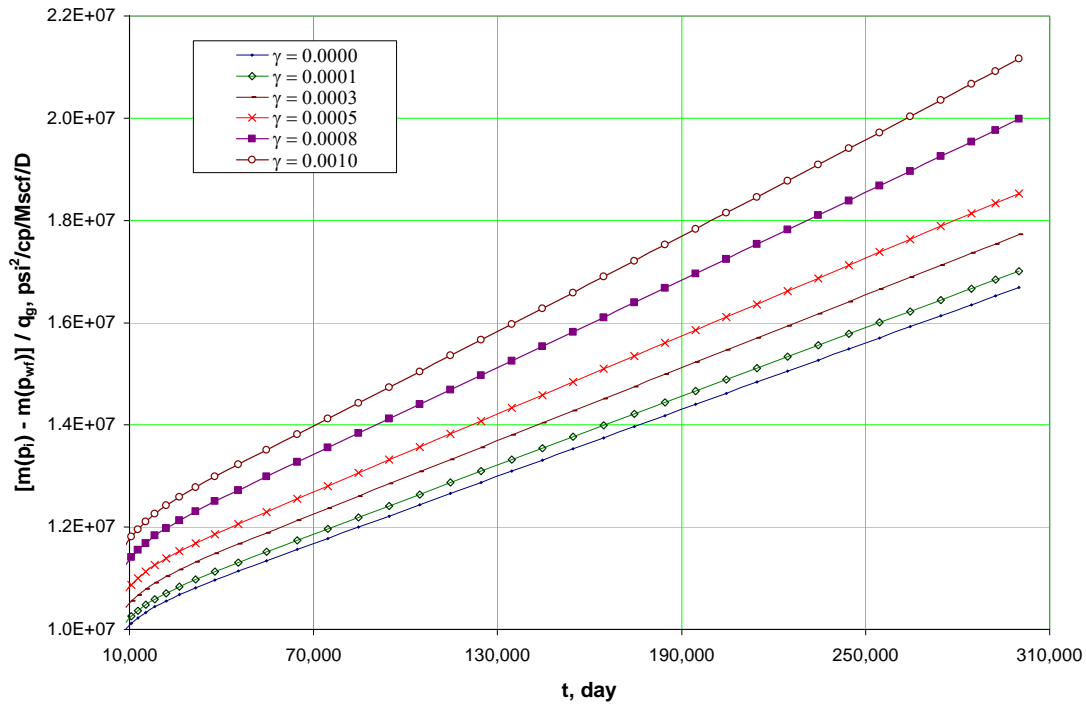


Fig. 4.20 – Cartesian plot, effect of pressure-dependent permeability for a finite acting radial reservoir producing at constant  $q_g = 10$  Mscf/D.

In **Fig. 4.20** are shown the numerical simulation results considering stress dependent permeability, this is, regarding several values of gamma. This is a Cartesian plot of pseudo pressure versus time and it reflect the pseudo steady state (PSS) period, the portion of the curve go from  $t=10,000$  days to  $t=300,000$  days. From the plot is seen that for each gamma a different curve is obtained, in all cases they are straight lines with different slopes. Non linearity has no significant effects over results due to a low pressure draw down considered in this case ( $q_g = 10$  MScf/D), that is way results show straight lines for all values of gamma. As the gamma increase results imply that PSS period start earlier in the model, that agree with the fact that a larger pressure drop is necessary as the permeability decrease in the reservoir due to depletion, and this lead to hit the borders of the reservoir in a smaller time. This is represented in Fig. 4.20 by a higher slope in the line as the value of gamma increase.

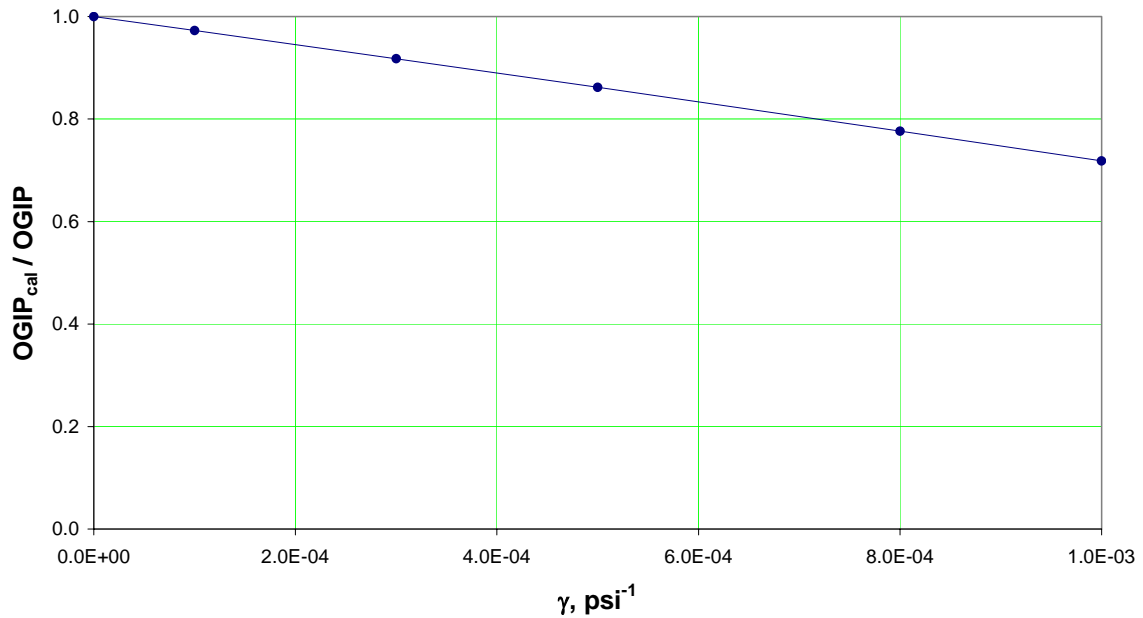


Fig. 4.21 – OGIP ratio vs. gamma, radial case, constant  $q_g = 10$  Mscf/D.

Now, it is made a discussion about the calculation of OGIP. The pore volume of the reservoir is calculated from the slope of each line in Fig. 4.20. Then, using initial gas saturation,  $S_{gi}$ , of 53% is calculated the OGIP from the volumetric equation. Results are presented in **Fig. 4.21**. This figure plot the ratio of gas in place versus gamma, it is, the OGIP calculated for each value of gamma divided for the OGIP considering a non-stress sensitive formation,  $\gamma=0$ . Fig. 4.21 indicates a proportional reduction of calculated gas in place in the reservoir as gamma increase. The meaning of that result is that the reservoir looks to be of smaller dimensions as gamma increase. This obeys the facts that for higher values of gamma, a larger pressure drop occurs and the limits of the reservoir are reached in an earlier time.



4.3.2 Case 6:  $q_g = 20$  Mscf/D

Case 6 correspond with a higher constant gas rate to deplete the reservoir, here is considered a gas rate of 20 Mscf/D.

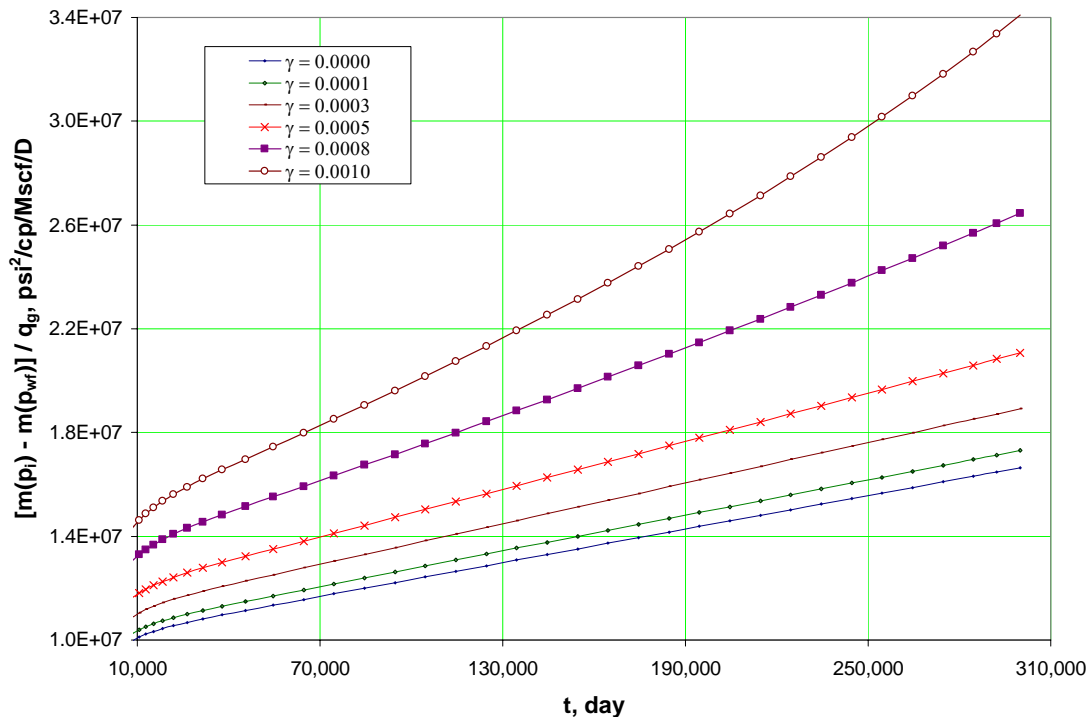


Fig. 4.22 – Cartesian plot, effect of pressure-dependent permeability for a finite acting radial reservoir producing at constant  $q_g = 20$  Mscf/D.

The point here is to analyze a case with a higher draw down imposed in the reservoir. **Fig. 4.22** present results for this case. Similar to previous case 5, Fig. 4.22 is a Cartesian plot of pseudo pressure versus time. The portion of the time important to analyze correspond with the pseudo steady state period. It is visible that for low values of gamma a straight line is obtained; however, for larger values of gamma, as  $\gamma = 0.001$ , the curve start to tilt upward and no longer is straight line. This is the direct effect of larger draw down and higher level of permeability reduction introduced by high value of gamma. It is clear that each curve is affected by non-linearity in the solution. From that plot is

obtained a wrong value of OGIP. To overcome the problem, in this project is used the concept of normalized pseudo time, introduced by Ibraim<sup>22</sup> and described in chapter 2. The normalized pseudo time provides a plotting function for smoothing the production data by taking the effect of reservoir properties change with average pressure.

**Fig. 4.23** shows the result of calculating pseudo time,  $t_n$ , for the case where  $\gamma = 0.0$ . It is visible that the new function linearizes production data by considering reservoir properties changes. Consequently, from the slope of the straight line is calculated the OGIP with more accuracy.

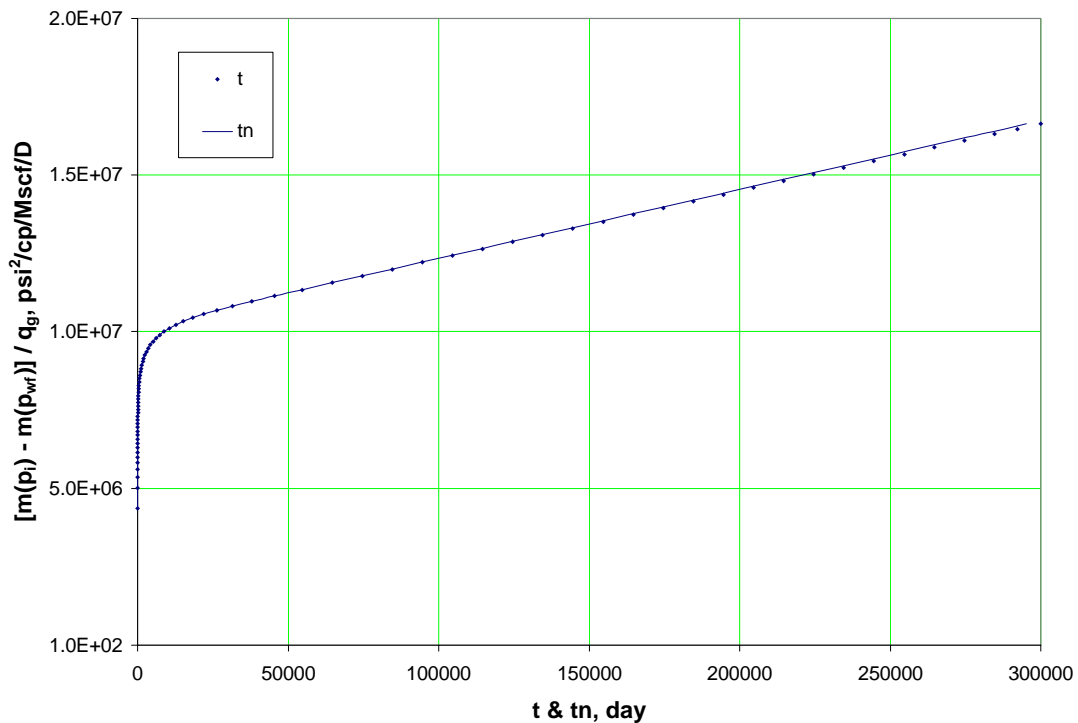


Fig. 4.23 – Time and normalized pseudo time for a finite acting radial reservoir producing at constant  $q_g = 20$  Mscf/D, Case  $\gamma = 0.0$ .

A similar method is applied for each curve in Fig. 4.22; they are linearized in terms of reservoir properties variation. Then, calculating the slope of each curve, allow us to get the values of pore volume and OGIP. Results are presented in **Fig. 4.24**.

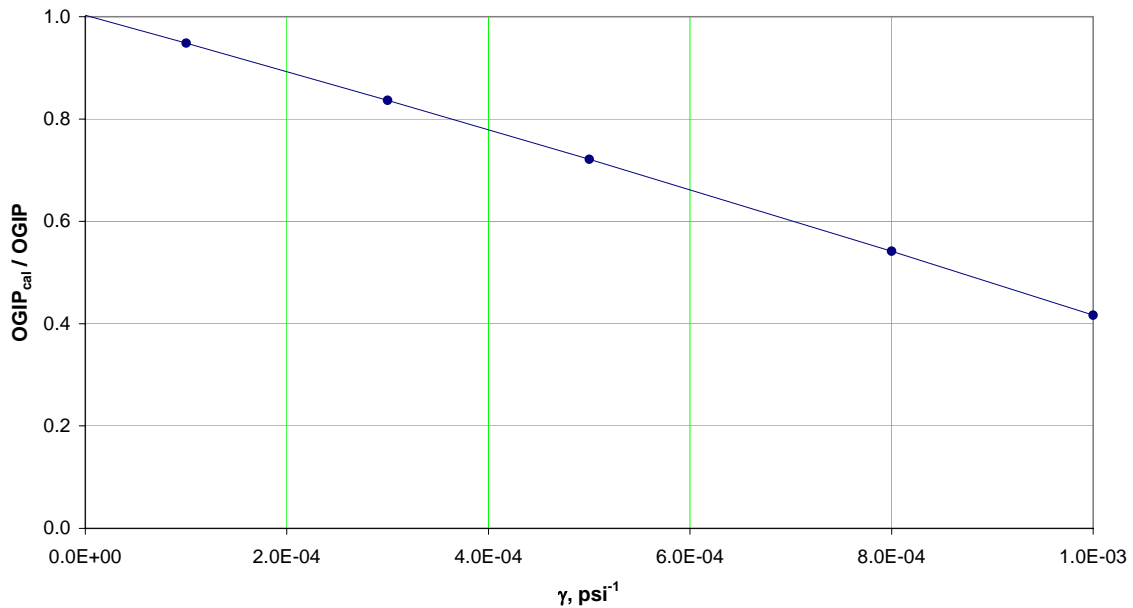


Fig. 4.24 - OGIP ratio vs. gamma, radial case, constant  $q_g = 20$  Mscf/D.

Fig. 4.24 shows the level of reduction in the calculated OGIP considering a stress sensitive formation. For  $\gamma=0.001$  the total reduction in the calculated OGIP is about 58%.

#### 4.4 Finite Acting, Constant $p_{wf}$

This section discusses the results of numerical simulation by depleting the radial reservoir at constant bottom hole pressure. Two cases are considered, the first one with  $p_{wf} = 4,000$  psi and second one with  $p_{wf} = 2,000$  psi. The major interest is to analyze the PSS period and estimate pore volume and OGIP in the reservoir.

4.4.1 Case 7:  $p_{wf} = 4,000$  psi

Case 7 correspond with a constant pressure drop of 4,800 psi in the reservoir. Numerical results are presented in the form  $[m(p_i)-m(p_{wf})]/qg$  versus time in **Fig. 4.25**.

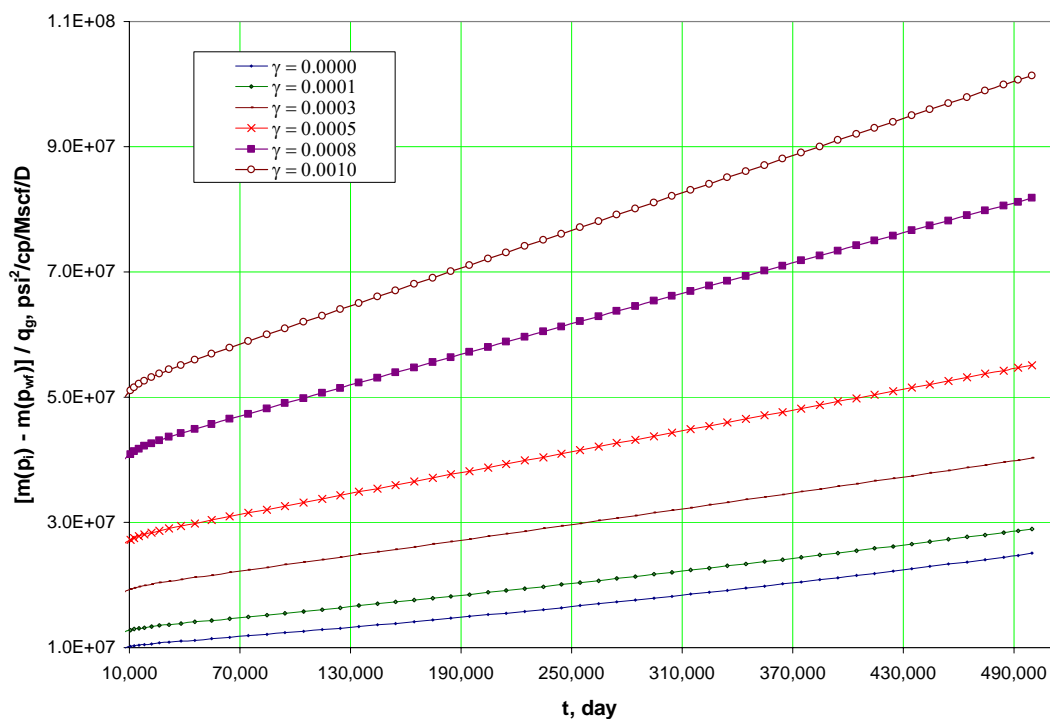


Fig. 4.25 – Cartesian plot, effect of pressure-dependent permeability for a finite acting radial reservoir producing at constant  $p_{wf} = 4000$  psi.

Fig. 4.25 is a Cartesian plot that shows the reservoir response during PSS period, in this particular plot the solution follows a straight-line behavior. The results are presented for different level of stress dependent permeability, from the line in the bottom to the line in the top, the gamma values increase. For all the range of gamma a straight line is obtained, with different slopes. As gamma is higher, the slope form the curve is higher. Pore volume and OGIP are calculated from that slope. In **Fig. 4.26** it is observable the effect of a stress dependent permeability on the OGIP calculated. The results indicate a significant reduction of calculated gas in place in the reservoir as gamma increase. These

results are similar to the cases with constant gas rate, the reservoir behave like being of smaller dimensions for higher values of gamma.

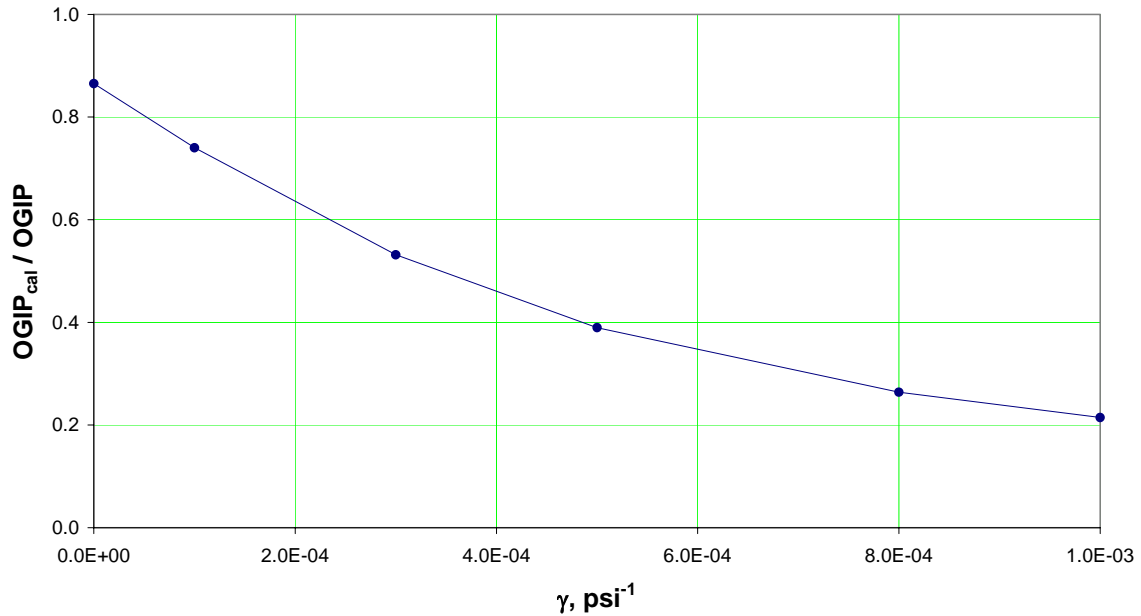


Fig. 4.26 - OGIP ratio vs. gamma, radial case, constant  $p_{wf} = 4000$  psi.

#### 4.4.2 Case 8: $p_{wf} = 2,000$ psi

Case 8 correspond with a lower bottom hole pressure to deplete the reservoir, here is considered a  $p_{wf}$  of 2,000 psi. The main interest is to analyze a case with a higher draw down imposed in the reservoir. **Fig. 4.27** shows the results for this case.

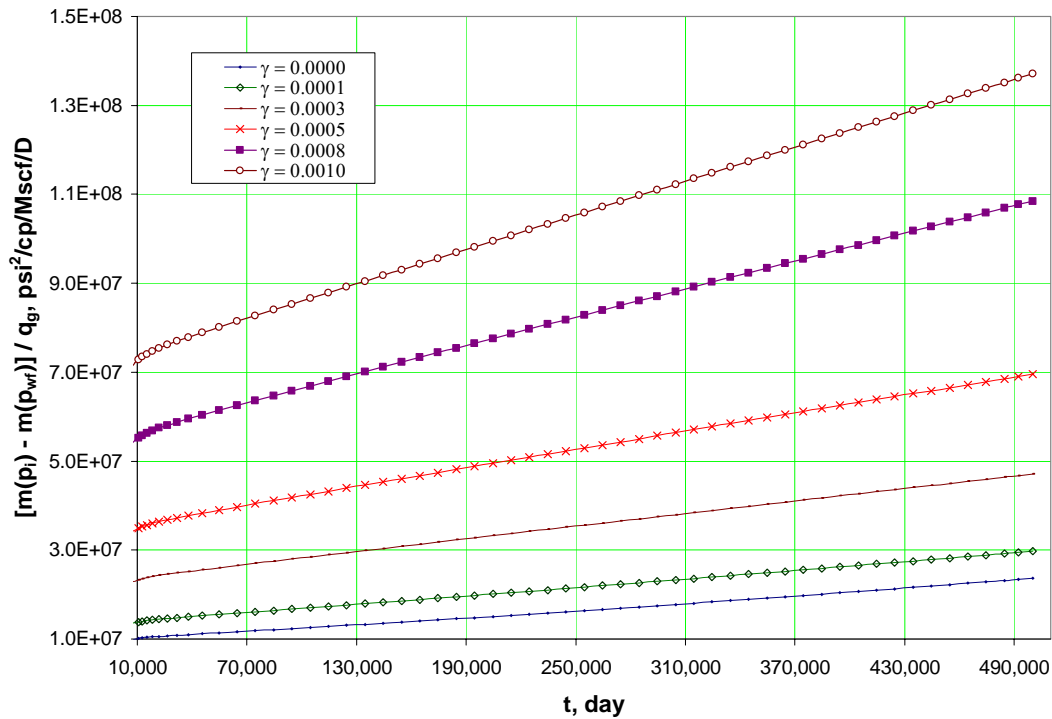


Fig. 4.27 – Cartesian plot, effect of pressure-dependent permeability for a finite acting radial reservoir producing at constant  $p_{wf} = 2000$  psi.

Similar to case 7, Fig. 4.27 is a Cartesian plot of  $[m(p_i) - m(p_{wf})] / q_g$  versus time. Results are presented for the PSS period in the reservoir. It is important to mention that for all the range of gamma studied and for a 6,800 constant pressure drop in the reservoir, a straight line is obtained. Each curve has a higher slope than previous one as gamma increase. These results lead to the conclusion that no matter the range of pressure drop in the reservoir; the Cartesian plot is always a straight line with different slopes. Calculating the slope of each curve, we come out with reservoir pore volume and OGIP. Results are shown in **Fig. 4.28**.

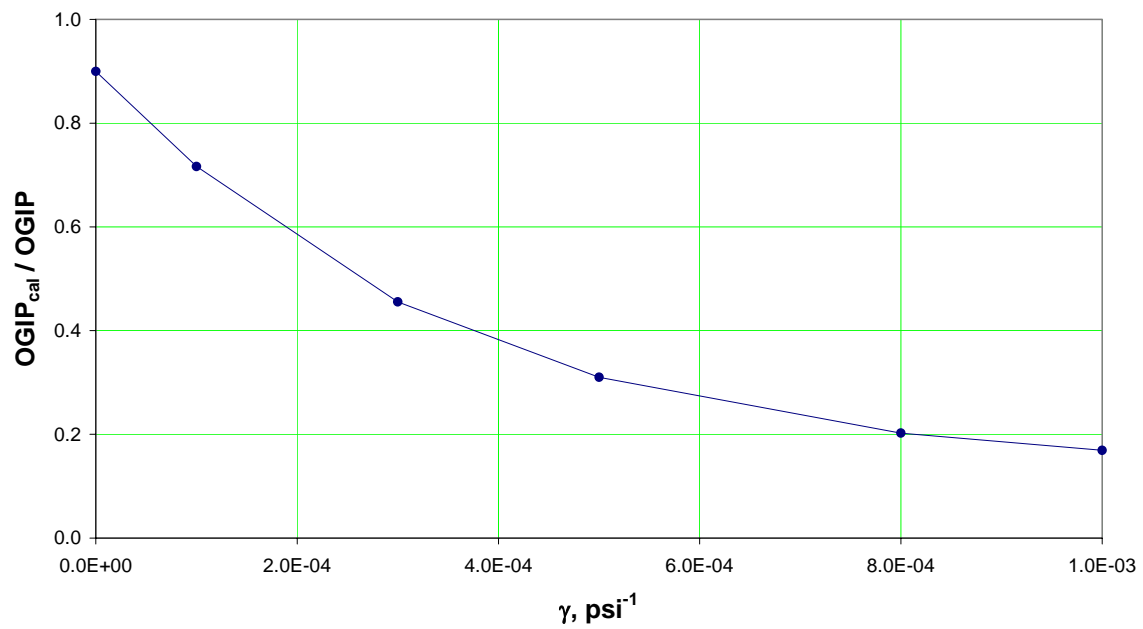


Fig. 4.28 - OGIP ratio vs. gamma, radial case, constant  $p_{wf} = 2000$  psi.

Fig. 4.28 shows the level of reduction in the calculated OGIP considering a stress sensitive formation. For  $\gamma=0.001$  the total reduction in the calculated OGIP is about 83%.

## CHAPTER V

## STRESS-DEPENDENT PERMEABILITY LINEAR CASES

This chapter includes results and discussion of analytical and numerical simulation of stress-dependent permeability considering a reservoir with linear geometry. The analysis is presented for transient flow and pseudo-steady state flow, as well as constant gas rate and constant bottom hole pressure cases. Data files used in simulations are included in Appendix D. In addition, derivation of equations used to calculate permeability and skin factor as well as reservoir pore volume and OGIP are described in Appendix F.

### 5.1 Infinite Acting, Constant $q_g$

This section starts presenting the numerical results from GASSIM simulator for the case with constant gas rate 10 Mscf/D. The main objective here is analyze the portion of the curve that correspond with infinite acting or transient flow, to calculate permeability and skin factor from the slope of each curve that correspond with different values of gamma,  $\gamma$ . The analysis for linear flow is made in terms of pseudo-pressure  $m(p)$ ; the plot of  $\log[m(p)]$  versus  $\log(t)$  indicate a straight line with a slope of 1/2 that is related directly to the value of permeability. **Fig. 5.1** show results of analytical and numerical simulation for  $\gamma = 0$ , that means; no stress-dependent permeability is considered.



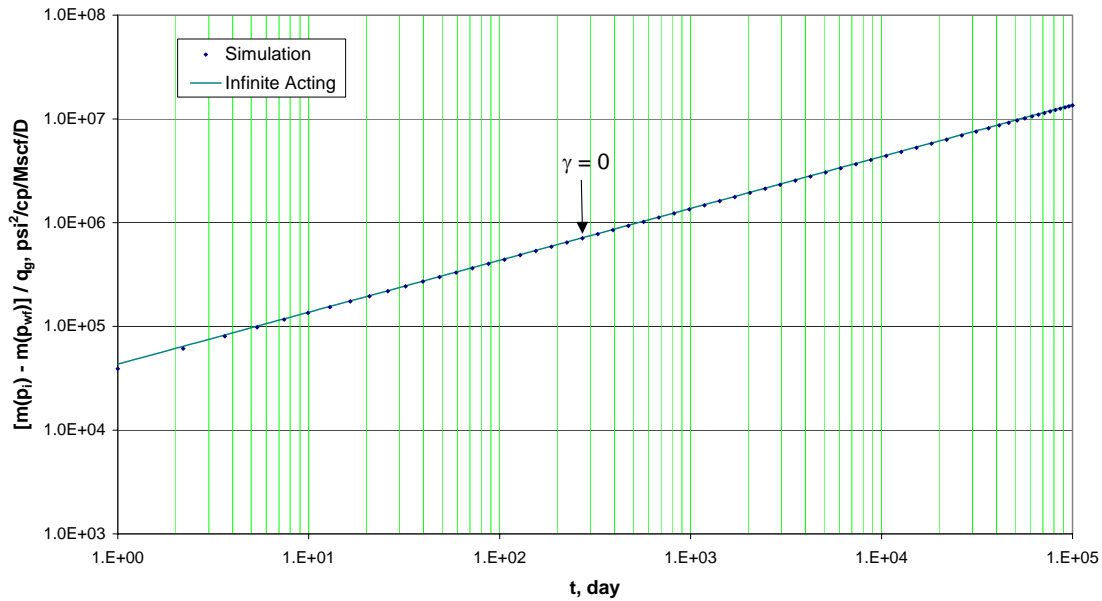


Fig. 5.1 – Log-log plot, analytical and numerical match for infinite acting linear case, constant  $q_g$ .

Fig. 5.1 indicates a satisfactory match between analytical solution and numerical simulation regarding a linear model, constant gas rate and non-stress-dependent permeability. It is also visible a very small separation for early time, between 1 and 2 days due to numerical error. The numerical error can be minimized reducing the grid dimensions and time steps in the simulator. This results validate the simulation model for  $\gamma = 0$ .

To investigate the effect of stress-dependent permeability on the reservoir response, scenarios with different values of gamma ( $\gamma$ ) are considered. As the value of gamma increase, means that exists a stronger dependency of permeability on pressure. **Fig. 5.2** presents results in terms of pseudo pressure for a linear reservoir in transient flow condition.

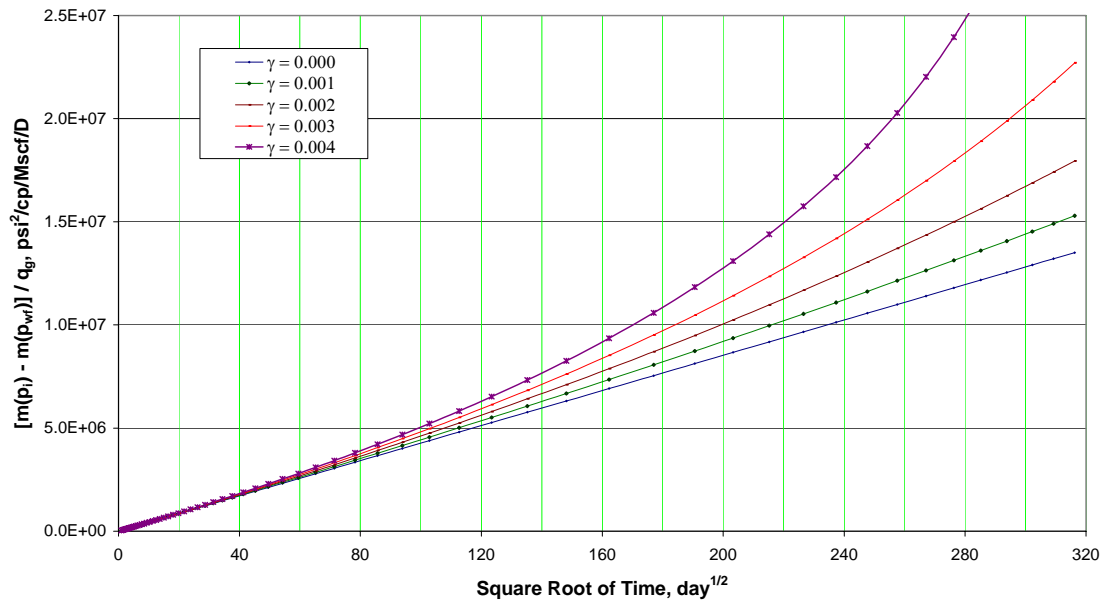


Fig. 5.2 – Square root of time plot, effect of pressure-dependent permeability for an infinite acting linear reservoir producing at constant  $q_g = 10$  Mscf/D.

For this scenario, analysis of linear flow is represented by a plot of variables  $[m(p_i) - m(p_{wf})]/q_g$  versus  $\sqrt{t}$ . For a non-stress sensitive formation,  $\gamma=0$ , the slope of that plot correspond with a straight line. Observing Fig. 5.2, it is seen that for values of gamma ( $\gamma$ ) less than 0.001, the response can be considered as straight line, having each straight line a different slope, which is directly related to permeability and skin using the analytical solution equations. A very important result is that for values of gamma greater than 0.001, the reservoir response is not longer straight line, curves start to bending upward, indicating a stronger dependency of permeability on pore pressure. It means that at each time, a different tangent is obtained and different results are obtained for permeability and skin calculated using analytical solution.

As expected, the permeability ( $k$ ) and skin factor ( $s$ ) calculated from the slope of the curve gamma zero ( $\gamma=0$ ) is the original reservoir permeability and zero skin. In other words; for  $\gamma=0$ ,  $k_{calc} = 0.0025$  md and  $s = 0$ . As the value of gamma increase, the slope obtained is higher; it is due to the permeability reduction in the reservoir as it is being

depleted at constant gas rate. These results make sense and agree with Darcy's law; keeping the gas rate constant, whatever reduction in reservoir permeability during depletion time lead to a higher pressure drop, that explain the higher value of each slope as gamma increase.

Now, is included some discussion about permeability calculations. Permeability is calculated from the slope of each curve in Fig. 5.2 using the analytical solution equation. The initial reservoir permeability used in the GASSIM simulator was 0.0025 md. **Fig. 5.3** shows the results of calculations.

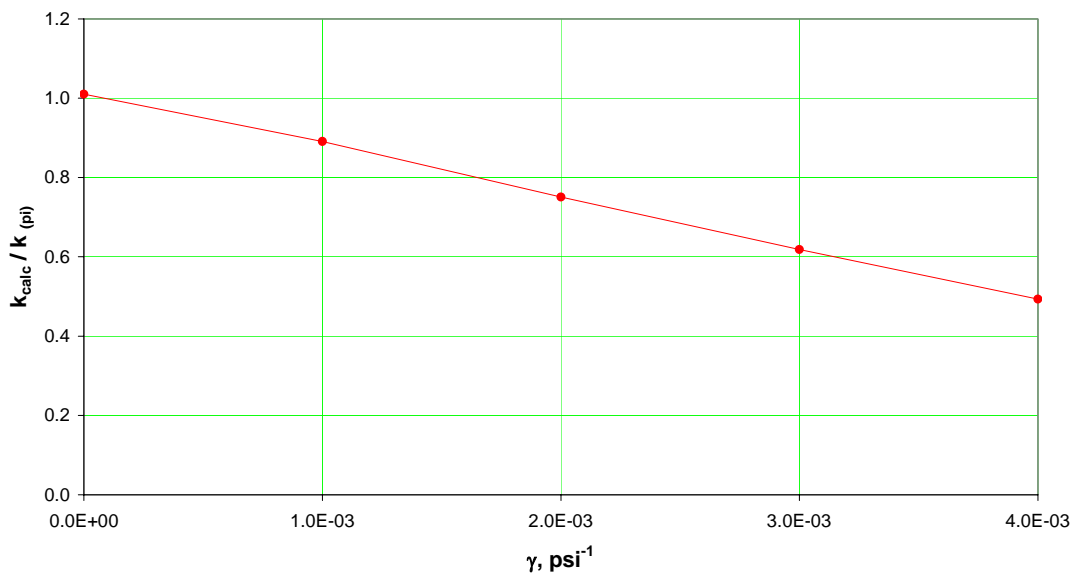


Fig. 5.3 – Permeability ratio vs. gamma, linear case, constant  $q_g = 10$  Mscf/D.

Fig. 5.3 is a plot of permeability reduction versus gamma. Permeability ratio is the permeability calculated in each run divided by the initial permeability ( $k=0.0025$  md). From that plot is clear that the higher the value of gamma the higher is the permeability reduction in the reservoir, a 50% permeability reduction occur for  $\gamma=0.004$ . In addition, can be concluded that for this particular case, where  $q_g=10$  Mscf/D, a linear relation is obtained between permeability ratio and gamma.

The same analysis can be drawn for skin factor calculations. It is used the definition of skin factor to investigate the magnitude of permeability reduction in the reservoir in terms of pore pressure. That means, the additional pressure drop necessary in the reservoir to maintain a gas rate constant meanwhile the permeability is reduced due to reservoir depletion. Skin factor is calculated from Fig. 5.2 and using equations from analytical solution of linear flow constant gas rate described in appendix E. Fig. 5.4 shows the results.

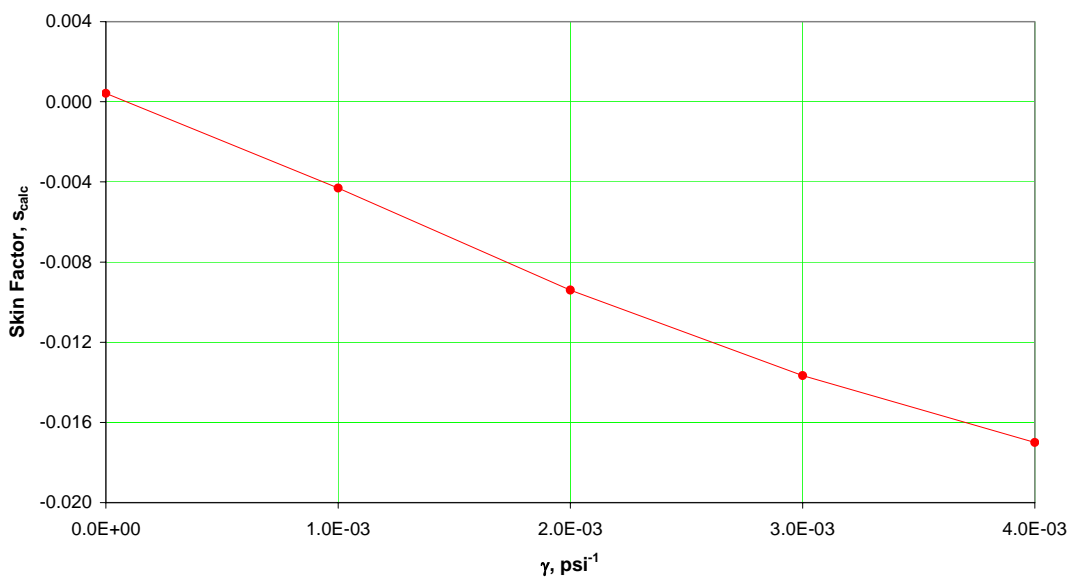


Fig. 5.4 – Skin factor vs. gamma, linear case, constant  $q_g = 10$  MScf/D.

Fig. 5.4 corresponds with a plot of skin factor versus gamma. The analytical solution imply a non-skin case,  $s=0$ . For the range of gamma considered in this case, skin varies between 0.0004 and -0.016. The fact that from numerical simulation we do not get a skin  $s=0$  for gamma  $\gamma=0$ , is explained as numerical error in the simulation runs. However, it is also understandable that the variation of skin factor for the range of gammas analyzed is very small. The greater gamma the more negative is skin factor.

Now, is investigated the range of pressure drop originated by the production at constant gas rate of 10 Mscf/D. Comparison is made in terms of  $m(p)$  and  $m'(p)$ . The term  $m(p)$

correspond to the pseudo pressure defined originally by Al-Hussainy<sup>1</sup>. The term  $m'(p)$  is the pseudo pressure including the stress-dependent permeability function. **Fig. 5.5** shows the results.

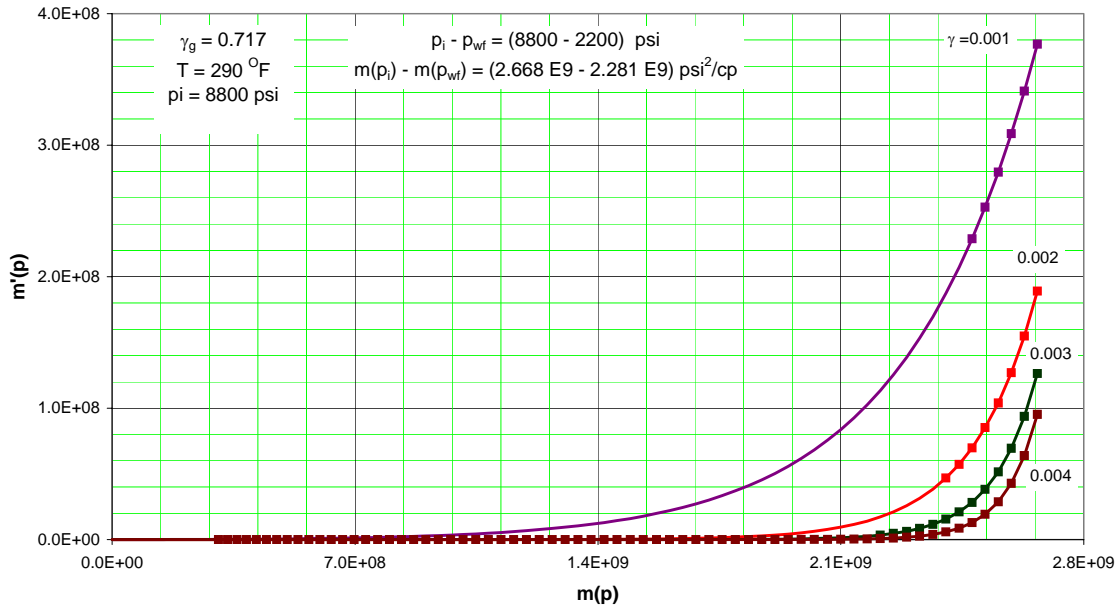


Fig. 5.5 - Plot  $m'(p)$  vs.  $m(p)$ , linear case, constant  $q_g = 10$  MScf/D.

In Fig. 5.5 the plot correspond with  $m'(p)$  versus  $m(p)$ . Gas properties were calculated using a reservoir temperature of 290 °F, gas specific gravity of 0.717 and initial pressure of 8,800 psi. Each curve corresponds with a different value of gamma. For a non-stress sensitive scenario,  $\gamma = 0$ , a straight line is obtained (not shown in the plot). As gamma start to increase from 0 to 0.004, the curves start to bend downward, and the relation is not longer linear. The maximum pressure drop ( $p_i - p_{wf}$ ) occurred for the case with  $\gamma = 0.004$  and it was 6,600 psi ( $p_i = 8,800$  psi;  $p_{wf} = 2,200$  psi). The squared dots localized at the end of each line indicate the range of pressure studied in this case ( $q_g = 10$  Mscf/D). Can be seen that for gamma between 0 and 0.001 the squared dots are localized in a region over the continuous line where still exist a linear relation between  $m'(p)$  and  $m(p)$ , that explain the results analyzed in this case, where a linear response is obtained for  $[m(p_i) - m(p_{wf})]/q_g$  vs. time for all gamma. For values of gamma greater than 0.001, dots are

localized in the curve section of each line, indicating that there is not a linear relation between  $m(p)$  and  $m'(p)$ .

## 5.2 Infinite Acting, Constant $p_{wf}$

This case corresponds with a simulation run where the control mode is the bottom hole pressure and it is kept constant to 8,000 psi. An important point is to investigate the reservoir response for a stress-dependent permeability in terms of pseudo pressure and time, then calculate permeability and skin factor from transient flow period. First at all, it is considered a comparison between the numerical and the analytical solution for non-stress-dependent permeability reservoir; that means gamma is zero ( $\gamma=0$ ). **Fig. 5.6** shows the match between both solutions.

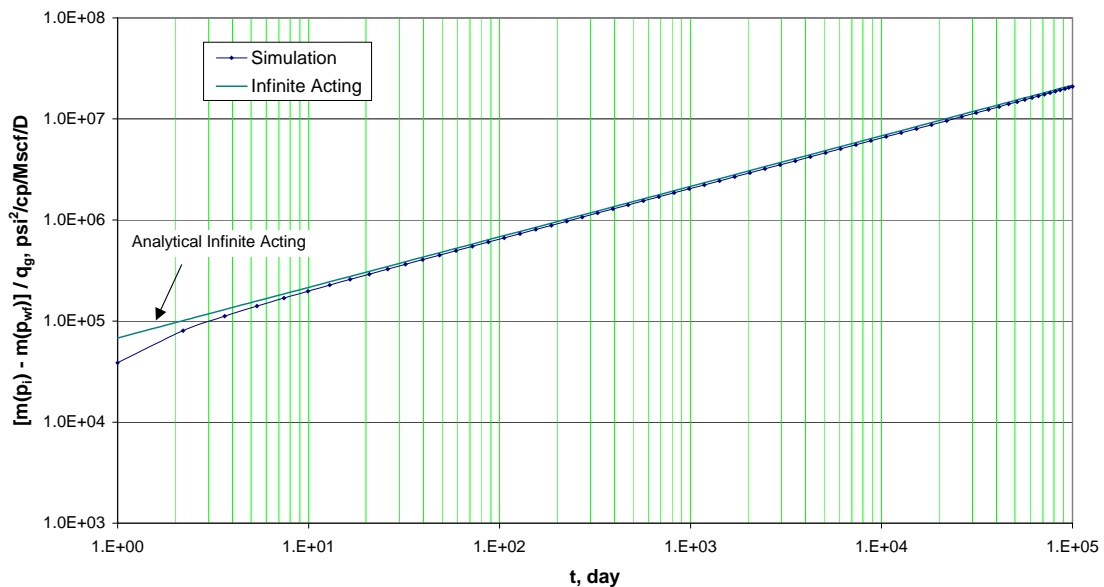


Fig. 5.6 – Log-log plot, analytical and numerical match for infinite acting linear case, constant  $p_{wf}$ .

In Fig. 5.6 is presented the numerical and analytical results in terms of pseudo pressure,  $m(p)$ , and time. Log-Log plot of this variables indicate a straight line with slope 1/2 for

transient flow period in a linear reservoir. Can be observed from the plot that there is a pretty good match between the numerical and analytical solution, however, the first 10 days of simulation there is a numerical error, due to time and space dimension specified in the simulator. The numerical error can be minimized reducing the grid dimensions and time steps in the simulator. This results validate the simulation model for  $\gamma = 0$ .

Then, we will move forward to see the results by incorporating the stress-dependent permeability by increasing the values of gamma in each simulation run. Results are shown in **Fig. 5.7**.

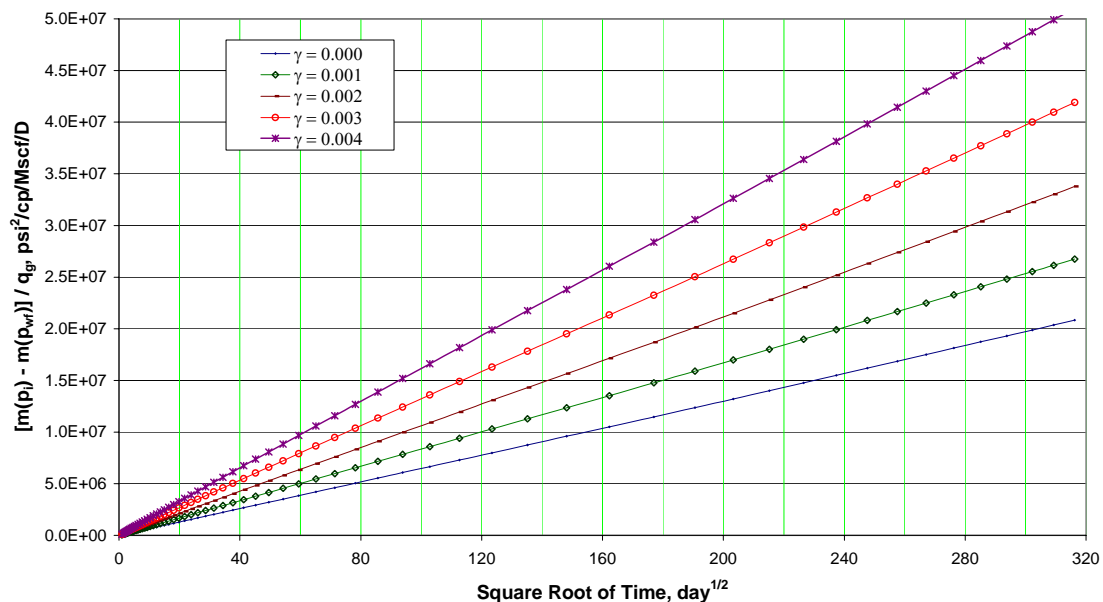


Fig. 5.7 – Square root of time plot, effect of pressure-dependent permeability for an infinite acting linear reservoir producing at constant  $p_{wf} = 8000$  psi.

Fig. 5.7 corresponds with the numerical simulation results for a linear reservoir with constant bottom hole pressure (8,000 psi) considering pressure-dependent permeability. The plot is in the form  $[m(p_i) - m(p_{wf})] / q_g$  vs.  $\sqrt{t}$ . For a non-stress-dependent permeability formation this plot leads to a straight line and from the slope we calculate permeability and skin factor. As it is included pressure-dependent permeability by considering different values of gamma, the result indicate also a straight line for the

transient flow period with a different slope. The higher the value of gamma the higher is the slope of the curve. That results imply a reduction on gas rate production with time as the permeability is reduced in the reservoir and the bottom hole pressure is kept constant, that results obey Darcy's law. An important point to mention here is that for that particular case with a pressure draw down of 8,000 psi all the curves are straight lines.

Then, from each curve in Fig. 5.7 it is calculated the slope and consequently, the permeability of each simulation run to be compared with the initial permeability considered in the reservoir. Results are in **Fig. 5.8**.

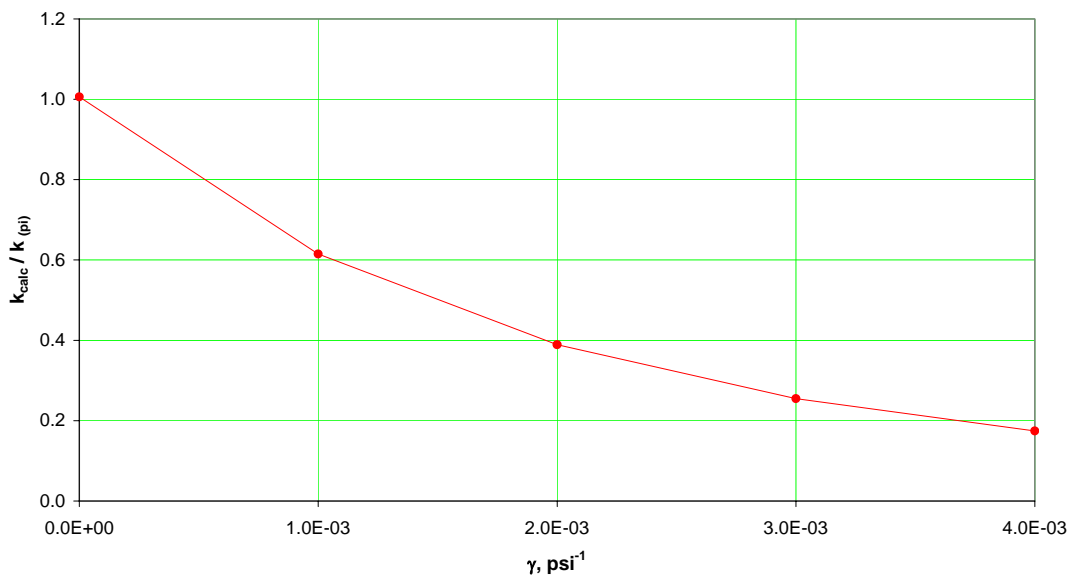


Fig. 5.8 - Permeability ratio vs. gamma, linear case, constant  $p_{wf} = 8000$  psi.

Fig. 5.8 shows permeability ratio versus gamma. It is noticed that for gamma zero there is not reduction on permeability ( $k_{\text{calc}} / k_{\text{pi}} = 1$ ). For higher values of gamma, the permeability calculated from each slope in Fig. 5.7 is lower, becoming almost 82% reduction on permeability for the case with  $\gamma = 0.004$ . The correlation between permeability reduction and gamma has an exponential form.



Skin factor is calculated in a similar way, using the slope of each curve from Fig. 5.7. Equations are described in Appendix E. Results are shown in **Fig. 5.9**. The calculation of skin factor for  $\gamma=0$  is very close to zero ( $s=0.0003$ ); difference is caused by numerical error introduced in the simulator by dimensions in the grid and time steps. The higher values of gamma the more negative is calculated skin factor. The lower value of skin is about  $-0.0319$  and correspond with gamma,  $\gamma = 0.003$ .

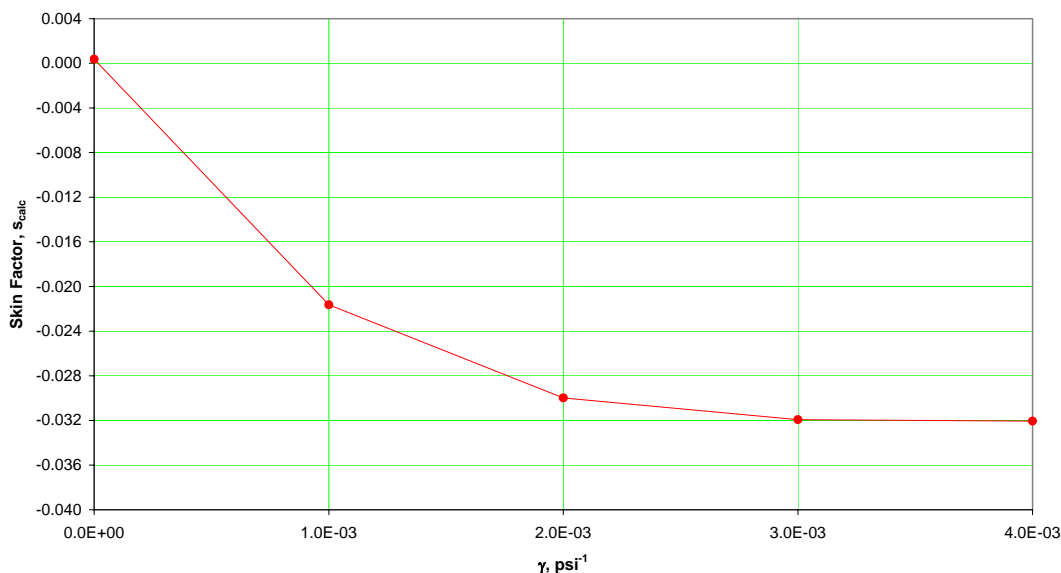


Fig. 5.9 - Skin factor vs. gamma, linear case, constant  $p_{wf} = 8000$  psi.

As it was discussed in the constant gas rate cases, for this constant bottom hole pressure case, an investigation on the range of pressure drop imposed in the reservoir is made. The important point here is to investigate the range of pressure where  $m(p)$  and  $m'(p)$  have a linear relation. Results are discussed in **Fig. 5.10**. The plot is  $m'(p)$  vs.  $m(p)$ . Both variables are the pseudo pressure defined by Al-Hussainy<sup>1</sup>, but the first include the effect of having a stress sensitive formation. Gas properties are calculated using as initial values, a specific gravity of 0.717 and a reservoir temperature of 290°F. Current case corresponds with a constant bottom hole pressure of 8,000 psi, which imply that the pressure drop in the reservoir is constant to 800 psi. Each curve corresponds

with a different value of gamma. For a non-stress sensitive scenario,  $\gamma = 0$ , a straight line is obtained. As gamma start to increase from 0 to 0.004, the curves start to tilt downward, and the relation is not longer linear. The squared dots localized over the continuous lines indicate the range of pressure studied in this case ( $p_{wf}=8,000$  psi). From Fig. 5.10 we can notice a very important difference between this case and the one with constant gas rate (previous case). The squared dots are localized in a region over the continuous line where there is not a linear relation between  $m(p)$  and  $m'(p)$ . That results suggest that lines in Fig. 5.7  $\{[m(p_i)-m(p_{wf})]/q_g \text{ vs. } \sqrt{t}\}$  should not be straight lines, however, based in simulation results they are straight lines. This is a particular result for cases with constant bottom hole pressure; same results were obtained in chapter 4 for cases with a radial geometry.

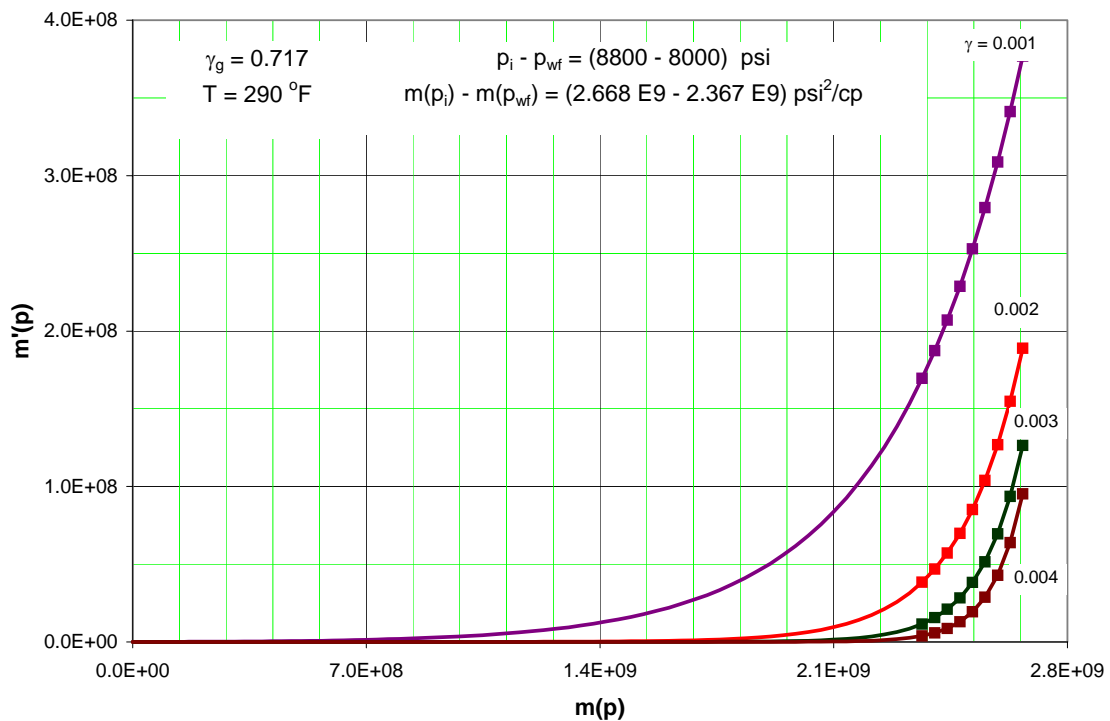


Fig. 5.10 - Plot  $m'(p)$  vs.  $m(p)$ , linear case, constant  $p_{wf} = 8000$  psi.

### 5.3 Finite Acting, Constant $q_g$

In this section the discussion is focused on the pseudo steady state simulation results, and particularly to calculate the Original Gas in Place (OGIP) in the reservoir. It is desirable to investigate how is affected the calculation of OGIP considering the stress dependent permeability through the introduction of the gamma function. The methodology is to deplete the reservoir at constant rate until it reaches the borders, then estimate the dimensions, pore volume and estimate the original volume of hydrocarbon in place. Data files used in simulations are described in Appendix D. Derivation of equations used in this section is described in Appendix E.

Discussion starts with the first case that corresponds with a constant gas rate of 10 Mscf/D in a linear reservoir.

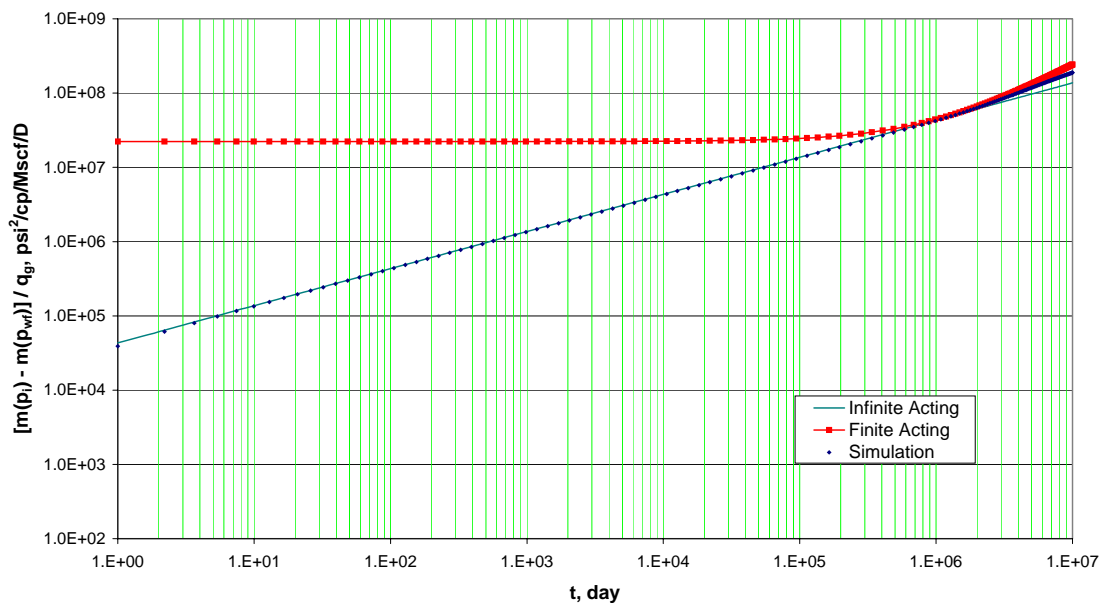


Fig. 5.11- Log-log plot, analytical and numerical match for finite acting linear case, constant  $q_g$ .

It is used the analytical solution of pseudo steady state at the inner boundary, then estimate the reservoir pore volume from the slope of the cartesian plot  $[m(p_i)-m(p_{wf})]/q_g$  vs. time.

**Fig. 5.11** shows the results of compare analytical and numerical solutions for a non-stress sensitive formation. From plot is visible a satisfactory match only for early time. Early time corresponds with transient flow where the reservoir behaves like to be infinite; no limits are found in that portion, and the match is between numerical and transient analytical solutions curves. For about 1,000,000 days start the transition time to pseudo steady state (PSS) period and the match corresponds with the PSS analytical solution curve; we observe from the plot that the match is not satisfactory for that condition of flow, simulation results are always below the analytical solution during PSS. Differences are due to non-linearity in the diffusivity equation, it means that reservoir properties as  $\phi \mu c_t$ , have a significant change with pore pressure.

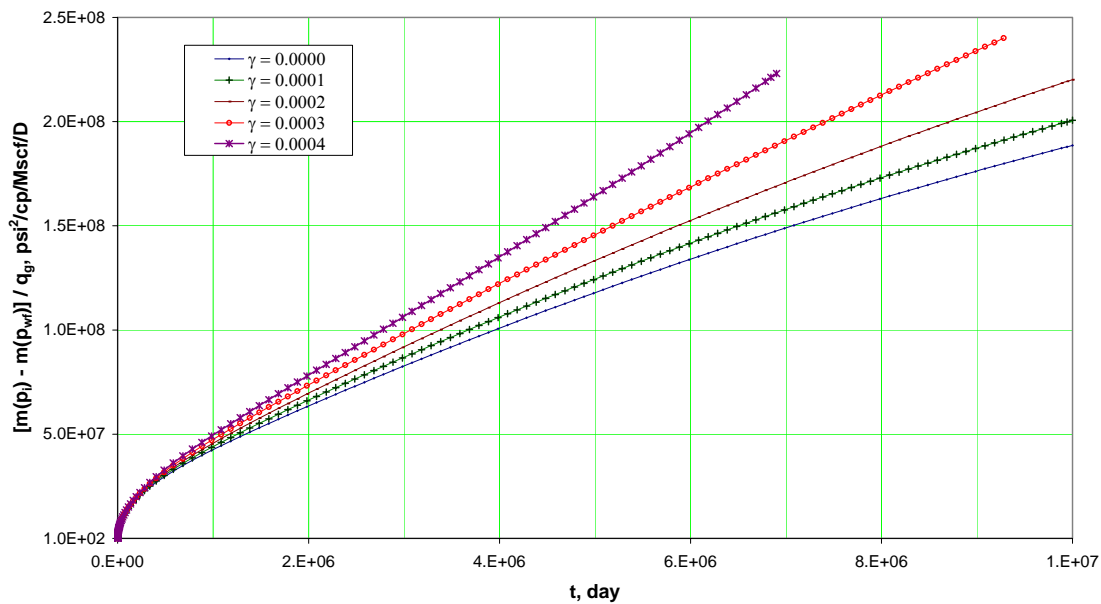


Fig. 5.12 – Cartesian plot, effect of pressure-dependent permeability for a finite acting linear reservoir producing at constant  $q_g = 10$  Mscf/D.

In Fig. 5.12 are shown the numerical simulation results considering stress dependent permeability, this is, regarding several values of gamma. This is a Cartesian plot of pseudo pressure versus time and it reflects the pseudo steady state (PSS) period, analytical solution imply a straight line for a non pressure dependent permeability and small change in term  $\phi\mu c_t$ . Can be noticed that for each gamma a different curve is obtained, and each curve is affected by non-linearity in the diffusivity equation. From that plot is not good to calculate the OGIP, we would obtain a wrong value. To overcome the problem, in this project is used the concept of normalized pseudo time, introduced by Ibraim<sup>22</sup> and described in detail in chapter 2. The normalized pseudo time provides a plotting function for smoothing the production data by taking the effect of reservoir properties change with average pressure.

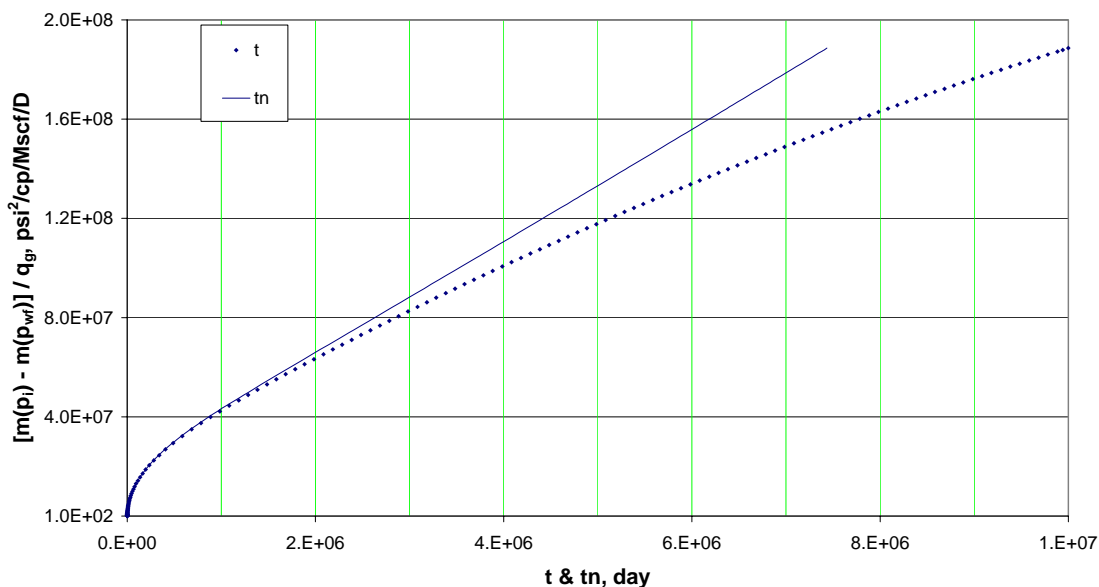


Fig. 5.13 – Normalized pseudo time for  $\gamma = 0$ , linear case, constant  $q_g = 10$  Mscf/D.

Fig. 5.13 shows the result of calculating normalized pseudo time,  $t_n$  for the non pressure dependent permeability, case  $\gamma=0$ . It is clear that the new variable linearizes production

data by considering reservoir properties changes. Then, from the slope of the straight line is calculated the OGIP with more accuracy.

From this analysis can be concluded that the normalized pseudo time gives the correct OGIP because it takes into account the effect of properties change with average reservoir pressure.

A similar method is applied for each curve in Fig. 5.12; they are linearized in terms of reservoir properties variation. As an example of these calculations, result for the case of  $\gamma=0.0003$  is shown in Fig. 5.14.

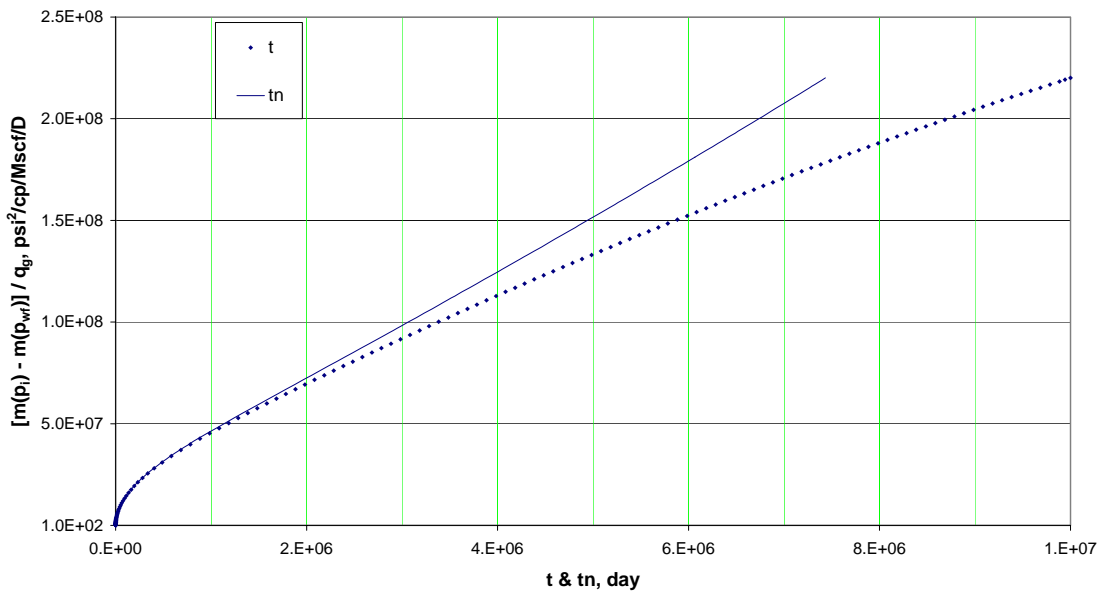


Fig. 5.14 - Normalized pseudo time for  $\gamma = 0.0003$ , linear case, constant  $q_g = 10$  Mscf/D.

It is important to notice that, as the gamma increase, results imply that PSS period start earlier in the model, that agree with the fact that a larger pressure drop is necessary as the permeability decrease in the reservoir due to depletion, and this lead to hit the borders of the reservoir in a smaller time. This is derived making a comparison between Fig. 5.13 and Fig. 5.14; there is a higher slope in the line for a higher gamma.

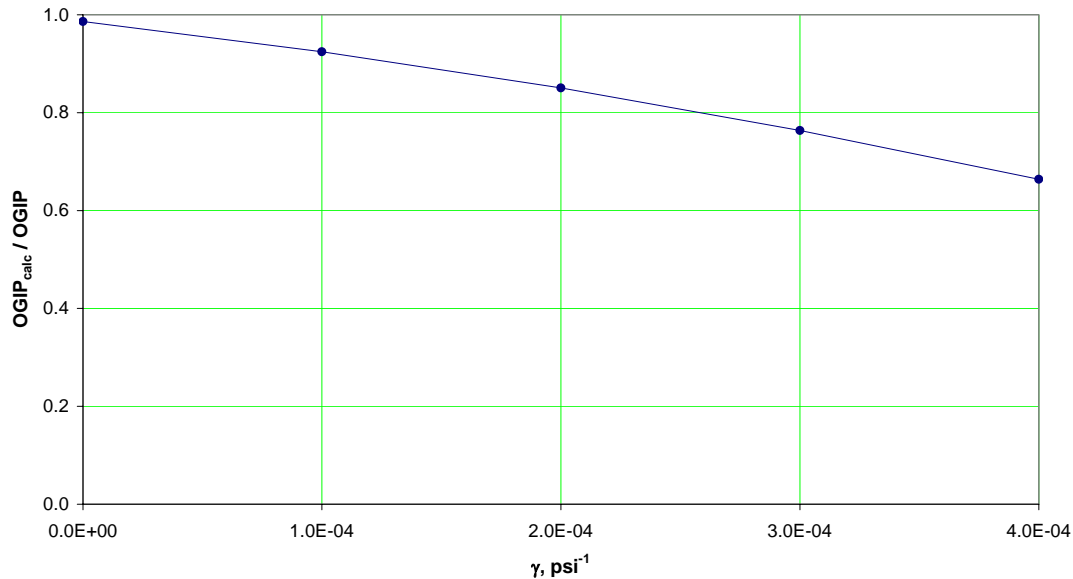


Fig. 5.15 – OGIP ratio vs. gamma, linear case, constant  $q_g = 10$  Mscf/D.

Now, will be discussed the calculation of OGIP. The pore volume of the reservoir is calculated from the slope of each straight line in Fig. 5.13 and 5.14, see Appendix E for detailed description of equations. Then, using initial gas saturation  $S_{gi}$ , of 53% is calculated the OGIP from the volumetric equation. Results are presented in **Fig. 5.15**. This figure plot the ratio of gas in place versus gamma, it is, the OGIP calculated for each value of gamma divided for the OGIP considering a non-stress sensitive formation,  $\gamma=0$ . Fig. 5.15 indicates a proportional reduction of calculated gas in place in the reservoir as gamma increase. The meaning of that result is that the reservoir looks to be of smaller dimensions as gamma increase. This obeys the facts that for higher values of gamma, a larger pressure drop occurs and the limits of the reservoir are reached in an earlier time.

#### 5.4 Finite Acting, Constant $p_{wf}$

This section discusses the results of numerical simulation by depleting the linear reservoir at constant bottom hole pressure. The case considered correspond with a  $p_{wf} = 8,000$  psi, data file is described in Appendix D. The major interest is to analyze the PSS period and estimate pore volume and OGIP in the reservoir.

This case corresponds with a constant pressure drop of 800 psi in the reservoir. To check the validity of the simulation, numerical results are compared with analytical solution for  $\gamma=0$ , this is presented in **Fig. 5.16**.

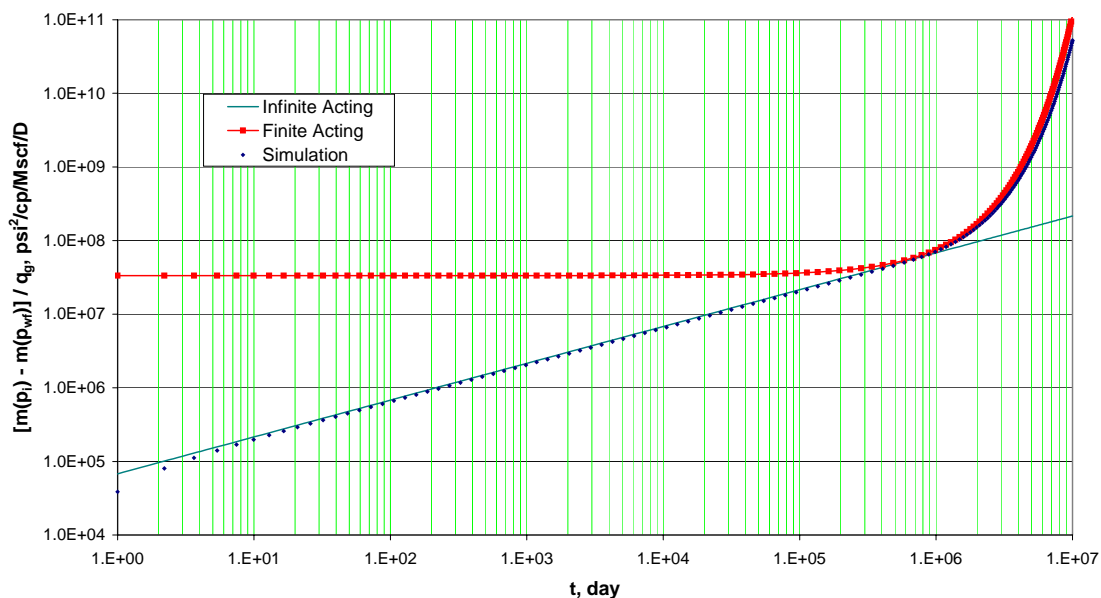


Fig. 5.16 – Log-log plot, analytical and numerical match for finite acting linear case, constant  $p_{wf}$ .

Results are presented in the form  $\log\{[m(p_i)-m(p_{wf})]/q_g\}$  versus  $\log(t)$  in **Fig. 5.16**. From the plot is clear that there is a satisfactory match for infinite acting period, but for PSS condition the match is not good enough. Simulations results are always below the analytical solution during PSS flow, differences are due to non-linearity in the



term  $\phi \mu c_t$ , it means that reservoir properties have a significant change with reservoir pressure.

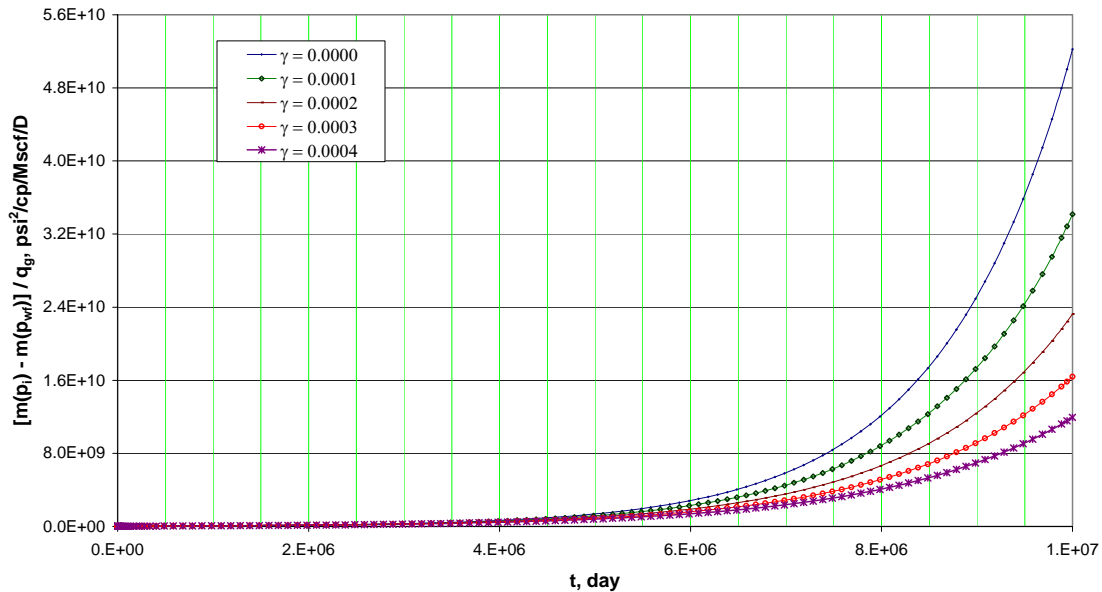


Fig. 5.17 – Cartesian plot, effect of pressure-dependent permeability for a finite acting linear reservoir producing at constant  $p_{wf} = 8000$  psi.

Fig. 5.17 is a Cartesian plot that shows the reservoir response during PSS period, the results are presented for different level of stress dependent permeability, from the line in the top to the line in the bottom, the gamma values increase. For all the range of gamma a different curve is obtained. The analytical solution described in Appendix E imply that a plot of  $\log\{[m(p_i)-m(p_{wf})]/qg\}$  versus  $t$ , lead to a straight line behavior. These results are presented in **Fig. 5.18**. In that figure is made linear the PSS portion of the production data.

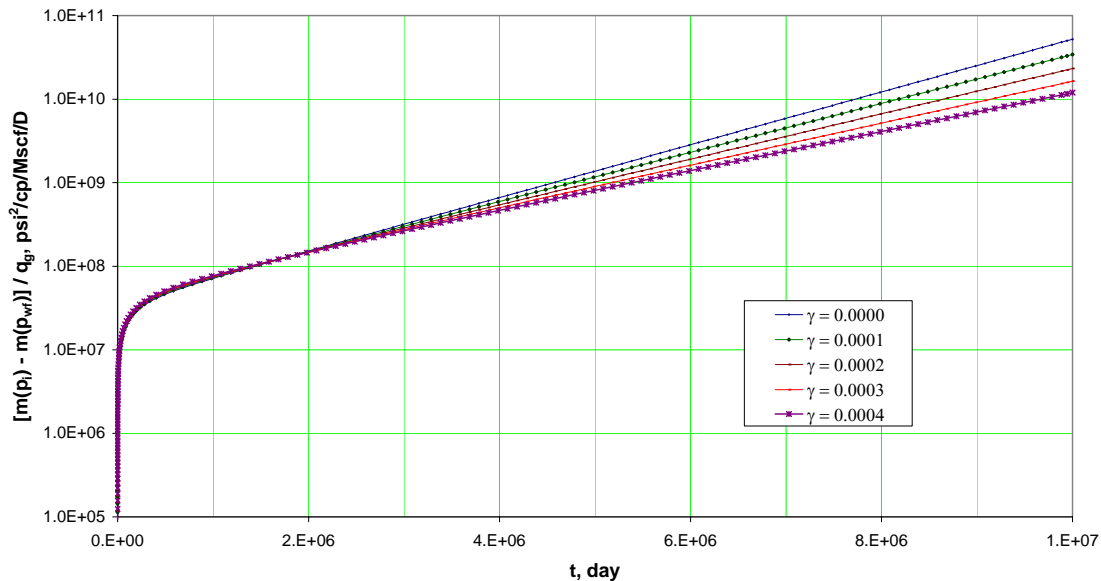


Fig. 5.18 – Semilog plot, pressure-dependent permeability, linear case, constant  $p_{wf} = 8000$  psi.

As gamma is higher, the slope from the curve is higher. Each curve in Fig. 5.18 look straight line, but a closer view reflects that they are not, and are affected by non-linearity in the term  $\phi \mu c_t$ . From that plot we would obtain a wrong value for OGIP. To solve the problem, is used again the concept of normalized pseudo time in a similar way was done in previous case with constant gas rate, it is described in chapter 2 and taken from Ibrahim<sup>22</sup>. **Fig. 5.19** shows the result of calculating normalized pseudo time,  $t_n$  for the non pressure dependent permeability, case  $\gamma = 0$ . From the plot is observable that the new variable linearizes production data by considering reservoir properties changes. Then, from the slope of the straight line is calculated the OGIP with more accuracy. The same method is applied for each curve in Fig. 5.18.

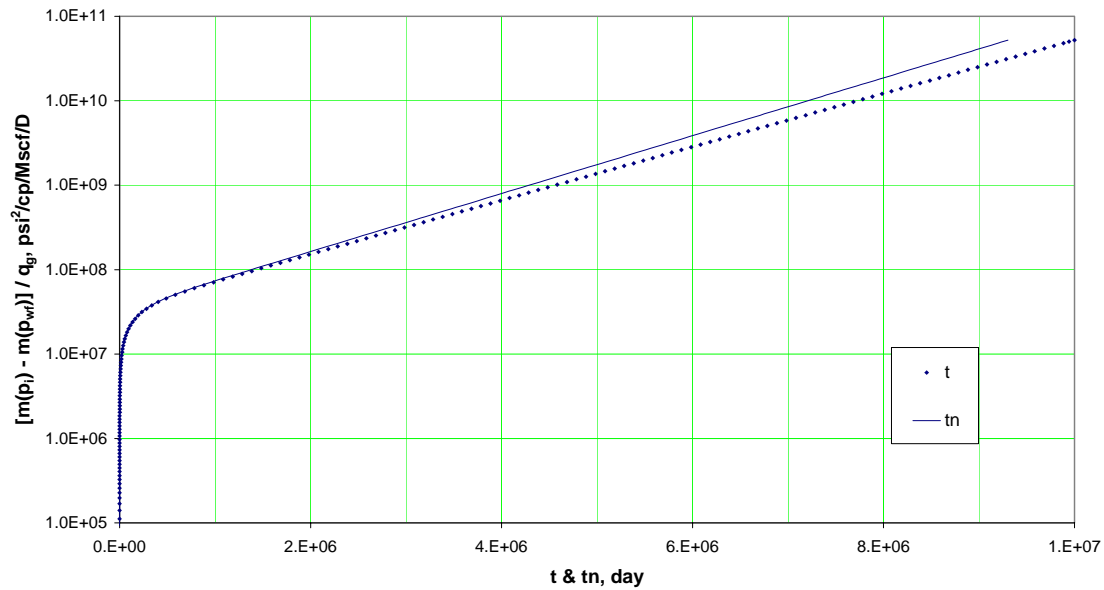


Fig. 5.19 - Normalized pseudo time for  $\gamma = 0.0$ , linear case, constant  $p_{wf} = 8000$  psi.

Then, pore volume and OGIP are calculated from the slope in Fig. 5.19 using the normalized pseudo time. Results are shown in **Fig. 5.20**, and can be seen the effect of a stress dependent permeability on the OGIP calculated. The results indicate a significant increment of calculated gas in place in the reservoir as gamma increase. These results are opposite to the cases with constant gas rate, the reservoir behave like being of larger dimensions for higher values of gamma.

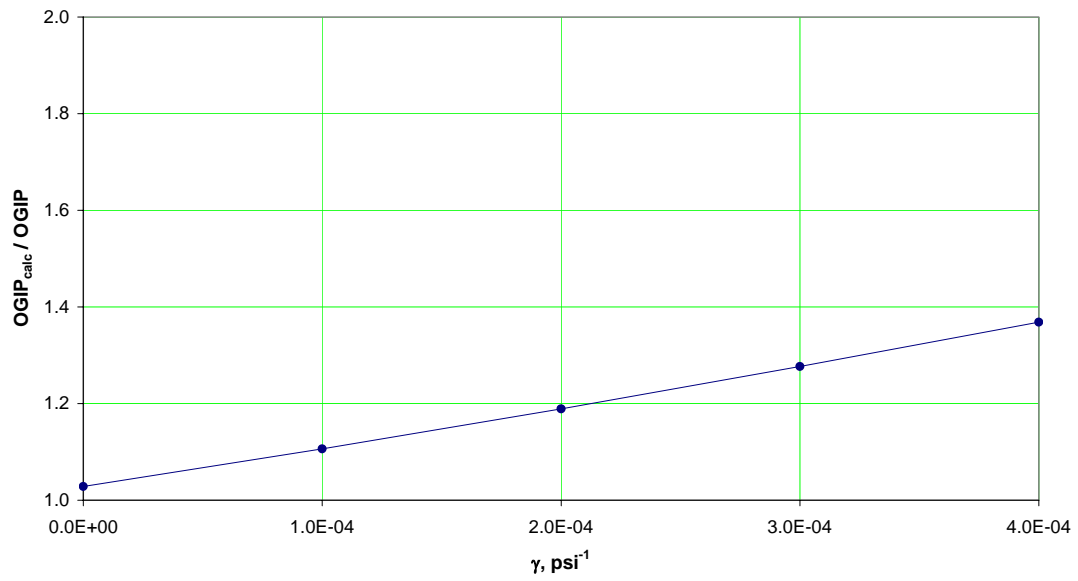


Fig. 5.20 – OGIP ratio vs. gamma, linear case, constant  $p_{wf} = 8000$  psi.

## CHAPTER VI

### ANALYSIS OF RESULTS

This section concerns with the results obtained in chapters IV and V. As it was presented previously, chapter IV refers to a reservoir with a radial geometry and chapter V a linear reservoir. Discussion is based on the results of analytical solution and numerical simulation considering stress dependent permeability.

The analysis is oriented toward solving the problem originally defined at the beginning of this project in chapter I. In that section, was mentioned the necessity to investigate the errors introduced estimating some reservoir parameters by using conventional well testing analysis of a tight gas reservoir. Tight gas reservoirs exhibit stress sensitive permeability, and for such reservoirs, pressure transient analysis and forecast performance based on constant rock properties, especially permeability, can lead to significant errors in parameters estimation.

Now, following is a discussion of some important results from this project:

- 1) For all cases analyzed, radial and linear models, a satisfactory match was reached between the analytical solution and numerical simulation. Both, infinite acting and finite acting period time have been matched with the corresponding analytical solution considering constant  $q_g$  and  $p_{wf}$  cases. This validates the performance of simulator GASSIM.
- 2) For radial and linear model cases with low constant  $q_g$ , a straight line is obtained in the plot of pseudo pressure versus time during infinite acting period. That means, for low draw down cases a straight line with different slope is obtained when considering pressure dependent permeability. Permeability calculated from that slope is lower than the correct value of the reservoir. Skin factor is also miscalculated.

- 3) When considering a larger draw down for radial and linear model, constant  $q_g$ , infinite acting results indicate that curves in the plot pseudo pressure versus time are straight lines for low values of gammas and start to bending upward for large values of gammas. These cases introduce significantly larger errors when calculating permeability and skin factor.
- 4) In all cases with constant  $p_{wf}$ , radial and linear geometry, an important conclusion is derived. For low and large draw down, results indicate a straight line for infinite acting period in all range of gamma. That means a straight line with different slope is obtained for each value of gamma. These results differ from that obtained with constant  $q_g$  cases. A significant error is introduced when estimating permeability and skin factor. That results lead to the conclusion that is not possible to identify a stress dependent permeability from the constant bottom hole pressure draw down scenario.
- 5) From results of reservoir infinite acting period we can conclude that permeability reduction depends on gamma and reservoir draw down,  $q_g$  or  $p_{wf}$ , and that no correlation can be made.
- 6) For finite acting period analysis, in all cases considered with constant  $q_g$  and  $p_{wf}$ , the OGIP is miscalculated. The level of error on calculations depends on the draw down in the reservoir. The use of normalized pseudo time was necessary to correct for changes in reservoir properties.
- 7) From results of reservoir finite acting period we can say that no correlation can be made for calculation of OGIP; results depend on reservoir draw down,  $q_g$  or  $p_{wf}$  and gamma.

In this project have been demonstrated the level of errors in the determination of permeability, skin factor and OGIP using conventional well test analysis instead of a pressure dependent permeability model. All of these results have a great impact in business decisions and profitability for the oil company.

Miscalculation in the permeability and skin factor can lead to take wrong decisions regarding well stimulation. That means to invest additional money to make well stimulation jobs when there are not necessary, and it reduces the well profitability.

In the case of OGIP calculation, in most of the cases it is sub estimated, calculated values are lower than the correct value. It can be taken as an advantage; if we consider that additional gas wells and reserves would be incorporated in the exploitation plan.

## CHAPTER VII

### CONCLUSIONS

During the development of this project, the following conclusions were obtained:

- If pressure-dependence of permeability  $k(p)$  is ignored, erroneous values of permeability, skin factor and OGIP will be calculated from well test analysis of tight gas reservoirs.
- In constant gas rate cases, for both radial and linear reservoir geometry, the plot of pseudo pressure versus time give a straight line with different slopes for cases with small draw down during infinite acting flow. For large draw down (larger pressure range) curves start to bending up and straight line not longer exist. Then, calculated  $k$  and  $s$  are wrong and depend on the case ( $q_g$  considered).
- In constant bottom hole pressure cases, radial and linear reservoir geometry, the plot of pseudo pressure versus time give a straight line during infinite acting flow for all range of  $p_{wf}$  considered, small and large draw down. A straight line with different slope is obtained for each value of gamma. Results imply that is not possible to identify a stress dependent permeability from a constant bottom hole pressure draw down scenario. Calculated  $k$  and  $s$  are wrong and depend on the case ( $p_{wf}$  considered).
- From results of reservoir infinite acting period we can conclude that permeability reduction depends on gamma and reservoir draw down,  $q_g$  or  $p_{wf}$ , and that no correlation can be made.
- For finite acting period analysis, in all cases considered with constant  $q_g$  and  $p_{wf}$ , the OGIP is miscalculated. The level of error on calculations depends on the



draw down in the reservoir. The use of normalized pseudo time was necessary to correct for changes in reservoir properties.

- From results of reservoir finite acting period we can say that no correlation can be made for calculation of OGIP; results depend on reservoir draw down,  $q_g$  or  $p_{wf}$  and gamma.
- In this project I have demonstrated the level of errors in the determination of permeability, skin factor and OGIP using conventional well test analysis instead of a pressure dependent permeability model
- The great impact of permeability, skin factor and OGIP calculations are traduced in business decisions and profitability for the oil company. Miscalculation in the permeability and skin factor can lead to take wrong decisions regarding well stimulation. That means to invest additional money to make well stimulation jobs when there are not necessary, and it reduces the well profitability.
- In the case of OGIP calculation, in most of the cases it is sub estimated, calculated values are lower than the correct value. It can be taken as an advantage; if we consider that additional gas wells and reserves would be incorporated in the exploitation plan.
- In the absence of lab data, this project proves that permeability modulus concept is a good mathematical approximation to define a relationship for permeability and pore pressure in the tight gas reservoir.

## NOMENCLATURE

$B$  = formation volume factor, rcf/scf

$c$  = fluid compressibility, 1/psi

$c_f$  = rock compressibility, 1/psi

$c_t$  = total system compressibility, 1/psi

$J_g$  = gas productivity index, Mscf.cp/D/psi<sup>2</sup>

$k$  = permeability, md

$m(p)$  = real gas pseudo pressure, psi<sup>2</sup>/cp

$m(p_{bar})$  =  $m(p)$  at average reservoir pressure, psi<sup>2</sup>/cp

$m(p_i)$  =  $m(p)$  at initial reservoir pressure, psi<sup>2</sup>/cp

$m(p_{wf})$  =  $m(p)$  at flowing wellbore pressure, psi<sup>2</sup>/cp

$OGIP$  = Original Gas in Place, m<sup>3</sup>, scf

$p$  = pore pressure, psia

$p_{bar}$  = average reservoir pressure, psi

$p_D$  = dimensionless pressure

$p_i$  = initial pore pressure, psia

$PSS$  = pseudo-steady state condition

$p_{wf}$  = bottom-hole pressure, psi

$q_g$  = gas flow rate, Mscf/D

$r$  = radial distance from center of well, ft

$r_d$  = drainage boundary radius, ft

$r_w$  = wellbore radius, ft

$T$  = temperature, °R

$t_D$  = dimensionless time

$z$  = gas deviation factor

$\phi$  = porosity

$\mu$  = viscosity, cp

$\rho$  = fluid density, lbm/ft<sup>3</sup>

$\nabla$  = gradient

$\gamma$  = “gamma” permeability modulus

$\mu(p)$  = viscosity as function of pressure, cp

$\tilde{m}_{PSS}$  = Cartesian slope of  $m(p_i) - m(p_{wf})/q_g$  versus pseudo time, psi<sup>2</sup>/cp/Mscf

$m(p)$  = modified gas pseudo pressure considering  $k(p)$ , md\*psia<sup>2</sup>/cp

### Subscripts

$Ac$  = cross sectional area

$calc$  = calculated

$D$  = dimensionless

$g$  = gas

$i$  = initial

$r$  = radial

$z$  = vertical

## REFERENCES

- 1) Al-Hussainy, R., Ramey, H.R. Jr., and Crawford, P.B.: "The Flow of Real Gases Through Porous Media," *JPT* (May 1966) 624-36; Trans. AIME, **237**.
- 2) Raghavan, R., Scorer, J. D. T., and Miller, F. G.: "An Investigation by Numerical Methods of the Effect of Pressure-Dependent Rock and Fluid Properties on Well Flow Tests," *SPEJ* (June 1972) 267-75; Trans., AIME **253**.
- 3) Vairogs, J., and Rhoades, V.W. : "Pressure Transient Tests in Formations Having Stress-Sensitive Permeability," *JPT* (Aug. 1973) 965-970; Trans., AIME **255**.
- 4) Samaniego-V, F., Brigham, W. E., and Miller, F. G.: "An Investigation of Transient Flow of Reservoir Fluids Considering Pressure-Dependent Rock and Fluid Properties," *SPEJ* (Apr. 1977) 140-50; Trans., AIME **263**.
- 5) Gochmour, J.R., and Slater, G.E.: "Well Test Analysis in Tight Gas Reservoirs," Paper SPE 6842 presented at the 52<sup>nd</sup> Annual Fall Technical Conference and Exhibition, Denver, Colorado, Oct. 1977, 1-10.
- 6) Walls, J.D.: "Tight Gas Sands: Permeability, Pore Structure and Clay," Paper SPE 9871 presented at the 1981 SPE/DOE Low Permeability Symposium, Denver, Colorado, May 1981.
- 7) Pedrosa, O.A.: "Pressure Transient Response in Stress-Sensitive Formations," Paper SPE 15115 presented at the 56<sup>th</sup> California Regional Meeting, Oakland, CA, Apr. 1986, 203-210.

- 8) Ostensen, R.W.: "The Effect of Stress-Dependent Permeability on Gas Production and Well Testing," *SPE Formation Evaluation* (June 1986) 227-235.
- 9) Samaniego, F., and Cinco-Ley, H.: "On the Determination of the Pressure-Dependent Characteristics of a Reservoir Through Transient Pressure Testing," Paper SPE 19774 presented at the 64<sup>th</sup> Annual Technical Conference and Exhibition, San Antonio, Texas, Oct. 1989, 9-20.
- 10) Kikani, J., and Pedroza, O.A.: "Perturbation Analysis of Stress-Sensitive Reservoirs," *SPE Formation Evaluation* (Sept. 1991) 379-386.
- 11) Zhang, M.Y., and Ambastha, A.K.: "New Insights in Pressure-Transient Analysis for Stress-Sensitive Reservoirs," Paper SPE 28420 presented at the SPE 69<sup>th</sup> Annual Technical Conference and Exhibition, New Orleans, LA, Sept. 1994, 617-628.
- 12) Jelmert, T.A., and Selseng, H.: "Pressure Transient Behavior of Stress-Sensitive Reservoirs," Paper SPE 38970 presented at the 1997 SPE Latin American/Caribbean Petroleum Engineering Conference, Rio de Janeiro, Brazil, Aug. 1997, 1-10.
- 13) Davies, J.P., and Davies, D.K. : "Stress-Dependent Permeability: Characterization and Modeling," Paper SPE 56813 presented at the 1999 SPE Annual Technical Conference and Exhibition, Houston, Texas, Oct. 1999, 1-16.
- 14) Lee, W.J., and Hopkins, C.W.: "Characterization of Tight Reservoirs," *JPT* (Nov. 1994) 956-964.
- 15) Lee, W. J.: *Well Testing*, SPE Textbook Series, Texas, Vol. 1, 1982.

- 16) Wattenbarger, R.A., and Ramey, H.J.: "Gas Well Testing with Turbulence, Damage and Wellbore Storage" Paper SPE 1835 presented at the SPE 42nd Annual Fall Meeting, Houston, Texas, Oct. 1967, 1-11.
- 17) Agarwal, R.G.: "Real Gas Pseudo-Time. A New Function for Pressure Buildup Analysis of MHF Gas Wells" Paper SPE 8279 presented at the SPE 54th Annual Fall Technical Conference and Exhibition, Las Vegas, Nevada, Sept. 1979, 1-12.
- 18) Vairogs, J., Hearn, C. L., Dareing, D. W., and Rhoades, V. W.: "Effect of Rock Stress on Gas Production from Low-Permeability Reservoirs," *JPT* (September 1971) 1161-67; *Trans., AIME*, **251**.
- 19) Davies, J.P., and Holditch, S.A.: "Stress Dependent Permeability in Low Permeability Gas Reservoirs: Travis Peak Formation, East Texas," Paper SPE 39917 presented at the 1998 SPE Rocky Mountain Regional/Low Permeability Reservoirs Symposium and Exhibition, Denver, Colorado, Apr. 1998, 117-128.
- 20) Nur A., and Yilmaz, O.: "Pore Pressure in Fronts in Fractured Rock Systems," Dept. of Geophysics, Stanford U., Stanford, CA (1985).
- 21) Wattenbarger, R. A., El-Banbi A. H., Villegas M. E. and Maggard, J. B.: "Productivity Analysis of Linear Flow Into Fractured Tight Gas Wells," Paper SPE 39931 presented at the 1998 SPE Rocky Mountain Regional/Low-Permeability Reservoirs Symposium and Exhibition, Denver, Colorado, Apr. 5-8, 1-15.
- 22) Arevalo-Villagran, J. A., Wattenbarger, R. A., Samaniego-Verduzco, F., and Pham, T. T.: "Production Analysis of Long-Term Linear Flow in Tight Gas Reservoirs: Case Histories," Paper SPE 71516 presented at the 2001 Annual Technical Conference and Exhibition, New Orleans, LA, Sept. 30 - Oct. 3, 1-15.

- 23) Lee, W. J., and Wattenbarger, R. A.: *Gas Reservoir Engineering*, SPE Textbook Series, Texas, Vol. 5, 1996.
  
- 24) Ibrahim, M., Wattenbarger, R. A., and Helmy, W.: "Determination of *OGIP* for Wells in Pseudo-steady-State-Old Techniques, New Approaches," Paper SPE 84286, presented at the 2003 SPE Annual Technical Conference and Exhibition, Denver, Colorado, Oct. 5-8, 1-12.

## APPENDIX A

## REAL GAS DIFFUSIVITY EQUATION

Following is the derivation of the diffusivity equation considering real gas fluid. It begins with definition of continuity equation, Darcy's Law and equation of state for real gas as:

Continuity Equation:

$$\nabla \cdot \rho \bar{u} = - \frac{\partial(\phi\rho)}{\partial t} \dots\dots\dots(A.1)$$

Darcy's Law:

$$\bar{u} = -\frac{k}{\mu} \nabla p \dots\dots\dots(A.2)$$

Equation of State:

$$\rho = \frac{pM}{zRT} \dots\dots\dots(A.3)$$

Substituting Eq. (A.2) and (A.3) in Eq. (A.1) yield:

$$\nabla \cdot \frac{pM}{zRT} \left( -\frac{k}{\mu} \nabla p \right) = - \frac{\partial}{\partial t} \left( \phi \frac{pM}{zRT} \right) \dots\dots\dots(A.4)$$

Simplifying eq. (A.4):

$$\nabla \cdot k \frac{p}{z\mu} \nabla p = \frac{\partial}{\partial t} \left( \phi \frac{p}{z} \right) \dots\dots\dots(A.5)$$

Defining a pseudo pressure variable as:

$$m(p) = 2 \int_{p_o}^p \frac{p}{z\mu} dp \dots\dots\dots(A.6)$$

And we can write a derivative of Eq. (A.6) as follow:

$$\frac{dm}{d\xi} = \frac{2p}{z\mu} \frac{dp}{d\xi} \text{ and } \nabla m = \frac{2p}{z\mu} \nabla p \dots\dots\dots(A.7) \text{ \& (A.8)}$$



Rearranging Eq. (A.5) yield:

$$\nabla \cdot \frac{2p}{z\mu} \nabla p = \frac{2}{k} \frac{\partial}{\partial t} \left( \phi \frac{p}{z} \right) \dots \dots \dots (A.9)$$

Substituting Eq. (A.8) into Eq. (A.9) yield:

$$\nabla \cdot \nabla m = \frac{2}{k} \frac{\partial}{\partial t} \left( \phi \frac{p}{z} \right) \dots \dots \dots (A.10)$$

Expanding and using chain rule in Eq. (A.10) yield:

$$\nabla^2 m = \frac{2}{k} \left[ \phi \frac{d}{dp} \left( \frac{p}{z} \right) + \frac{p}{z} \frac{d\phi}{dp} \right] \frac{\partial p}{\partial t} \dots \dots \dots (A.11)$$

Multiplying and dividing by the same factor in Eq. (A.11):

$$\nabla^2 m = \frac{2}{k} \frac{z\mu}{2p} \left[ \phi \frac{d}{dp} \left( \frac{p}{z} \right) + \frac{p}{z} \frac{d\phi}{dp} \right] \frac{2p}{z\mu} \frac{\partial p}{\partial t} \dots \dots \dots (A.12)$$

Substituting Eq. (A.7) into Eq. (A.12) yield:

$$\nabla^2 m = \frac{\phi\mu}{2} \left[ \frac{z}{p} \frac{d}{dp} \left( \frac{p}{z} \right) + \frac{1}{\phi} \frac{d\phi}{dp} \right] \frac{\partial m}{\partial t} \dots \dots \dots (A.13)$$

Using definition of real gas compressibility:

$$c = \frac{1}{\rho} \frac{d\rho}{dp} = \frac{zRT}{pM} \frac{d}{dp} \left( \frac{pM}{zRT} \right) = \frac{z}{p} \frac{d}{dp} \left( \frac{p}{z} \right) \dots \dots \dots (A.14)$$

Eq. (A.13) is simplified by:

$$\nabla^2 m = \frac{\phi\mu}{k} (c + c_f) \frac{\partial m}{\partial t} \dots \dots \dots (A.15)$$

Finally, real gas diffusivity equation is:

$$\boxed{\nabla^2 m = \frac{\phi\mu c_t}{k} \frac{\partial m}{\partial t}} \dots \dots \dots (A.16)$$

## APPENDIX B

REAL GAS DIFFUSIVITY EQUATION CONSIDERING PRESSURE DEPENDENT  
PERMEABILITY

Following is the derivation of the diffusivity equation considering real gas fluid and pressure-dependent permeability. It begins with definition of continuity equation, Darcy's Law and equation of state for real gas as:

Continuity Equation:

$$\nabla \bullet \rho \vec{u} = - \frac{\partial(\phi\rho)}{\partial t} \dots\dots\dots(B.1)$$

Darcy's Law:

$$\vec{u} = -\frac{k}{\mu} \nabla p \dots\dots\dots(B.2)$$

Equation of State:

$$\rho = \frac{pM}{zRT} \dots\dots\dots(B.3)$$

Substituting Eq. (B.2) and (B.3) into Eq. (B.1) yield:

$$\nabla \bullet \frac{pM}{zRT} \left( -\frac{k}{\mu} \nabla p \right) = - \frac{\partial}{\partial t} \left( \phi \frac{pM}{zRT} \right) \dots\dots\dots(B.4)$$

Simplifying Eq. (B.4) yield:  $\nabla \bullet k \frac{p}{z\mu} \nabla p = \frac{\partial}{\partial t} \left( \phi \frac{p}{z} \right) \dots\dots\dots(B.5)$

Defining pseudo pressure as follow:

$$m'(p) = 2 \int_0^p \frac{kp}{z\mu} dp \dots\dots\dots(B.6)$$

Derivative of pseudo pressure is defined as:

$$\frac{dm'(p)}{d\xi} = \frac{2kp}{z\mu} \frac{dp}{d\xi} \dots\dots\dots(B.7)$$

Eq. (B.7) can expressed as:

$$\nabla m'(p) = \frac{2kp}{z\mu} \nabla p \dots\dots\dots(B.8)$$

Substituting Eq. (B.8) in Eq. (B.5) yield:

$$\nabla \bullet \nabla m'(p) = 2 \frac{\partial}{\partial t} \left( \phi \frac{p}{z} \right) \dots\dots\dots(B.9)$$

Expanding Eq. (B.9) and using chain rule:

$$\nabla^2 m'(p) = 2 \left[ \phi \frac{d}{dp} \left( \frac{p}{z} \right) + \frac{p}{z} \frac{d\phi}{dp} \right] \frac{dp}{dt} \dots\dots\dots(B.10)$$

Multiplying and dividing by the same factor in Eq. (B.10):

$$\nabla^2 m'(p) = 2 \frac{z\mu}{2kp} \left[ \phi \frac{d}{dp} \left( \frac{p}{z} \right) + \frac{p}{z} \frac{d\phi}{dp} \right] \frac{2kp}{z\mu} \frac{\partial p}{\partial t} \dots\dots\dots(B.11)$$

Rearranging Eq. (B.11) yield:

$$\nabla^2 m'(p) = \frac{\phi\mu}{k} \left[ \frac{z}{p} \frac{d}{dp} \left( \frac{p}{z} \right) + \frac{1}{\phi} \frac{d\phi}{dp} \right] \frac{\partial m'(p)}{\partial t} \dots\dots\dots(B.12)$$

Using definition of real gas compressibility:

$$c = \frac{1}{\rho} \frac{d\rho}{dp} = \frac{zRT}{pM} \frac{d}{dp} \left( \frac{pM}{zRT} \right) = \frac{z}{p} \frac{d}{dp} \left( \frac{p}{z} \right) \dots\dots\dots(B.13)$$

Eq. (B.13) is simplified by:

$$\nabla^2 m'(p) = \frac{\phi\mu}{k} (c + c_f) \frac{\partial m'(p)}{\partial t} \dots\dots\dots(B.14)$$

Finally, real gas diffusivity equation is:

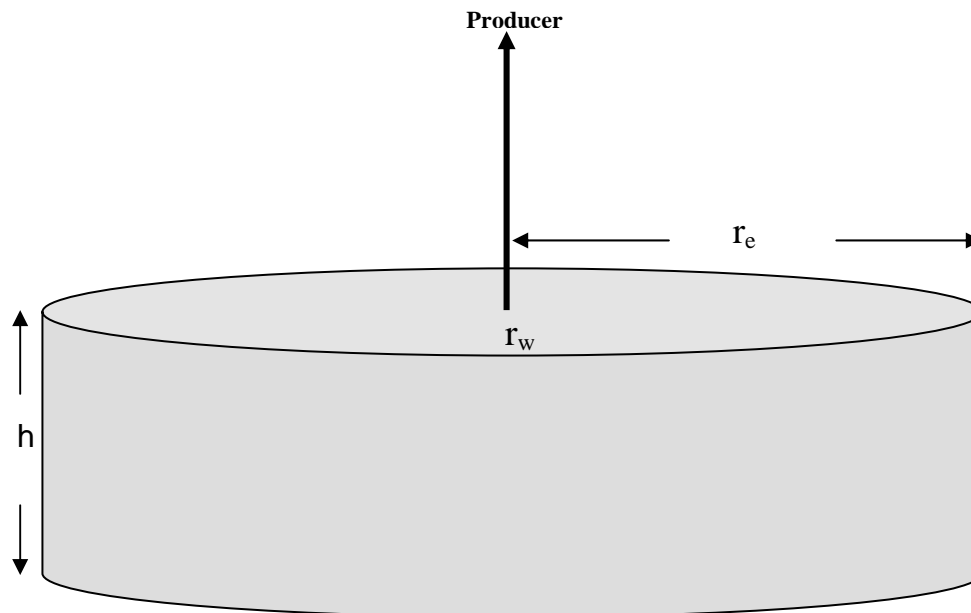
$$\boxed{\nabla^2 m'(p) = \frac{\phi\mu c_t}{k} \frac{\partial m'(p)}{\partial t}} \dots\dots\dots(B.15)$$

## APPENDIX C

## RADIAL AND LINEAR MODELS

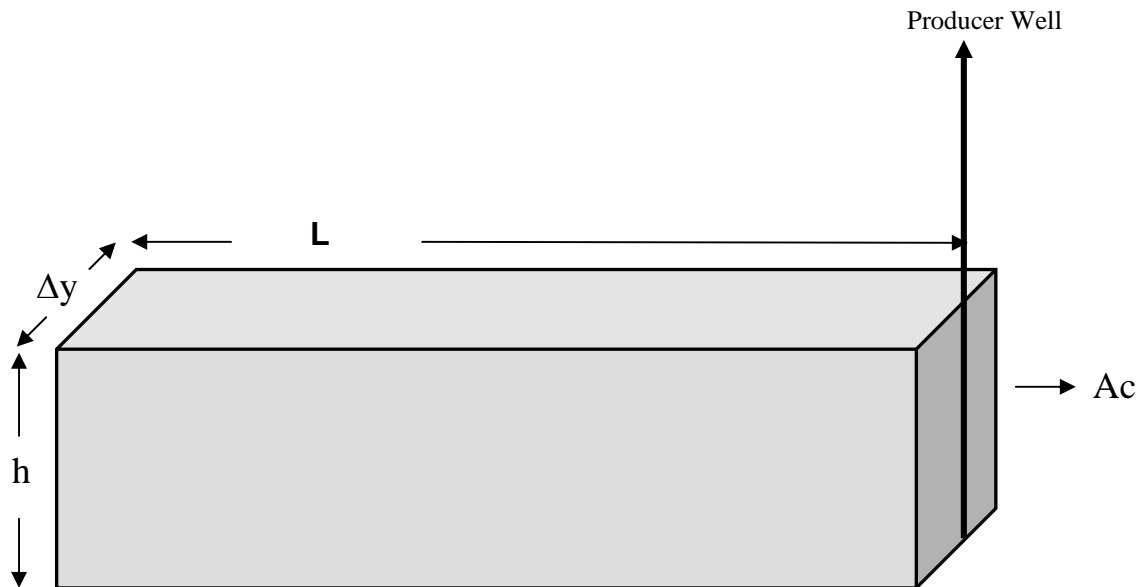
Following is a brief description of the radial and linear models used in the current project. It is included the dimensions of each models as well as some initial reservoir parameters.

## 1) Radial Model



Property	Value
$r_e$ , ft	3,000
$r_w$ , ft	0.25
$h$ , ft	362
$T$ , °R	750
$B_{gi}$ , rcf/scf	0.0031371
$S_{wi}$ , fraction	0.47
$\phi$ , fraction	0.15
$k$ , md	0.0025
Pore Volume, PV, Brcf	1.53
OGIP, Bscf	259.37

## 2) Linear Model



Property	Value
L, ft	15,994
$A_c$ , ft <sup>2</sup>	640,000
h, ft	800
$\Delta y$ , ft	800
T, °R	750
B <sub>gi</sub> , rcf/scf	0.0031371
S <sub>wi</sub> , fraction	0.47
$\phi$ , fraction	0.15
k, md	0.0025
Pore Volume, PV, Brcf	1.53
OGIP, Bscf	259.37

APPENDIX D  
GASSIM DATA FILES

1) Radial Case, Constant  $q_g$

```

CMNT Radial Case, Pressure-Dependent Permeability, Constant Rate for Gas well
CMNT
CMNT Single Value Data
CMNT
IMAX 53
JMAX 1
CMNT (cf)model = (cf + Swi*cw)/(1-Correction for water
RWEL 0.25
CROC 4.08E-06
GRAV 0.717
PREF 8800
TSC 520
PSC 14.65
T 750
NEWT 4
BETA 0
TABL 0
IMAP 1
SWAT 0.47
CWAT 4.1E-06
GAMMA 0
END
CMNT
CMNT Grid Data
CMNT
KX 0.0025
KY 0.0025
PHI 0.15
POI 8800
CMNT
RR -1
0.3 0.36 0.43 0.51 0.61 0.72 0.86 1.03 1.23 1.47
1.76 2.1 2.5 2.99 3.57 4.26 5.09 6.07 7.25 8.65
10.33 12.34 14.73 17.58 20.99 25.06 29.92 35.73 42.65 50.92
60.8 72.58 86.66 103.46 123.52 147.47 176.06 210.2 250.96 299.62
357.71 427.07 509.88 608.74 726.77 867.68 1035.92 1236.78 1474.59 1762.89
2104.7 2512.79 3000
CMNT
DELY 361.99
END
CMNT
CMNT Schedule Data
CMNT
PMAP 2
PLOT 2
CMNT
NAME 1 1 1 0 0
ALPH 1.2
DELT 1
DTMX 20
QG 1 10000
PMIN 1 100
TIME 1000
END

```

2) Radial Case, Constant  $p_{wf}$ 

```

CMNT Radial Case, Pressure-Dependent Permeability, Constant Pwf for Gas well
CMNT
CMNT Single Value Data
CMNT
IMAX 53
JMAX 1
CMNT (cf)model = (cf + Swi*cw)/(1-Correction for water
RWEL 0.25
CROC 4.08E-06
GRAV 0.717
PREF 8800
TSC 520
PSC 14.65
T 750
NEWT 4
BETA 0
TABL 0
IMAP 1
SWAT 0.47
CWAT 4.1E-06
GAMMA 0
END
CMNT
CMNT Grid Data
CMNT
KX 0.0025
KY 0.0025
PHI 0.15
POI 8800
CMNT
RR -1
0.3 0.36 0.43 0.51 0.61 0.72 0.86 1.03 1.23 1.47
1.76 2.1 2.5 2.99 3.57 4.26 5.09 6.07 7.25 8.65
10.33 12.34 14.73 17.58 20.99 25.06 29.92 35.73 42.65 50.92
60.8 72.58 86.66 103.46 123.52 147.47 176.06 210.2 250.96 299.62
357.71 427.07 509.88 608.74 726.77 867.68 1035.92 1236.78 1474.59 1762.89
2104.7 2512.79 3000
CMNT
DELY 361.99
END
CMNT
CMNT Schedule Data
CMNT
PMAP 2
PLOT 2
CMNT
NAME 1 1 1 0 0
ALPH 1.2
DELT 1
DTMX 20
QG 1 10000
PWF 1 4000
TIME 1000
END

```

3) Linear Case, Constant  $q_g$ 

```

CMNT Linear Case, Pressure-Dependent Permeability, Constant Rate for Gas well
CMNT
CMNT Single Value Data
CMNT
IMAX 105
JMAX 1
CMNT (cf)model = (cf + Swi*cw)/(1-Correction for water
CMNT 0.25
CROC 4.08E-06
GRAV 0.717
PREF 8800
TSC 520
PSC 14.65
T 750
NEWT 4
BETA 0
TABL 0
IMAP 1
SWAT 0.47
CWAT 0.0000041
GAMMA 0
END
CMNT
CMNT Grid Data
CMNT
KX 0.0025
KY 0.0025
PHI 0.15
POI 8800
CMNT
DELX -1
0.5 0.6 0.7 1 2 4 8 10 15 20
25 30 35 40 50 70 100 100 100 100
100 100 100 100 100 150 150 150 150 150
150 150 150 150 150 150 150 150 150 150
200 200 200 200 200 200 200 200 200 200
200 200 200 200 200 200 200 200 200 200
200 200 200 200 200 200 200 200 200 200
200 200 200 200 200 200 200 200 200 200
200 200 200 200 200 200 200 200 200 200
200 200 200 200 232
CMNT
DELY 800
H 800
WIND 1 1 1 1
PHI 0.075
KX 0.0025
KY 0.0025
END
CMNT
CMNT Schedule Data
CMNT
PMAP 2
PLOT 2
CMNT
NAME 1 1 1 0 0
ALPH 1.2
DELT 1
DTMX 100000
QG 1 10000
PMIN 1 100
TIME 10000000
END

```



4) Linear Case, Constant  $p_{wf}$ 

```

CMNT Linear Case, Pressure-Dependent Permeability, Constant Pwf for Gas well
CMNT
CMNT Single Value Data
CMNT
IMAX 105
JMAX 1
CMNT (cf)model = (cf + Swi*cw)/(1-Correction for water
CMNT 0.25
CROC 4.08E-06
GRAV 0.717
PREF 8800
TSC 520
PSC 14.65
T 750
NEWT 4
BETA 0
TABL 0
IMAP 1
SWAT 0.47
CWAT 0.0000041
GAMMA 0
END
CMNT
CMNT Grid Data
CMNT
KX 0.0025
KY 0.0025
PHI 0.15
POI 8800
CMNT
DELX -1
0.5 0.6 0.7 1 2 4 8 10 15 20
25 30 35 40 50 70 100 100 100 100
100 100 100 100 100 150 150 150 150 150
150 150 150 150 150 150 150 150 150 150
150 150 150 150 150 150 150 150 150 150
200 200 200 200 200 200 200 200 200 200
200 200 200 200 200 200 200 200 200 200
200 200 200 200 200 200 200 200 200 200
200 200 200 200 200 200 200 200 200 200
200 200 200 200 200 200 200 200 200 200
200 200 200 200 232
CMNT
DELY 800
H 800
WIND 1 1 1 1
PHI 0.075
KX 0.0025
KY 0.0025
END
CMNT
CMNT Schedule Data
CMNT
PMAP 2
PLOT 2
CMNT
NAME 1 1 1 0 0
ALPH 1.2
DELT 1
DTMX 100000
QG 1 10000
PWF 1 8000
TIME 10000000
END

```

## APPENDIX E

## ANALYTICAL SOLUTION FOR RADIAL DIFFUSIVITY EQUATION

Analytical Solution: Infinite Acting Radial Case

1) Constant  $q_g$

The solution of diffusivity equation is:

$$m_D = \frac{1}{2} \ln(t_D) + 0.4045 + s \dots\dots\dots(E.1)$$

Dimensionless variables are defined as:

$$m_D = \frac{kh[m(p_i) - m(p_{wf})]}{1422Tq_g} = \frac{kh\Delta m(p)}{1422Tq_g} \dots\dots\dots(E.2)$$

$$t_D = \frac{0.00633kt}{\phi\mu c_i r_w^2} \dots\dots\dots(E.3)$$

Substituting and reordering;

$$\frac{kh\Delta m(p)}{1422Tq_g} = \frac{1}{2} \ln \left[ \frac{0.00633kt}{\phi\mu c_i r_w^2} \right] + 0.4045 + s \dots\dots\dots(E.4)$$

$$\frac{\Delta m(p)}{q_g} = \frac{1422T}{kh} \left[ \frac{2.303}{2} \log \left( \frac{0.00633kt}{\phi\mu c_i r_w^2} \right) + 0.4045 + s \right] \dots\dots\dots(E.5)$$

$$\frac{\Delta m(p)}{q_g} = \frac{1637.4T}{kh} \left[ \log \left( \frac{0.00633k}{\phi\mu c_i r_w^2} \right) + \log(t) + \frac{0.4045}{1.1515} + \frac{s}{1.1515} \right] \dots\dots\dots(E.6)$$

$$\frac{\Delta m(p)}{q_g} = \frac{1637.4T}{kh} \log(t) + \frac{1637.4T}{kh} \left[ \log \left( \frac{0.00633k}{\phi\mu c_i r_w^2} \right) + \frac{0.4045}{1.1515} + \frac{s}{1.1515} \right] \dots\dots\dots(E.7)$$

Plotting,  $\frac{\Delta m(p)}{q_g}$  vs  $\log(t)$  the slope correspond to:  $m = \frac{1637.4T}{kh}$

Solving for Skin, s:

$$\frac{\Delta m(p)}{q_g} \frac{1}{m} = \log\left(\frac{0.00633k}{\phi\mu c_i r_w^2}\right) + \log(t) + \frac{0.4045}{1.1515} + \frac{s}{1.1515} \dots\dots\dots(E.8)$$

$$\frac{s}{1.1515} = \frac{\Delta m(p) / q_g}{m} - \log\left(\frac{k}{\phi\mu c_i r_w^2}\right) - \log(t) - \log(0.00633) - \frac{0.4045}{1.1515} \dots\dots\dots(E.9)$$

For t = 1 day imply that log(t) = 0

$$s = 1.1515 \left[ \frac{\Delta m(p) / q_g}{m} - \log\left(\frac{k}{\phi\mu c_i r_w^2}\right) + 1.8473 \right] \dots\dots\dots(E.10)$$

2) Constant  $p_{wf}$

The solution of diffusivity equation is:

$$m_D = \frac{1}{q_D} = \frac{1}{2} \ln(t_D) + 0.4045 + s \dots\dots\dots(E.11)$$

Dimensionless variables are defined as:

$$m_D = \frac{1}{q_D} = \frac{kh[m(p_i) - m(p_{wf})]}{1422Tq_g} = \frac{kh\Delta m(p)}{1422Tq_g} \dots\dots\dots(E.12)$$

$$t_D = \frac{0.00633kt}{\phi\mu c_i r_w^2} \dots\dots\dots(E.13)$$

Substituting and reordering;

$$\frac{kh\Delta m(p)}{1422Tq_g} = \frac{1}{2} \ln\left[\frac{0.00633kt}{\phi\mu c_i r_w^2}\right] + 0.4045 + s \dots\dots\dots(E.14)$$

$$\frac{\Delta m(p)}{q_g} = \frac{1422T}{kh} \left[ \frac{2.303}{2} \log\left(\frac{0.00633kt}{\phi\mu c_t r_w^2}\right) + 0.4045 + s \right] \dots\dots\dots(E.15)$$

$$\frac{1}{q_g} = \frac{1637.4T}{kh\Delta m(p)} \left[ \log\left(\frac{0.00633k}{\phi\mu c_t r_w^2}\right) + \log(t) + \frac{0.4045}{1.1515} + \frac{s}{1.1515} \right] \dots\dots\dots(E.16)$$

$$\frac{1}{q_g} = \frac{1637.4T}{kh\Delta m(p)} \log(t) + \frac{1637.4T}{kh\Delta m(p)} \left[ \log\left(\frac{0.00633k}{\phi\mu c_t r_w^2}\right) + \frac{0.4045}{1.1515} + \frac{s}{1.1515} \right] \dots\dots(E.17)$$

Plotting,  $\frac{1}{q_g}$  vs  $\log(t)$  the slope correspond to:  $m = \frac{1637.4T}{kh\Delta m(p)}$

Solving for Skin, s:

$$\frac{1/q_g}{m} = \log\left(\frac{0.00633k}{\phi\mu c_t r_w^2}\right) + \log(t) + \frac{0.4045}{1.1515} + \frac{s}{1.1515} \dots\dots\dots(E.18)$$

$$\frac{s}{1.1515} = \frac{1/q_g}{m} - \log\left(\frac{k}{\phi\mu c_t r_w^2}\right) - \log(t) - \log(0.00633) - \frac{0.4045}{1.1515} \dots\dots\dots(E.19)$$

For t = 1 day imply that  $\log(t) = 0$

$$s = 1.1515 \left[ \frac{1/q_g}{m} - \log\left(\frac{k}{\phi\mu c_t r_w^2}\right) + 1.8473 \right] \dots\dots\dots(E.20)$$

### Analytical Solution: Finite Acting Radial Case

#### 1) Constant $q_g$

The analytical solution of the diffusivity equation for radial flow during pseudo steady state (PSS) condition in dimensionless terms is:

$$m_D = \frac{2}{r_{eD}^2} t_D + \ln(r_{eD}) - \frac{3}{4} \dots\dots\dots (E.21)$$

Dimensionless variables are defined as:

$$m_D = \frac{kh[m(p_i) - m(p_{wf})]}{1422Tq_g} \dots\dots\dots (E.22)$$

$$t_D = \frac{0.00633kt}{\phi\mu c_t r_w^2} \dots\dots\dots (E.23)$$

Substituting Eqs. 2 and 3 in Eq. 1:

$$\frac{kh[m(p_i) - m(p_{wf})]}{1422Tq_g} = \frac{2}{r_{De}^2} \left( \frac{0.00633kt}{\phi\mu c_t r_w^2} \right) + \ln(r_{De}) - \frac{3}{4} \dots\dots\dots (E.24)$$

Reordering;

$$\frac{[m(p_i) - m(p_{wf})]}{q_g} = \frac{1422T}{kh} \frac{2}{r_{De}^2} \left( \frac{0.00633kt}{\phi\mu c_t r_w^2} \right) + \frac{1422T}{kh} \left[ \ln(r_{De}) - \frac{3}{4} \right] \dots\dots\dots (E.25)$$

$$\frac{[m(p_i) - m(p_{wf})]}{q_g} = \frac{18T}{h\phi\mu c_t r_e^2} t + \frac{1422T}{kh} \left[ \ln(r_{De}) - \frac{3}{4} \right] \dots\dots\dots (E.26)$$

Pore volume,  $V_p$ , is calculated as:

$$V_p = \pi r_e^2 h \phi \dots\dots\dots (E.27)$$

Substituting pore volume in equation:

$$\frac{[m(p_i) - m(p_{wf})]}{q_g} = \frac{18\pi T}{V_p \mu c_t} t + \frac{1422T}{kh} \left[ \ln(r_{De}) - \frac{3}{4} \right] \dots\dots\dots(E.28)$$

Then, plotting  $\frac{[m(p_i) - m(p_{wf})]}{q_g}$  vs t, we get the slope, m, as:

$$m = \frac{18\pi T}{V_p \mu c_t} \dots\dots\dots(E.29)$$

OGIP is calculated as:

$$OGIP = \frac{V_p S_{gi}}{B_{gi}} \dots\dots\dots(E.30)$$

$$B_{gi} = 0.0282 \frac{T z_i}{p_i} \dots\dots\dots(E.31)$$

$$OGIP = 18\pi \frac{T}{\mu c_t} \left( \frac{1}{\tilde{m}_{PSS}} \right) \left( \frac{p_i}{0.0282 T z_i} \right) S_{gi} \dots\dots\dots(E.32)$$

$$OGIP = \frac{2 p_i S_{gi}}{z_i \mu c_t} \left( \frac{1}{\tilde{m}_{PSS}} \right) \dots\dots\dots(E.33)$$

## 2) Constant $p_{wf}$

The analytical solution of the diffusivity equation for radial flow during pseudo steady state (PSS) condition in dimensionless terms is:

$$m_D = \frac{1}{q_D} = \frac{2}{r_{eD}^2} t_D + \ln(r_{eD}) - \frac{3}{4} \dots\dots\dots(E.34)$$

Dimensionless variables are defined as:

$$m_D = \frac{1}{q_D} = \frac{kh[m(p_i) - m(p_{wf})]}{1422Tq_g} \dots\dots\dots(E.35)$$

$$t_D = \frac{0.00633kt}{\phi\mu_c r_w^2} \dots\dots\dots(E.36)$$

Substituting Eqs. 2 and 3 in Eq. 1:

$$\frac{kh[m(p_i) - m(p_{wf})]}{1422Tq_g} = \frac{2}{r_{De}^2} \left( \frac{0.00633kt}{\phi\mu_c r_w^2} \right) + \ln(r_{De}) - \frac{3}{4} \dots\dots\dots(E.37)$$

Reordering;

$$\frac{[m(p_i) - m(p_{wf})]}{q_g} = \frac{1422T}{kh} \frac{2}{r_{De}^2} \left( \frac{0.00633kt}{\phi\mu_c r_w^2} \right) + \frac{1422T}{kh} \left[ \ln(r_{De}) - \frac{3}{4} \right] \dots\dots(E.38)$$

$$\frac{[m(p_i) - m(p_{wf})]}{q_g} = \frac{18T}{h\phi\mu_c r_e^2} t + \frac{1422T}{kh} \left[ \ln(r_{De}) - \frac{3}{4} \right] \dots\dots\dots(E.39)$$

Pore volume,  $V_p$ , is calculated as:

$$V_p = \pi r_e^2 h \phi \dots\dots\dots(E.40)$$

Substituting pore volume in equation:

$$\frac{[m(p_i) - m(p_{wf})]}{q_g} = \frac{18\pi T}{V_p \mu_c} t + \frac{1422T}{kh} \left[ \ln(r_{De}) - \frac{3}{4} \right] \dots\dots\dots(E.41)$$

Then, plotting  $\frac{[m(p_i) - m(p_{wf})]}{q_g}$  vs  $t$ , we get the slope,  $m$ , as:

$$m = \frac{18\pi T}{V_p \mu c_t} \dots\dots\dots (E.42)$$

OGIP is calculated as:

$$OGIP = \frac{V_p S_{gi}}{B_{gi}} \dots\dots\dots (E.43)$$

$$B_{gi} = 0.0282 \frac{Tz_i}{p_i} \dots\dots\dots (E.44)$$

$$OGIP = 18\pi \frac{T}{\mu c_t} \left( \frac{1}{\tilde{m}_{PSS}} \right) \left( \frac{p_i}{0.0282 T z_i} \right) S_{gi} \dots\dots\dots (E.45)$$

$$OGIP = \frac{2 p_i S_{gi}}{z_i \mu c_t} \left( \frac{1}{\tilde{m}_{PSS}} \right) \dots\dots\dots (E.46)$$



## APPENDIX F

## ANALYTICAL SOLUTION FOR LINEAR DIFFUSIVITY EQUATION

Analytical Solution: Infinite Acting Linear Case

1) Constant  $q_g$

The solution of diffusivity equation is:

$$m_D = 4\sqrt{\pi * t_{D_{Ac}}} + s \dots\dots\dots(F.1)$$

Dimensionless variables are defined as:

$$m_D = \frac{[m(p_i) - m(p_{wf})] k \sqrt{A_c}}{1,422 T q_g} \dots\dots\dots(F.2)$$

$$t_{D_{Ac}} = \frac{0.00633 k t}{\phi \mu c_t A_c} \dots\dots\dots(F.3)$$

Substituting and reordering;

$$\frac{[m(p_i) - m(p_{wf})] k \sqrt{A_c}}{1,422 T q_g} = 4 \sqrt{\frac{0.00633 \pi k t}{\phi \mu c_t A_c}} + s \dots\dots\dots(F.4)$$

$$\frac{[m(p_i) - m(p_{wf})]}{q_g} = \frac{4 * 1,422 T}{k \sqrt{A_c}} \sqrt{\frac{0.00633 \pi k t}{\phi \mu c_t A_c}} + \frac{1,422 T}{k \sqrt{A_c}} s \dots\dots\dots(F.5)$$

$$\frac{[m(p_i) - m(p_{wf})]}{q_g} = 4 * 1,422 * \sqrt{0.00633 \pi} * \frac{T}{\sqrt{k} A_c} \frac{1}{\sqrt{\phi \mu c_t}} * \sqrt{t} + \frac{1,422 T}{k \sqrt{A_c}} s \dots\dots\dots(F.6)$$

$$\frac{[m(p_i) - m(p_{wf})]}{q_g} = 802.11 * \frac{T}{\sqrt{k} A_c} \frac{1}{\sqrt{\phi \mu c_t}} * \sqrt{t} + \frac{1,422 T}{k \sqrt{A_c}} s \dots\dots\dots(F.7)$$

Plotting,  $\frac{[m(p_i) - m(p_{wf})]}{q_g}$  vs  $\sqrt{t}$  the slope corresponds to:  $m = \frac{802.11T}{\sqrt{k} A_c} \frac{1}{\sqrt{\phi\mu c_t}}$

Solving for permeability, k:

$$m = \frac{802.11T}{\sqrt{k} A_c} \frac{1}{\sqrt{\phi\mu c_t}} \dots\dots\dots(F.8)$$

$$\sqrt{k} = \frac{802.11T}{m A_c} \frac{1}{\sqrt{\phi\mu c_t}} \dots\dots\dots(F.9)$$

$$k = \left[ \frac{802.11T}{m A_c} \right]^2 \frac{1}{\phi\mu c_t} \dots\dots\dots(F.10)$$

Solving for Skin, s:

$$\frac{[m(p_i) - m(p_{wf})]}{q_g} = 802.11 * \frac{T}{\sqrt{k} A_c} \frac{1}{\sqrt{\phi\mu c_t}} * \sqrt{t} + \frac{1,422T}{k\sqrt{A_c}} s \dots\dots\dots(F.11)$$

$$\frac{1,422T}{k\sqrt{A_c}} s = \frac{[m(p_i) - m(p_{wf})]}{q_g} - 802.11 * \frac{T}{\sqrt{k} A_c} \frac{1}{\sqrt{\phi\mu c_t}} * \sqrt{t} \dots\dots\dots(F.12)$$

$$s = \frac{k\sqrt{A_c}}{1,422T} \frac{[m(p_i) - m(p_{wf})]}{q_g} - \frac{802.11}{1,422} * \frac{k\sqrt{A_c}}{\sqrt{k} A_c} \frac{1}{\sqrt{\phi\mu c_t}} * \sqrt{t} \dots\dots\dots(F.13)$$

$$s = \frac{k\sqrt{A_c}}{1,422T} \frac{[m(p_i) - m(p_{wf})]}{q_g} - 0.564075 * \sqrt{\frac{k}{\phi\mu c_t A_c}} * \sqrt{t} \dots\dots\dots(F.14)$$

2) Constant  $p_{wf}$ 

The solution of diffusivity equation is:

$$\frac{1}{q_D} = 2\pi \sqrt{\pi * t_{D_{Ac}}} + s \dots\dots\dots(F.15)$$

Dimensionless variables are defined as:

$$\frac{1}{q_D} = \frac{[m(p_i) - m(p_{wf})] k \sqrt{A_c}}{1,422 T q_g} \dots\dots\dots(F.16)$$

$$t_{D_{Ac}} = \frac{0.00633 k t}{\phi \mu c_t A_c} \dots\dots\dots(F.17)$$

Substituting and reordering;

$$\frac{[m(p_i) - m(p_{wf})] k \sqrt{A_c}}{1,422 T q_g} = 2\pi \sqrt{\frac{0.00633 \pi k t}{\phi \mu c_t A_c}} + s \dots\dots\dots(F.18)$$

$$\frac{[m(p_i) - m(p_{wf})]}{q_g} = \frac{2\pi * 1,422 T}{k \sqrt{A_c}} \sqrt{\frac{0.00633 \pi k t}{\phi \mu c_t A_c}} + \frac{1,422 T}{k \sqrt{A_c}} s \dots\dots\dots(F.19)$$

$$\frac{[m(p_i) - m(p_{wf})]}{q_g} = 2\pi * 1,422 * \sqrt{0.00633\pi} * \frac{T}{\sqrt{k} A_c} \frac{1}{\sqrt{\phi \mu c_t}} * \sqrt{t} + \frac{1,422 T}{k \sqrt{A_c}} s \dots\dots(F.20)$$

$$\frac{[m(p_i) - m(p_{wf})]}{q_g} = 1,259.96 * \frac{T}{\sqrt{k} A_c} \frac{1}{\sqrt{\phi \mu c_t}} * \sqrt{t} + \frac{1,422 T}{k \sqrt{A_c}} s \dots\dots\dots(F.21)$$

Plotting,  $\frac{[m(p_i) - m(p_{wf})]}{q_g}$  vs  $\sqrt{t}$  the slope corresponds to:  $m = \frac{1,259.96 T}{\sqrt{k} A_c} \frac{1}{\sqrt{\phi \mu c_t}}$

Solving for permeability, k:

$$m = \frac{1,259.96T}{\sqrt{k} A_c} \frac{1}{\sqrt{\phi\mu c_t}} \dots\dots\dots(F.22)$$

$$\sqrt{k} = \frac{1,259.96T}{m A_c} \frac{1}{\sqrt{\phi\mu c_t}} \dots\dots\dots(F.23)$$

$$k = \left[ \frac{1,259.96T}{m A_c} \right]^2 \frac{1}{\phi\mu c_t} \dots\dots\dots(F.24)$$

Solving for Skin, s:

$$\frac{[m(p_i) - m(p_{wf})]}{q_q} = 1,259.96 * \frac{T}{\sqrt{k} A_c} \frac{1}{\sqrt{\phi\mu c_t}} * \sqrt{t} + \frac{1,422T}{k\sqrt{A_c}} s \dots\dots\dots(F.25)$$

$$\frac{1,422T}{k\sqrt{A_c}} s = \frac{[m(p_i) - m(p_{wf})]}{q_q} - 1,259.96 * \frac{T}{\sqrt{k} A_c} \frac{1}{\sqrt{\phi\mu c_t}} * \sqrt{t} \dots\dots\dots(F.26)$$

$$s = \frac{k\sqrt{A_c}}{1,422T} \frac{[m(p_i) - m(p_{wf})]}{q_q} - \frac{1,259.96}{1,422} * \frac{k\sqrt{A_c}}{\sqrt{k} A_c} \frac{1}{\sqrt{\phi\mu c_t}} * \sqrt{t} \dots\dots\dots(F.27)$$

$$s = \frac{k\sqrt{A_c}}{1,422T} \frac{[m(p_i) - m(p_{wf})]}{q_q} - 0.886047 * \sqrt{\frac{k}{\phi\mu c_t A_c}} * \sqrt{t} \dots\dots\dots(F.28)$$

## Analytical Solution: Finite Acting Linear Case

1) Constant  $q_g$ 

The analytical solution of the diffusivity equation for linear flow during pseudo steady state (PSS) condition in dimensionless terms is:

$$m_D = 2\pi \left( \frac{L}{\sqrt{A_c}} \right) \left[ \frac{1}{3} + \left( \frac{\sqrt{A_c}}{L} \right)^2 t_{DAc} \right] \dots\dots\dots \text{F.29}$$

Dimensionless variables are defined as:

$$m_D = \frac{k \sqrt{A_c} [m(p_i) - m(p_{wf})]}{1422 T q_g} \dots\dots\dots \text{F.30}$$

$$t_D = \frac{0.00633kt}{\phi \mu c_t A_c} \dots\dots\dots \text{F.31}$$

Substituting Eqs. 2 and 3 in Eq. 1:

$$\frac{k \sqrt{A_c} [m(p_i) - m(p_{wf})]}{1422 T q_g} = \frac{2\pi}{3} \frac{L}{\sqrt{A_c}} + 2\pi \frac{L}{\sqrt{A_c}} \left( \frac{\sqrt{A_c}}{L} \right)^2 \left( \frac{0.00633kt}{\phi \mu c_t A_c} \right) \dots\dots\dots \text{F.32}$$

Reordering;

$$\frac{[m(p_i) - m(p_{wf})]}{q_g} = \frac{1422 T}{k \sqrt{A_c}} \left[ \frac{2\pi}{3} \frac{L}{\sqrt{A_c}} + (2\pi * 0.00633) \frac{1}{L \sqrt{A_c}} \frac{kt}{\phi \mu c_t} \right] \dots\dots\dots \text{F.33}$$

$$\frac{[m(p_i) - m(p_{wf})]}{q_g} = 1422 \frac{2\pi}{3} \frac{LT}{k A_c} + (0.00633 * 1422 * 2\pi) \frac{T}{L A_c} \frac{1}{\phi \mu c_t} t \dots\dots\dots \text{F.34}$$

Pore volume,  $V_p$ , is calculated as:

$$V_p = L A_c \phi \dots\dots\dots \text{F.35}$$

Substituting pore volume in equation:

$$\frac{[m(p_i) - m(p_{wf})]}{q_g} = 1422 \frac{2\pi}{3} \frac{LT}{kA_c} + 56.56 \frac{T}{V_p} \frac{1}{\mu c_t} t \dots\dots\dots(F.36)$$

Then, plotting  $\frac{[m(p_i) - m(p_{wf})]}{q_g}$  vs t, we get the slope, m, as:

$$m = 56.56 \frac{T}{V_p \mu c_t} \dots\dots\dots(F.37)$$

OGIP is calculated as:

$$OGIP = \frac{V_p S_{gi}}{B_{gi}} \dots\dots\dots(F.38)$$

$$B_{gi} = 0.0282 \frac{T z_i}{p_i} \dots\dots\dots(F.39)$$

$$OGIP = 56.56 \frac{T}{\mu c_t} \left( \frac{1}{\tilde{m}_{PSS}} \right) \left( \frac{p_i}{0.0282 T z_i} \right) S_{gi} \dots\dots\dots(F.40)$$

$$OGIP = \frac{2 p_i S_{gi}}{z_i \mu c_t} \left( \frac{1}{\tilde{m}_{PSS}} \right) \dots\dots\dots(F.41)$$

## 2) Constant $p_{wf}$

The analytical solution of the diffusivity equation for linear flow during pseudo steady state (PSS) and constant bottom hole pressure condition in dimensionless terms is:

$$\frac{1}{q_D} = \frac{\pi \left( \frac{L}{\sqrt{A_c}} \right)}{\sum_{n_{odd}}^{\infty} \exp \left[ \frac{-n^2 \pi^2}{4} \left( \frac{\sqrt{A_c}}{L} \right)^2 t_{D_{Ac}} \right]} \dots \dots \dots (F.42)$$

Dimensionless variables are defined as:

$$\frac{1}{q_D} = \frac{k \sqrt{A_c} [m(p_i) - m(p_{wf})]}{1,422 T q_g} \dots \dots \dots (F.43)$$

$$t_D = \frac{0.00633 k t}{\phi \mu c_t A_c} \dots \dots \dots (F.44)$$

Substituting Eqs. 2 and 3 in Eq. 1:

$$\frac{k \sqrt{A_c} [m(p_i) - m(p_{wf})]}{1,422 T q_g} = \frac{\pi \frac{L}{\sqrt{A_c}}}{\exp \left[ \frac{-\pi^2}{4} \frac{A_c}{L^2} \frac{0.00633 k t}{\phi \mu c_t A_c} \right]} \dots \dots \dots (F.45)$$

Reordering;

$$\frac{[m(p_i) - m(p_{wf})]}{q_g} = \frac{1,422 \pi \frac{T L}{k A_c}}{\exp \left[ \frac{-\pi^2}{4} \frac{A_c}{L^2} \frac{0.00633 k t}{\phi \mu c_t A_c} \right]} \dots \dots \dots (F.46)$$

$$\ln \left[ \frac{m(p_i) - m(p_{wf})}{q_g} \right] = \ln \left( 1,422 \pi \frac{T L}{k A c} \right) + \left( \frac{0.00633 \pi^2}{4} \right) \frac{A_c k t}{L^2 \phi \mu c_t A_c} \dots \dots \dots (F.47)$$

Pore volume,  $V_p$ , is calculated as:

$$V_p = L A_c \phi \dots \dots \dots (F.48)$$

Substituting pore volume in equation:

$$\ln \left[ \frac{m(p_i) - m(p_{wf})}{q_g} \right] = \ln \left( 1,422\pi \frac{TL}{kAc} \right) + \left( \frac{0.00633\pi^2}{4} \right) \frac{A_c k t}{L\mu c_t V_p} \dots\dots\dots(F.49)$$

Then, plotting  $\ln \left[ \frac{m(p_i) - m(p_{wf})}{q_g} \right]$  vs t, we get the slope, m, as:

$$m = \left( 0.00633 \frac{\pi^2}{4} \right) \frac{A_c k}{L\mu c_t V_p} \dots\dots\dots(F.50)$$

OGIP is calculated as:

$$OGIP = \frac{V_p S_{gi}}{B_{gi}} \dots\dots\dots(F.51)$$

$$B_{gi} = 0.0282 \frac{Tz_i}{p_i} \dots\dots\dots(F.52)$$

$$OGIP = \left( 0.00633 \frac{\pi^2}{4} \right) \frac{A_c k}{\mu c_t L} \left( \frac{1}{\tilde{m}_{PSS}} \right) \left( \frac{p_i}{0.0282 T z_i} \right) S_{gi} \dots\dots\dots(F.53)$$

$$OGIP = 0.5538 \frac{A_c k p_i S_{gi}}{T z_i \mu c_t L} \left( \frac{1}{\tilde{m}_{PSS}} \right) \dots\dots\dots(F.54)$$



APPENDIX G  
MISCELLANEOUS

This section includes some discussion regarding pseudo properties in terms of pressure-dependent and non pressure-dependent permeability. Also show the change of non-linear term  $\phi \mu c_t$  for the pressure range analyzed in case 1: radial flow, constant  $q_g = 10$  Mscf/D.

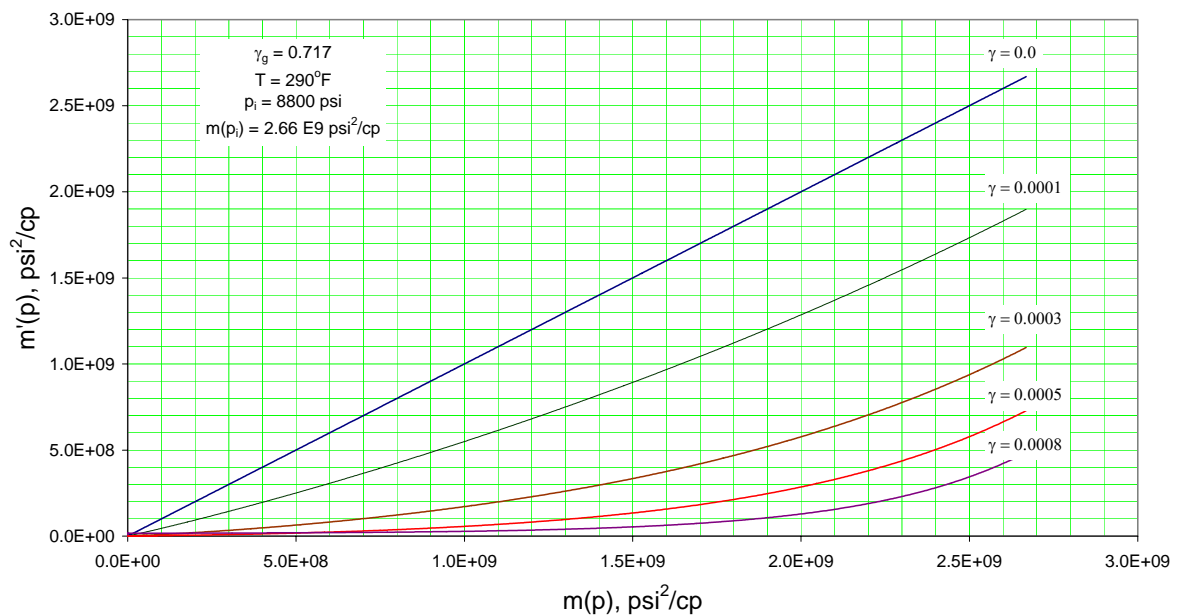


Figure G.1 – Cartesian plot  $m'(p)$  vs  $m(p)$  for a gas of gravity 0.717 and temperature  $290^\circ\text{F}$ . Comparison of pseudo pressure for a formation with and without stress-sensitive permeability is made. As gamma increase, the rock is more stress-dependent and permeability has a larger reduction, the relation between  $m'(p)$  vs  $m(p)$  is not longer linear.

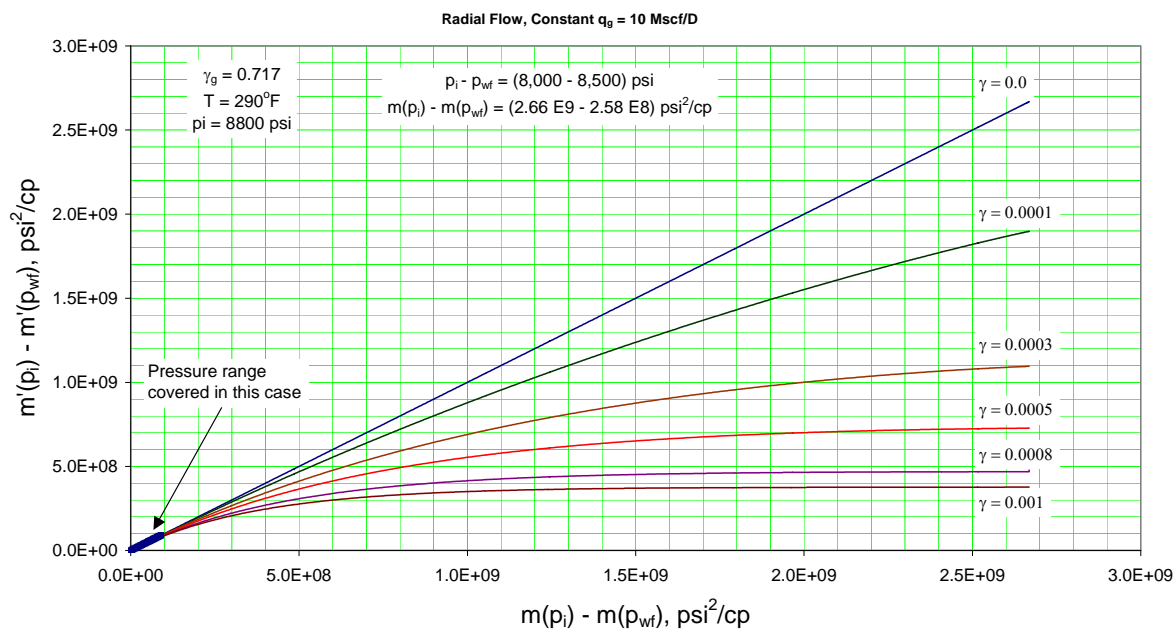


Fig. G.2 – Cartesian plot of pseudo pressure draw down. Comparison for a formation with  $[m'(p_i) - m'(p_{wf})]$  and without  $[m(p_i) - m(p_{wf})]$  stress-dependent permeability is made. Continuous lines are analytical solutions for several values of gamma. Darker lines represent the pressure range considered in the Case 1: radial flow, infinite acting period, constant  $q_g = 10$  Mscf/D. Case 1 considers a small pressure draw down range and still exists a linear relation between  $m'(p)$  vs  $m(p)$ .

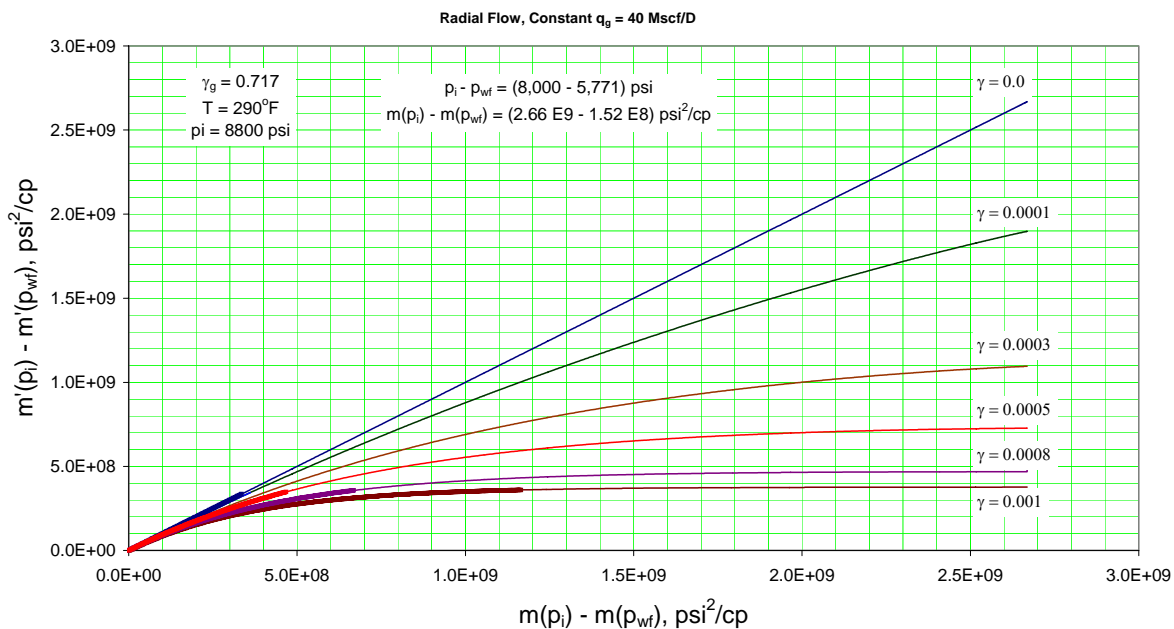


Fig. G.3 – Cartesian plot of pseudo pressure draw down. Comparison for a formation with  $[m'(p_i) - m'(p_{wf})]$  and without  $[m(p_i) - m(p_{wf})]$  stress-dependent permeability is made. Continuous lines are analytical solutions for several values of gamma. Darker lines represent the pressure range considered in the Case 2: radial flow, infinite acting period, constant  $q_g = 40$  Mscf/D. Case 2 considers a larger pressure draw down range and covers a long portion where there is not a linear relation between  $m'(p)$  vs  $m(p)$ .

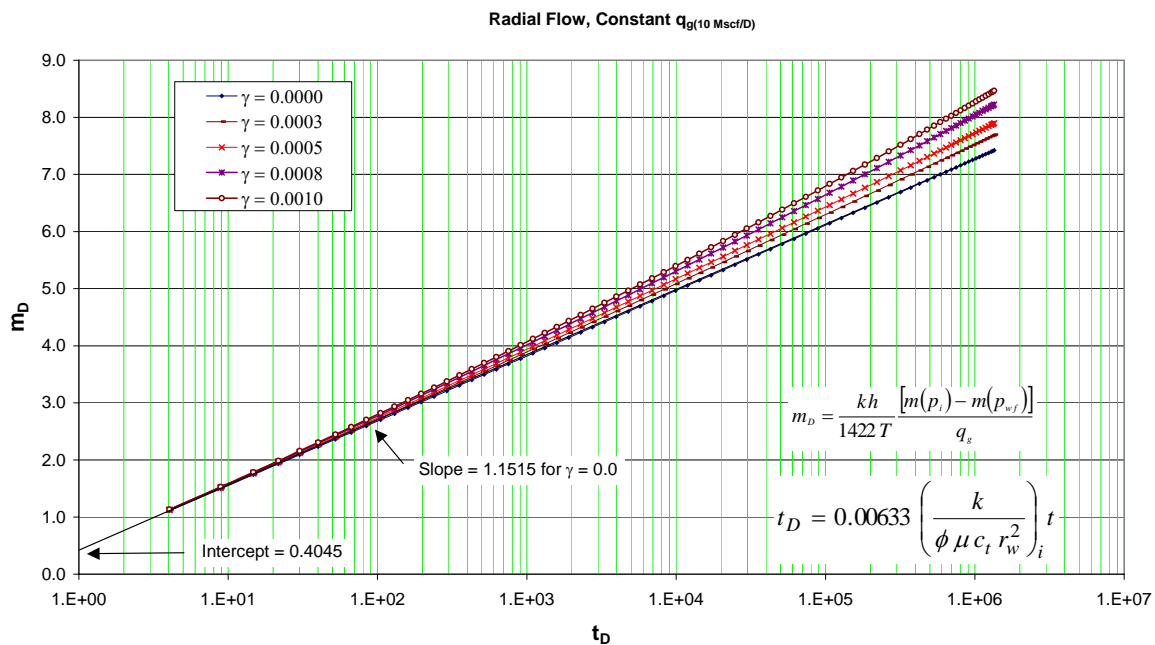


Fig. G.4 - Semi-log plot of dimensionless pseudo pressure vs. time. Values of gamma indicate a stress-dependent permeability. Numerical results are for Case 1: radial flow, infinite acting, constant  $q_g = 10 \text{ Mscf/D}$ . Analytical solution for  $\gamma = 0$  has the form:  $m_D = 1.1515 \log(t_D) + 0.4045 + s$ . As gamma increase results are straight line with a different slopes.

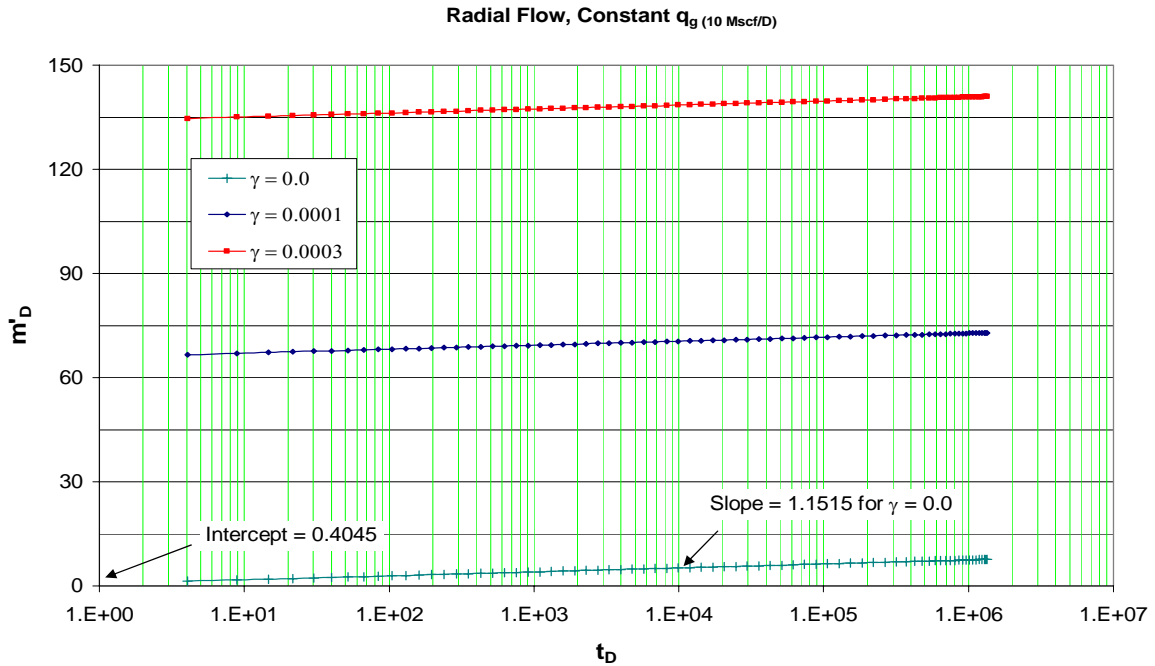


Fig. G.5 – Semi-log plot of dimensionless pseudo pressure prime vs. time. The value of  $m'(p)$  has been calculated analytically by the integral function including the

permeability modulus as:  $m'(p) = 2 \int_{P_{wf}}^{P_i} \frac{k}{k_i} \frac{p}{\mu z} dp$ . Values of gamma indicate a stress-

dependent permeability. Numerical results are for Case 1: radial flow, infinite acting,

constant  $q_g = 10$  Mscf/D. Analytical solution for  $\gamma = 0$  has the form:

$m_D = 1.1515 \log(t_D) + 0.4045 + s$ . As gamma increase results are straight line with same slopes and different intercept.

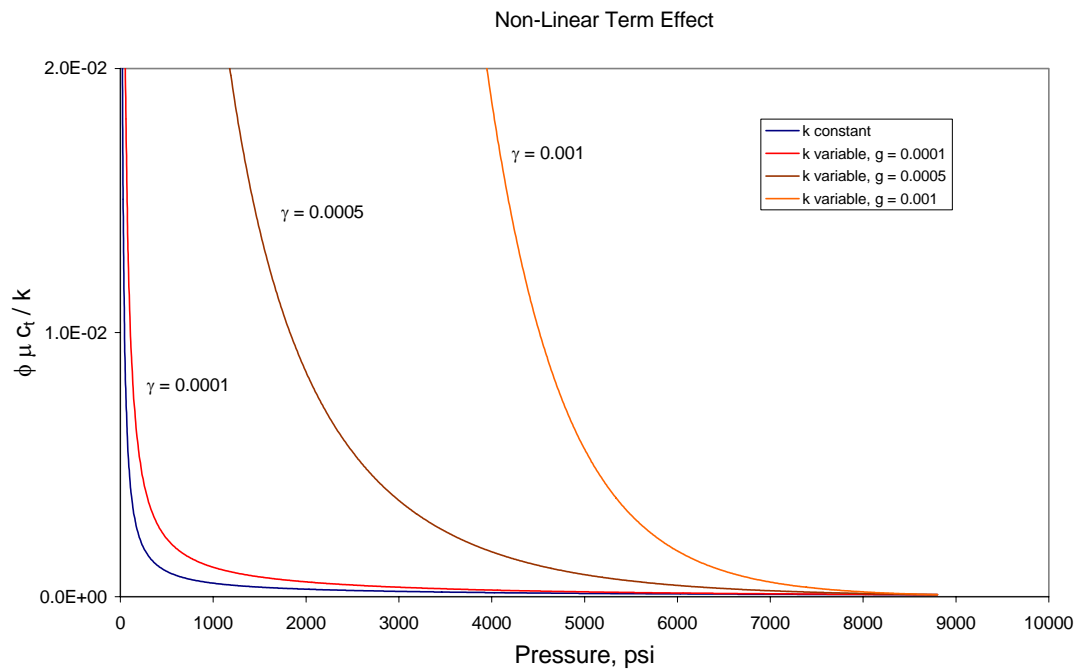


Fig. G.6 - Comparison of non-linear term  $\phi \mu c_t / k$  regarding a non-stress formation ( $k =$  constant) and a stress formation ( $k =$  function of pressure) as a function of pore pressure.

Values of gamma indicate a larger dependency on stress. For low pressure and large gamma the non-linear term has a significant variation.

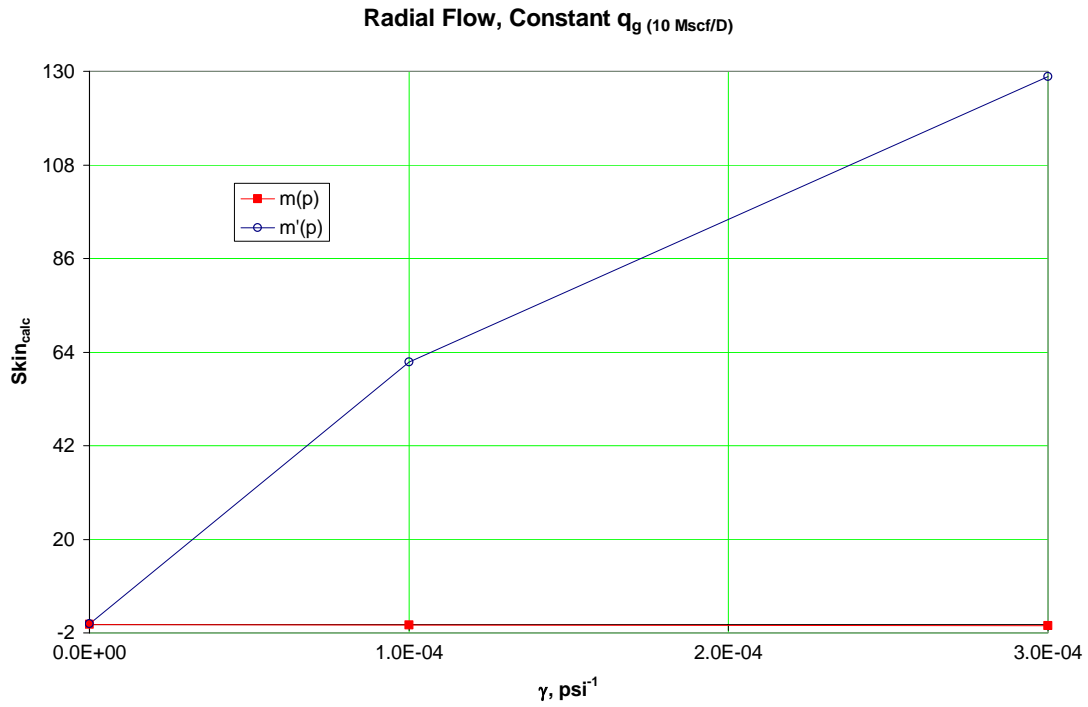


Fig. G.7 - Comparison of calculated skin factor from conventional real gas pseudo pressure numerical results,  $m(p)$ , and also using analytical real gas pseudo pressure

prime,  $m'(p)$ . Integral function used is: 
$$m'(p) = 2 \int_{P_{wf}}^{P_i} \frac{k}{k_i} \frac{p}{\mu z} dp .$$

The case considered correspond with radial flow, infinite acting and constant  $q_g = 10$  Mscf/D.

## VITA

Name: Cesar Alexander Rodriguez

Permanent Address: Apto 4-B, Residencias Dona Camila  
Av. El Milagro, Maracaibo  
Estado Zulia  
Venezuela

Email: car\_texas@hotmail.com

Education: B. S., Petroleum Engineering  
Universidad Central de Venezuela  
Caracas, Venezuela  
(August 1997)

M.S., Petroleum Engineering  
Texas A&M University  
College Station, TX 77843-3116  
(December 2004)